



UNIVERSITY
OF TRENTO - Italy

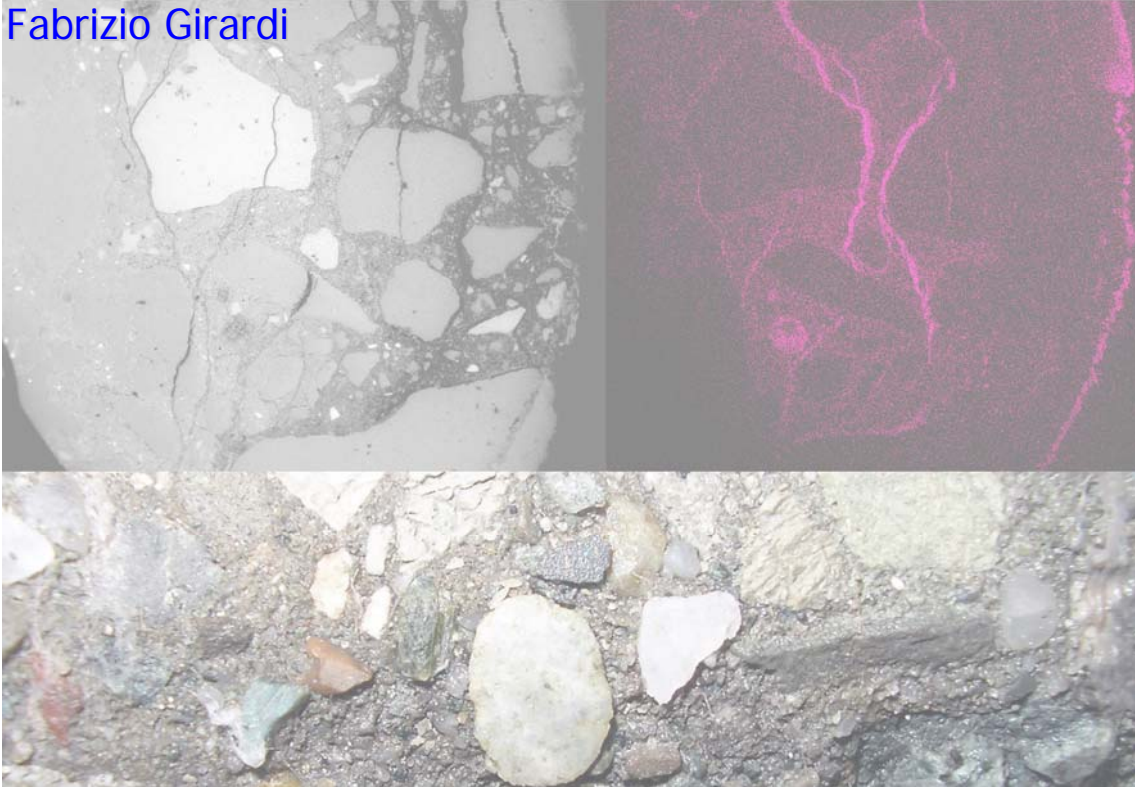
Department of Materials Engineering
and Industrial Technologies

Doctorate School in Materials Engineering – XXI cycle

A composite of two grayscale microscopic images showing the internal structure of concrete. The left image shows a circular cross-section with a textured, porous interior. The right image shows a more detailed view of the internal structure, highlighting the arrangement of fibers and the surrounding matrix.

Studies on concrete degradation in aggressive environment and development of protective system

Fabrizio Girardi



April 2009



UNIVERSITY
OF TRENTO - Italy

Department of Materials Engineering
and Industrial Technologies

Doctorate School in Materials Engineering – XXI cycle

Studies on concrete degradation in aggressive environment and development of protective system

Fabrizio Girardi

April 2009

Index

Index.....	i
List of figures.....	iv
List of tables.....	vii
Abbreviations	ix
Part 1 - Studies on concrete degradation in aggressive environment	1
Chapter 1 - Introduction	1
Chapter 2 - Degradation of concrete with limestone aggregates in sodium sulphate solution ...	7
2.1 Introduction	7
2.2 Materials	7
2.3 Chemical test	9
2.4 Testing program	9
2.5 Results	11
2.5.1 pH solution.....	11
2.5.2 Mass variation	11
2.5.3 Deformation.....	14
2.5.4 Characterization after 2000 hours of cyclic acid/sulphate attack	18
2.5.5 Characterization after 45000 hours.....	20
2.5.5.1 Phenolphthalein method (EN 9944).....	20
2.5.5.2 Microstructural analysis.....	22
2.6 Discussion.....	31
2.7 Conclusions	35
Chapter 3 – Degradation of concrete with limestone/silicates aggregates in complex sulphate solution	37
3.1 Introduction.....	37

3.2 Materials	37
3.3 Chemical test	38
3.4 Testing program	39
3.5 Results	41
3.5.1 Analysis of samples-L	41
3.5.1.1 pH and permeability in water	41
3.5.1.2 Mass variation	41
3.5.1.3 Deformation	45
3.5.1.4 Characterization after 40000 hours	47
3.5.1.4.1 Phenolphthalein method (EN 9944)	47
3.5.1.4.2 Microstructural analysis	48
3.5.2 Analysis of samples-S	56
3.5.2.1 pH and permeability in water	56
3.5.2.2 Aggregate analysis	56
3.5.2.3 Mass variation	58
3.5.2.4 Deformation results	60
2.5.2.5.1 Phenolphthalein method (EN 9944)	62
3.5.2.5.2 Microstructural analyses	63
3.6 Discussion and conclusions	71
Part 2 - Development of protective system	77
Chapter 4 – Silica coating	79
4.1 Introduction	79
4.2 Materials	79
4.3 Chemical test	81
4.4 Testing program	82
4.5 Results	83

4.5.1 Mass variation	83
4.5.2 Test on hardened concrete	89
4.5.3 Phenolphthalein and wettability tests	89
4.6 Discussion	91
4.7 Conclusions	93
Chapter 5 – Hybrid coating	95
5.1 Hybrid coating	95
5.2 Materials	95
5.3 Result and discussion	96
5.4 Conclusions	101
References	103
Acknowledgements	107
Publications	109

List of figures

Figure 1 – Sewer pipe degradation scheme	3
Figure 2 – pH values during acid attack (a) and during sulphate attack (b)	11
Figure 3 - Mass variation [%] during the sulphate attack.....	12
Figure 4 - Mass variation [%] during the cyclic acid/sulphate attack.	13
Figure 5 – Deformation [%] during the sulphate attack.....	15
Figure 6 - Deformation [%] during the cyclic acid/sulphate attack.....	16
Figure 7 – Phenolphthalein method results (EN 9944) on three mixtures (a) PTL-L, b) BLF-L and c) PZ-L+SF) after 2000 hour of acid/sulphate attack.....	18
Figure 8 – Micrographs of the mixtures BLF-L, PZ-L + SF and PTL-L (a, b and c respectively) after 2000 hours of acid/sulphate attack and the PTL-L (d) after 2000 hours of only sulphate attack.	19
Figure 9 - Phenolphthalein method results (EN 9944) after 45000 hours of sulphate attack (on the left) and acid/sulphate attack (on the right).....	21
Figure 10 - ESEM images (on the left) and X-ray maps for sulphur (on the right) of polished surface subjected to cyclic acid/sulphate attack.....	23
Figure 11 - Micrographs of the PTL-L after 45000 hours of cyclic acid/sulphate attack.	26
Figure 12 – EDAX results of the crystals in the crack reported in Figure 11b.....	26
Figure 13 – Micrographs of the PTL-L after 45000 hours of sulphate attack.	27
Figure 14 – Micrograph of the BLF-L after 45000 hours of cyclic acid/sulphate attack.....	27
Figure 15 – Micrograph of the BLF-L after 45000 hours of sulphate attack.....	27
Figure 16 – Micrograph of the PZ-L after 45000 hours of cyclic acid/sulphate attack.....	28
Figure 17 - EDAX results of the crystals in the crack reported in Figure 16b.....	28
Figure 18- Micrograph of the PZ-L after 45000 hours of sulphate attack.	28
Figure 19 – Micrograph of the BLF-L + SF after 45000 hours of cyclic acid/sulphate attack.	29
Figure 20 – Micrograph of the BLF-L + SF after 45000 hours of sulphate attack.....	29
Figure 21 – Micrograph of the PZ-L + SF after 45000 hours of cyclic acid/sulphate attack....	29
Figure 22 – Micrograph of the PZ-L + SF after 45000 hours of sulphate attack.	30
Figure 23 – pH values during acid attack (a) and during complex sulphate attack (b)	41
Figure 24 – Mass variation [%] during complex sulphate attack.	42
Figure 25 - Mass variation [%] (mean value of three samples for each typologies) during the cyclic acid/(complex)sulphate attack.....	44
Figure 26 – Deformation [%] during the complex sulphate attack.....	45

Figure 27 – Deformation [%] (mean value of three samples for each typologies) during cyclic acid/(complex) sulphate attack.	46
Figure 28 - Phenolphthalein methods results (EN 9944).....	48
Figure 29 ESEM images (on the left) and X-ray maps for sulphur (on the right) of polished surface subjected to cyclic acid and complex sulphate attack.	50
Figure 30 - Micrograph of PTL-L after 40000 hours of cyclic acid/(complex) sulphate attack.	52
Figure 31 - Micrograph of PTL-L after 40000 hours of complex sulphate attack.....	52
Figure 32 - Micrograph of BLF-L after 40000 hours of cyclic acid/(complex)sulphate attack.....	53
Figure 33 - Micrograph of BLF-L after 40000 hours of complex sulphate attack.....	53
Figure 34 – Micrograph of the PZ-L + SF after 40000 hours of cyclic acid/(complex) sulphate attack.	53
Figure 35 - EDAX results of the crystals in the crack reported Figure 34b.....	54
Figure 36 - Micrograph of PZ-L + SF after 40000 hours of complex sulphate attack.	54
Figure 37 – Micrograph of the mixtures stored in water after 40000 hours.	55
Figure 38 – pH values during acid attack (a) and during complex sulphate attack (b).....	56
Figure 39 – Mass variation [%] during the complex sulphate attack (mean value of two samples).....	58
Figure 40 – Mass variation [%] during the cyclic acid/(complex) sulphate attack (mean value of two samples).	59
Figure 41 – Deformation [%] during the complex sulphate attack (mean value of two samples).....	60
Figure 42 – Deformation [%] during the cyclic acid/(complex) sulphate attack (mean value of two samples).....	61
Figure 43 - Phenolphthalein methods (EN 9944) results on concretes prepared with silicates aggregate.....	63
Figure 44 - ESEM images (on the left) and X-ray maps for sulphur (on the right) of polished surface subjected to cyclic acid and complex sulphate attack.	65
Figure 45 - Micrograph of PTL-S after 25000 hours of complex sulphate attack.....	67
Figure 46 – Micrograph of PTL-S after 25000 hours of cyclic acid/(complex)sulphate attack.	67
Figure 47 - EDAX results of the crystals in the crack reported Figure 46b.....	67
Figure 48 – Micrograph of the mixture BLF-S after 25000 hours of complex sulphate attack.	68

Figure 49 – Micrograph of the BLF-S after 25000 hours of cyclic acid/(complex)sulphate attack.	68
Figure 50 – Micrograph of PZ-S + SF after 25000 hours of complex sulphate attack.	68
Figure 51 – Micrograph of the PZ-S + SF after 25000 hours of cyclic acid/(complex)sulphate attacks.	69
Figure 52 - EDAX results of the crystals in the crack reported Figure 51b.	69
Figure 53 – Micrographs of the mixtures stored in water.	70
Figure 54 – Mass variation [%] during the complex sulphate attack (mean value of two samples).	84
Figure 55 - Mass variation [%] during the acid/(complex)sulphate attack.	85
Figure 56 – Deformation [%] during the complex sulphate attack.	86
Figure 57 – Deformation [%] during the cyclic acid/(complex)sulphate attack.	87
Figure 58 – Effect of the silica coating on the grow of algae.	88
Figure 59 – Silica coating applied on hardened concrete.	89
Figure 60 - Phenolphthalein methods (EN 9944) results on LC sample.	90
Figure 61 - Wettability test of WC (a) and LCP (b, c).	90
Figure 62 - DSC curve of the solution VTMS/ZrNBB/BPO; Zr:Si 1:4 on the left; different ratio on the right.	96
Figure 63 – Bulk sample obtained heating the xerogel up to 130°C for 1 h.	97
Figure 64 - FTIR spectra of reagents (ZrNBB and VTMS) and hybrid gel.	98
Figure 65 - Evolution with temperature of 29Si MAS spectra of ZrNBB/VTMS hybrid materials on the left - 13C spectra of VAA and VTMS in d8-THF and 13C MAS spectra of ZrNBB and ZrNBB/VTMS hybrid material treated at different temperatures on the right.	99
Figure 66 - Viscoelastic properties of sample ZrNBB/VTMS (Zr:Si 1:4) hybrid material vs. temperature.	100
Figure 67 - Storage modulus (Zr:Si 1:4) vs. temperature of the same samples, subjected to five consecutive DMS tests.	100

List of tables

Table 1 – Exposure class XA: chemical attack.....	2
Table 2 – Concrete mixture prepared with limestone aggregates.....	8
Table 3 – Physical characteristic of the aggregates	8
Table 4 – Slope of the straight line of the mass variation during the sulphate attack. The rate is in 10^{-6} %/hours.	12
Table 5 - Slope of the straight line of the mass variation during type cyclic acid/sulphate attack. The rates are in 10^{-6} %/hours.....	14
Table 6 - Slope of the straight line of the deformation during the sulphate attack. The rates are in 10^{-7} %/hour.	15
Table 7 - Slope of the straight line of the deformation during the cyclic acid/sulphate attacks. The value of the rates are in 10^{-7} %/hour.	17
Table 8 – Concrete compression resistance	17
Table 9 – Concrete mixtures made with siliceous aggregates.....	38
Table 10 – Composition of attack sulphate solution	39
Table 11 - Slope of the straight line of mass variation during the complex sulphate attack. The values of the rate are in 10^{-4} %/hour.....	43
Table 12 - Slope of the straight line of mass variation during the cyclic acid/(complex)sulphate attack. The values of the rate are in 10^{-4} %/hour.....	44
Table 13 – Slope of the straight line of the deformation during the complex sulphate attack. The values of the rate are in 10^{-7} %/hour.	46
Table 14 – Slope of the straight line of the deformation during the cyclic acid/(complex)sulphate attack. The values of the rate are in 10^{-7} %/hour.	47
Table 15 – TG results.....	57
Table 16 –XRD results - % in weight ($\pm 1\%$).....	57
Table 17 - Slope of the straight line of mass variation during the complex sulphate attack. The values of the rate are in 10^{-4} %/hour.....	59
Table 18 - Slope of the straight line of mass variation during the cyclic acid/(complex)sulphate attack. The values of the rate are in 10^{-4} %/hour.....	60
Table 19 - Slope of the straight line of the deformation during the complex sulphate attack. The values of the rate are in 10^{-5} %/hour.	61
Table 20 - Slope of the straight line of the deformation during cyclic acid/(complex)sulphate attack. The values of the rate are in 10^{-5} %/hour.....	62

Table 21 - Concrete mixture and for silica coating.....	80
Table 22 – Silica sol composition	81
Table 23 – Composition of attack sulphate solution	81

Abbreviations

CSH calcium silicate hydrate

CH portlandite

MSH magnesium silicate hydrate

SF silica fume

samples-L; all the mixtures prepared with limestone aggregate

PTL-L portland limestone cement with limestone aggregate

BLF-L blast furnace cement with limestone aggregate

PZ-L pozzolanic cement with limestone aggregate

samples-S; all the mixtures prepared with silicates aggregate

PTL-S portland limestone cement with silicates aggregate

BLF-S blast furnace cement with silicates aggregate

PZ-S pozzolanic cement with silicates aggregate

TEOS tetra ethyl ortho silicate

FAS fluorine alkyl silane

ESEM environmental scanning electron microscopy

EDAX energy dispersive x-ray analysis

Part 1

Studies of concrete degradation in aggressive environment

Chapter 1 - Introduction

A lots of money are spent every year on the restoration of the concrete on structures and manufactured elements deteriorated by different types of degradation. A research was made by Cresme for the Progetto Ulisse in the 2006, and the data show that the prize of the rehabilitation for degraded concrete structures (17.038 billions €) exceeds the prize for new structures (14.525 billions €) in the public administration.

Degradation of concretes is attributable to inadequate mix-design; anyway some environments are so aggressive that requiring additional care in order to increase durability[1] .

One of the most aggressive environments for concrete is acidic one, such as in the inner walls of sewer pipes. There are hundred kilometres of problematic sewer pipes; for example, in the Los Angeles County over 320 km of pipes are interested by this problem, and the prize of the rehabilitation will exceed \$1 billion [12].

Deterioration of sewer pipes, made in concrete, is a great problem when service life is lower than 30 or less years, and maintenance or even replacement of damaged concrete sewer pipes are requested.

The prescriptions to be adopted are described in the European Standard EN 206-1 (“Concrete part 1: Specification, performance, production and conformity”). The main characteristic of this norm consists in the classification of the environments where the concrete construction will be erected. These six environment categories, called exposure classes, are XO, XC, XS, XF and XA. All the classes are divided into sub-classes, depending on the grade of the attack. As regard as the case of a sewer pipe, the exposure class is the XA3. This exposure class concerns concrete structures exposed to chemical attacks by sulphate ions and aggressive chemical agents (such as CO_2 , H^+ , NH_4^+ , Mg^+).

In Table 1 the different parameters of the XA3 exposure class related to the aggressive water are reported: the composition of the aggressive environment and some prescription like the maximum w/c ratio, the minimum strength class and the minimum cement content.

Table 1 – Exposure class XA: chemical attack

Exposition class	Environment description WATER					Maximum w/c	Minimum strength class (N/mm ²)	Minimum Cement Content (Kg/m ³)
	SO ₄ ^{=**} (mg/l)	pH	CO ₂ (mg/l)	NH ₄ ⁺ (mg/l)	Mg ⁺⁺ (mg/l)			
XA1	≥ 200	≤ 6.5	≥ 15	≥ 15	≥ 300	0,55	37	300
	≤ 600	≥ 5.5	≤ 40	≤ 30	≤ 1000			
XA2	> 600	<5.5	> 40	> 30	> 1000	0,50	37	320
	≤ 3000	≥ 4.5	≤ 100	≤ 60	≤ 3000			
XA3	> 3000	<4.5	> 100	> 60	> 3000	0,45	45	360
	≤ 6000	≥ 4,0	≥ 100	≤ 100	≤ 3000			

The problem of the degradation interests all the modern society, not only in term of money, but also in term of discomfort and safety.

To achieve a 30+ design life, materials exhibiting long-term durability have to be selected. However an extensive characterization of the most common concrete used for this application lacks due to the complexity of the chemical attack during service life.

The processes leading to corrosion of the concrete sewer pipes are really complex. As previously described by some authors [1-15,22], hydrogen sulphide produced by anaerobic wastewater is released into the flowing wastewater. Then, it diffuses into the atmosphere and re-dissolves in the condensate on the portion of the pipe above the wastewater, where micro-organisms, such as *Thiobacillus thiooxidans*, growing on this surface, convert aerobically hydrogen sulphite to sulphuric acid, which reacts with the concrete [9]. In most cases the pH on the surface is very low (in the worst case the pH is 0.5) [19]. The scheme of this process is reported in Figure 1.

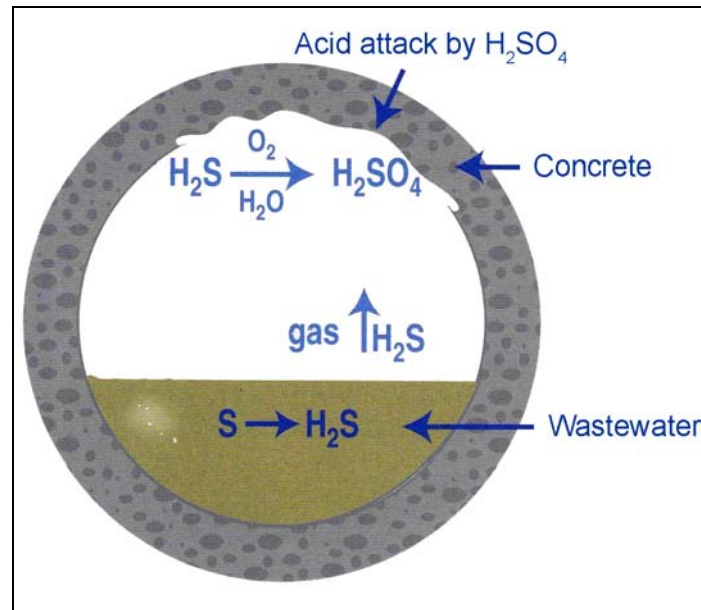
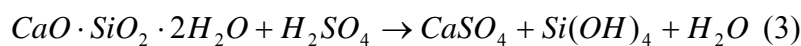


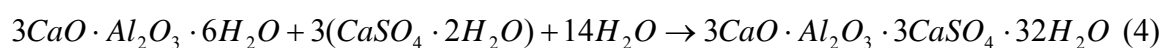
Figure 1 – Sewer pipe degradation scheme

The acid attacks first the calcium hydroxide and even tobermorite gel, when portlandite is not more available.

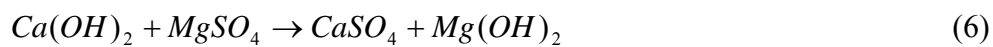
Accordingly, under attack, calcium hydroxide forms gypsum and the calcium silicate hydrate (C-S-H) forms both anhydrous gypsum and an incoherent mass hydrated silicate as reported in the following equations:



This layer is highly porous. The growth rate of the corroded layer is determined by the diffusion of the acid through the corroded layer to the reaction front and by the reaction rate of the acid with undamaged concrete. In a previous paper [1], it was reported that the rates of degradation of standard mortars are influenced by the presence and the thickness of the layer generated by the degradation products, e.g. calcium sulphate, which slow the diffusion of reactive species. In a second step calcium aluminates hydrate reacts with sodium sulphate ions from sulphuric acid to form ettringite:



However, different types of sulphate ions can be found in the wastewater. In the presence of a sodium sulphate source (>8000 ppm of SO_4^{2-}) [14], calcium hydroxide reacts to form secondary gypsum. Consequently, the latter can also participate in secondary ettringite formation. It is important to find out how to control these processes in order to increase the life of the facilities. The reaction equations in the cases of sodium, magnesium or ammonium sulphate are the following:



The literature results lacking in prediction of the concrete resistance, because the experiments neglected both the presence of aggregate and the real conditions in the sewage pipes. Actually, it has been observed that the rate of degradation is higher just above the waterline at the sides of the pipes, where the fluctuating water level continually wash away the sulphate deposits, reducing the degradation resistance. Moreover, anaerobic conditions for hydrogen sulphide formation occur mainly when the sewage flow is slow. Given that formation of hydrogen sulphide and sulphuric acid is the controlling factor, it is likely that pH is not continuously below 4, value for a fast concrete degradation, but shows a not well predictable wavy trend. It is worth noting that alternate wetting and drying of the concrete is even more detrimental than a continuous exposure to chemical attack. Thus the knowledge of the degradation rate is preliminary to the choice of a protection method or to design a suitable formulation of the mixes. Aim of this thesis is to develop procedures for evaluating the resistance of concrete mixes for sewage pipes. At this regard it seems that the concrete should be formulated for resisting cyclically to acid and sulphate attack. Indeed, the previous theories, which were developed so far upon testing standard mortars in acidic or sulphate solution, have

to be critically revised, taking into account that the real attack involves cyclically both acid and sulphates.

In this work new data, which were recorded on various concretes with different composition through a new chemical test, alternating acid and sulphate attack are described and discussed. The aim is to discriminate the effect and the behaviour of concrete compositions in an aggressive environment, as close as possible to the real attack condition, and in the meantime sufficiently fast. The concretes under investigation contain portland-limestone cement, blast furnace slag cement, sulphates resistance pozzolanic cement with or without silica fume, respectively, at constant water/cement ratio (w/c 0.39), and two type of aggregates, limestone and silicates.

This thesis is divided in two main parts: the first part regards the studies on concrete degradation in aggressive environment and the second one describes the development of protective system. After an introduction of the degradation problem in the chapter one, the chapter two describes the studies on degradation of different concretes prepared with various cements and limestone aggregate, using a cyclic acid/sulphate test with sulphuric acid and sodium sulphate. Chapter three shows the results regarding the degradation of different cements prepared with two type of aggregates, limestone and silicates, using a cyclic test with acid sulphuric and a complex (mixed) sulphate solution (containing sulphates).

The second part of the thesis describes the development of a pozzolanic coating and the results of the cyclic acid/complex sulphate test on a concrete with this protective coating. The last chapter shows preliminary results regarding the development of a new hybrid coating, which, contains also zirconium oxide, could have a protective effect without the drawbacks evidenced upon using pozzolanic addition or coating.

Chapter 2 –Degradation of concrete with limestone aggregates in sodium sulphate solution

2.1 Introduction

In order to understand the degradation on concrete sewer pipe, different sets of experiments were performed on concretes prepared with different cements. In this chapter the results on degradation of different concretes prepared with various cements and limestone aggregates are presented, using a cyclic acid/sulphate test with sulphuric acid and only sodium sulphate.

2.2 Materials

Five concrete pipes with limestone aggregate were prepared at the industrial plant Eurobeton S.p.a. situated in Salorno (BZ). The pipes have the following dimensions: diameter 30 cm and height 200 cm. The chemical composition and the concrete mixtures are described in details in Table 2 (for more clarity in the text, the labels of the concretes are acronyms, where the first three letters indicate the type of cement, and the last the type of aggregate). The physical properties of the aggregates are reported in Table 3. The aggregate is ground carbonate (dolomite) taken near Salorno (BZ). Two mixtures were prepared with both silica fume and an acrylic superplasticizer admixture.

To comparing the chemical resistance of different cements, a portland limestone cement (CEM II-A/LL 42.5 R PTL-L), a pozzolanic cement with a low content of “aluminates” (CEM IV-A 42.5 PZ-L) and a blast furnace cement (CEM III-A 42.5 BLF-L) were chosen.

Table 2 – Concrete mixture prepared with limestone aggregates.

Mixture n°	BLF-L + SF	PTL-L	PZ-L	BLF-L	PZ-L + SF
Elements	Measurement kg/m ³				
Aggregate	Limestone				
Fine	720	722	722	722	720
Fine 0/4	410	412	412	412	410
Coarse 3/8	620	621	621	621	620
Coarse 4/15	205	205	205	205	205
Cement type	CEM III-A	CEM II-A/LL	CEM IV-A	CEM III-A	CEM IV-A
Measuring	340	355	355	355	340
Silica Fume (Meyco, MS610)	30	--	--	--	30
Acrylic Superplasticizer (Glenium)	2.8	--	--	--	2.8
Water	133	140	140	140	133
w/c	0.39	0.39	0.39	0.39	0.39
Mass Volume Density (kg/dm ³)	2.490	2.501	2.502	2.532	2.516

N.B.: The measuring in Table 2 is theoretical. The data are referred to weighting industrial plant

Table 3 – Physical characteristic of the aggregates

Aggregate	Mass volume density [kg/m ³]	Mass volume density (SSD) [kg/m ³]	Water absorption [%]	Passing at 0.063 mm opening siege [%]
Fine 1	2785	2790	0.20	14.36
Fine 2	2803	2808	0.17	3.73
Coarse 3/8	2731	2756	0.90	0.53
Coarse 8/15	2698	2712	0.52	1.17

The pipes were removed from the mould after one day, then aged in open air. After 30 days, two series of cylindrical samples were cored from the pipes with two different sizes: a) diameter 69 mm, height 140 mm b) diameter 30mm, height 140 mm.

2.3 Chemical test

The chemical resistance was tested by the following types of attack:

- a) A cyclic immersion in sulphate solution with an attack in acid solution at pH=2 by sulphuric acid for 6 hours weekly (until 3000 hours of test) and monthly (after 3000 hours of test).
- b) Immersion in sulphate solution, replenished weekly (until 3000 hours of test) and monthly (after 3000 hours of test).

The sulphate solution was prepared with 50 g/l of sodium sulphate.

2.4 Testing program

Every week or month, the length and weight of each sample were measured. Before the weight measurement, samples were dried with a cloth and was used a technical balance with 0.001 g of sensitivity. The sample length was measured with a digital comparator with 0.001 mm of accuracy. The alkalinity level of the concrete samples was checked with the phenolphthalein method (EN 9944).

Morphological analyses were performed using an Environmental Scanning Electron Microscope (ESEM) (Philips XL30) and an Energy Dispersive X-ray (EDAX) detection system. Some samples were analyzed using XRD (40kV-22.5 mA). It was used an Imaging Plate diffractometer (Italstructure) in pure reflection geometry, with Cu-K α anode and Si multilayer monochromator on incident beam and a Ni filter on diffracted beam; the I.P. acquisition system was a Perkin-Elmer Pico Cyclon scanner. A full-profile Rietveld refinement was performed using MAUD software (Material Analysis Using Diffraction).

2.5 Results

2.5.1 pH solution

The pH values of the solutions were checked during every types of attack and in Figure 23 the trend is reported, during the 6 hours of acid attack (a) and during the 28 days of only sulphate attack (b).

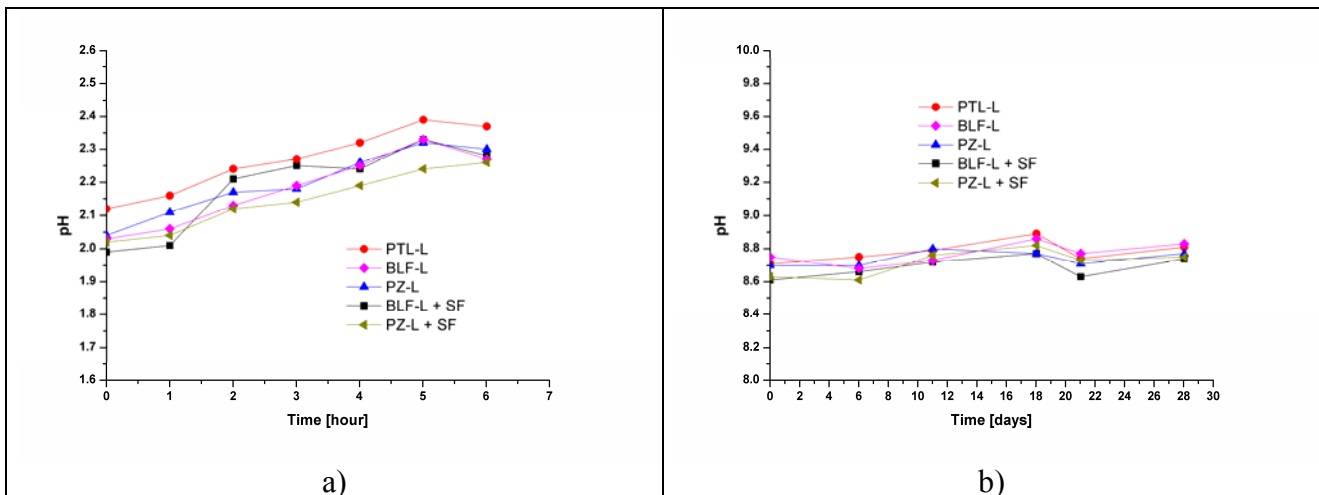


Figure 2 – pH values during acid attack (a) and during sulphate attack (b)

During the 6 hours of acid attack, the pH increases from 2 to 2.3 because degradation products release into the solution. In the case of the sulphate attack the pH values of every samples is stable in a range between 8.6 and 8.8 .

2.5.2 Mass variation

The concretes were prepared in accordance with EN 206 for the XA3 class with $w/c \leq 0.45$ and $R_{ck} \geq 45$ MPa. Figure 3 shows the mass variation vs. time during the sulphate attack in sodium sulphate (50 g/l Na_2SO_4). The trend is similar for all the mixtures and two behaviours appear: a sharp increment of the sample mass occurs in the first week due to absorption of the solution; then a small mass variation takes place, especially for the mixture prepared without silica fume, due to formation mainly calcium sulphate.

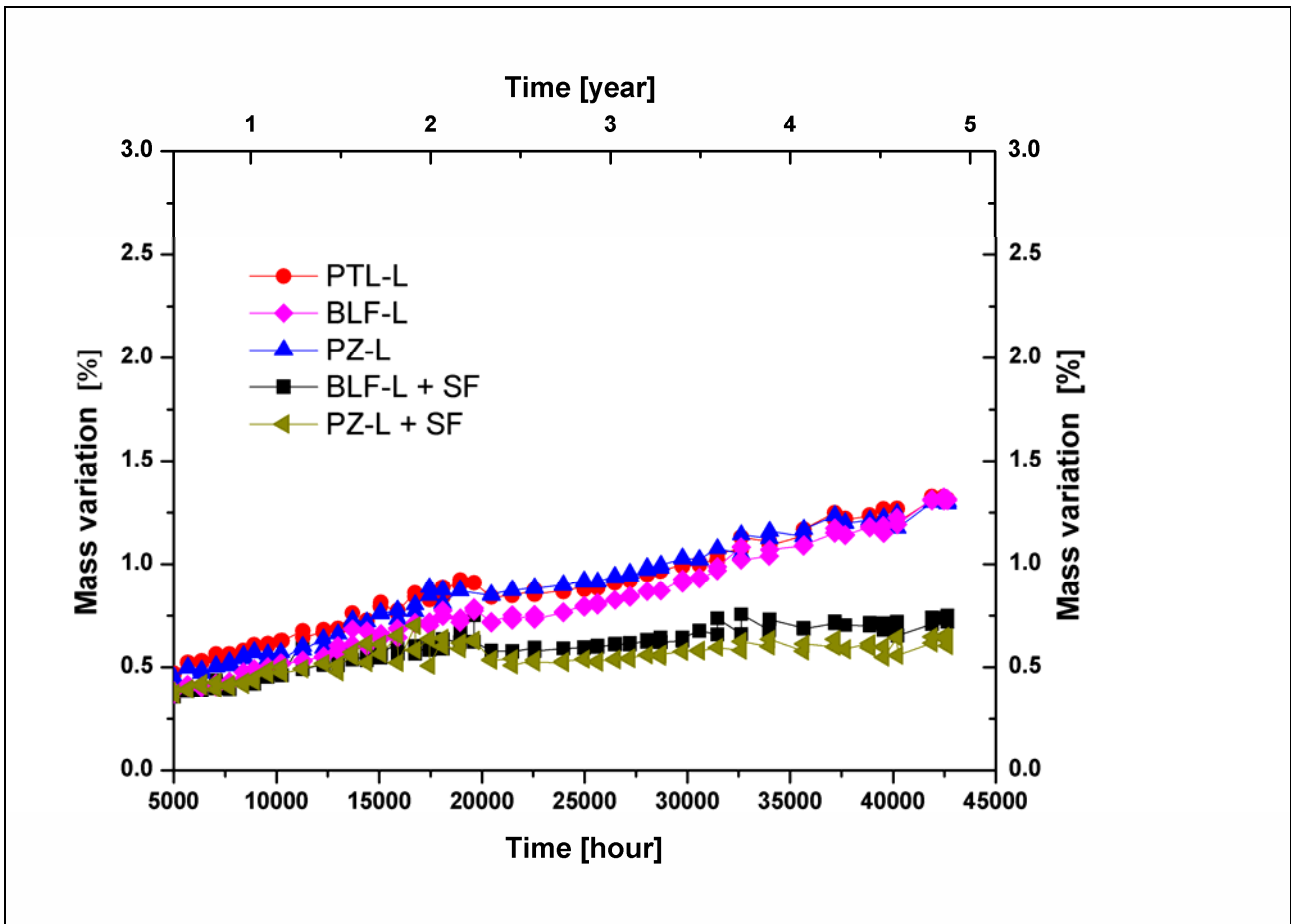


Figure 3 - Mass variation [%] during the sulphate attack.

The rate of the mass variation in two different periods during the 5 years of testing is reported in Table 4. The behaviour is similar for all the specimens but, in the range between 20000 and 45000 hours, the samples prepared without silica fume show a rate one order higher than the others prepared with silica fume. In general the specimens, in sodium sulphate solution, don't have evident degradation until 45000 hours of testing.

Table 4 – Slope of the straight line of the mass variation during the sulphate attack. The rate is in 10^{-6} %/hours.

Periods [hour]	5000-20000	20000-45000
PTL-L	24	30
BLF-L	25	30
PZ-L	21	21
BLF-L + SF	15	7
PZ-L + SF	3	8

Figure 4 shows the Δm (%) of specimens during the cyclic attack with sulphuric acid and sulphate solution.

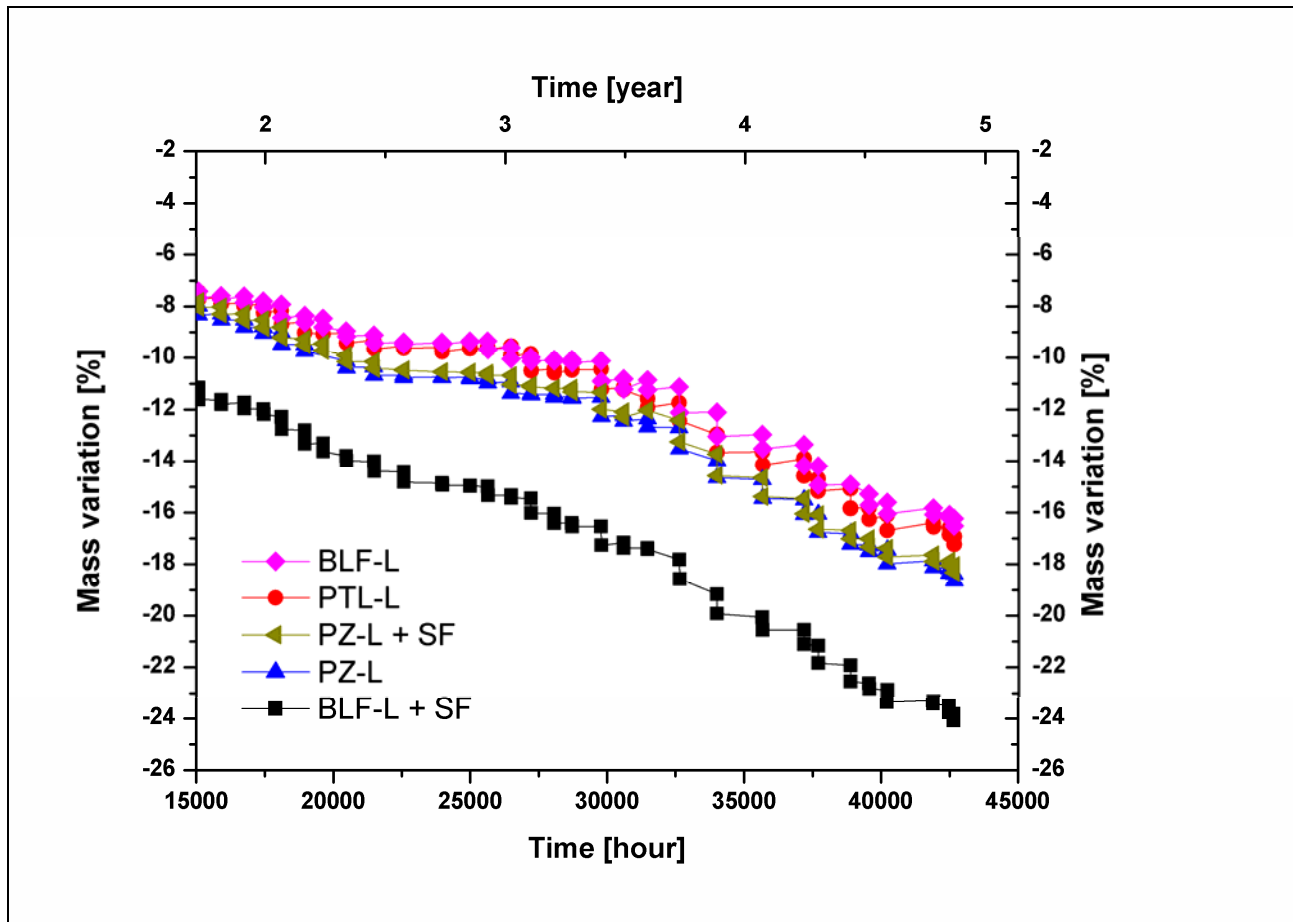


Figure 4 - Mass variation [%] during the cyclic acid/sulphate attack.

The sample mass is steady during the immersion in sulphate solution, but decreases during the acid attack. There are two regimes of mass variation: in the first the degradation rate is high when the acid attack occurs weekly; it is low in the second one, when the attack is monthly. The corrosion rates are calculated as the slope of the best linear interpolation of the experimental points, and are reported in Table 5.

Table 5 - Slope of the straight line of the mass variation during type cyclic acid/sulphate attack. The rates are in 10^{-6} %/hours.

Periods [hour]	2000-5000	5000-20000	20000-45000
BLF-L	-1160	-296	-433
PTL-L	-1320	-347	-464
PZ-L + SF	-1380	-366	-490
PZ-L	-1420	-387	-495
BLF-L + SF	-1450	-584	-536

The slopes are similar in the period between 2000 and 5000 hours, but in the others two, the BLF-L + SF has a high mass loss ($\Delta m = -24\%$ after about 5 years) [9]. The difference between the first and the second corrosion regimes depends on the frequency of the acid attack with sulphuric acid. The silica fume affects negatively the resistance to this attack. The sulphuric acid attacks both the cement phase and the carbonate aggregate. The portlandite and the C-S-H react with the sulphuric acid forming calcium sulphate and anhydrite, which are more soluble than portlandite. Also, aggregates are covered by incoherent calcium sulphate from the reaction with the acid. This is due to the high percentage of aggregate in concrete, which contributes more than cement paste to surface depletion.

2.5.3 Deformation

Figure 5 shows the deformation percentage of the samples subjected only to sulphate attack. The sample length is steady during the sulphate attack but, after 15000 hours, a remarkable expansion is recorded, especially for the mixtures prepared without silica fume. The slopes of the straight line of the expansion in three different periods are reported in Table 6

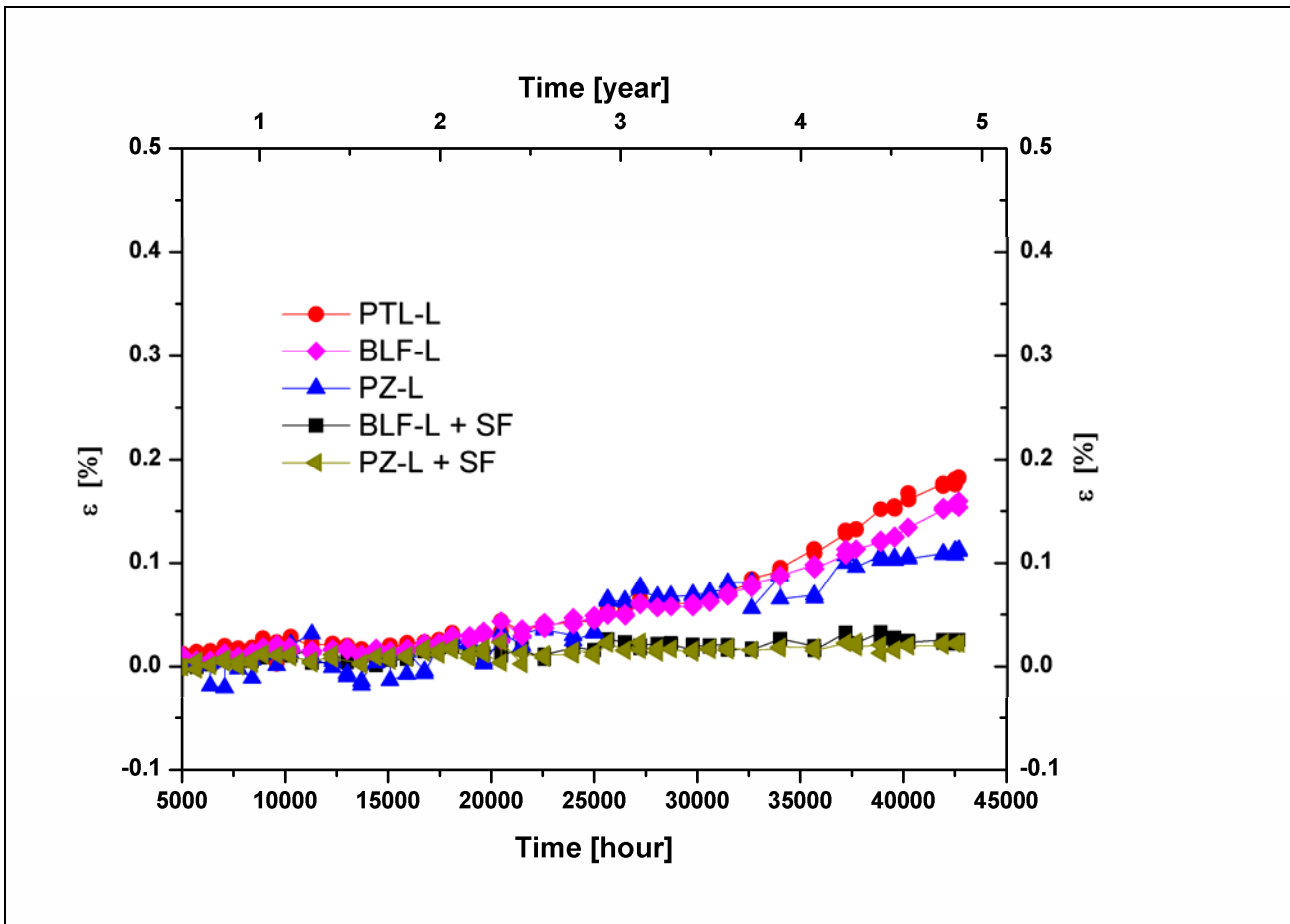


Figure 5 – Deformation [%] during the sulphate attack.

The concretes produced with SF don't show expansion, but PTL-L and BLF-L show a remarkable deformation after 15000 hours of attack. The mixture PZ-L, prepared only with pozzolanic cement, shows a little, but constant deformation, just only in the first periods.

Table 6 - Slope of the straight line of the deformation during the sulphate attack. The rates are in 10^{-7} %/hour.

Periods [hour]	5000-14000	14000-30000	30000-45000
PTL-L	13	31	99
BLF-L	12	31	76
PZ-L	5	51	37
BLF-L + SF	8	8	5
BLF-L + SF	7	4	4

The deformations of all specimens subjected to the cyclic acid and sulphate attack are reported in Figure 6. It is clear that, just after 13000 hours, PTL-L and BLF-L show a remarkable expansion.

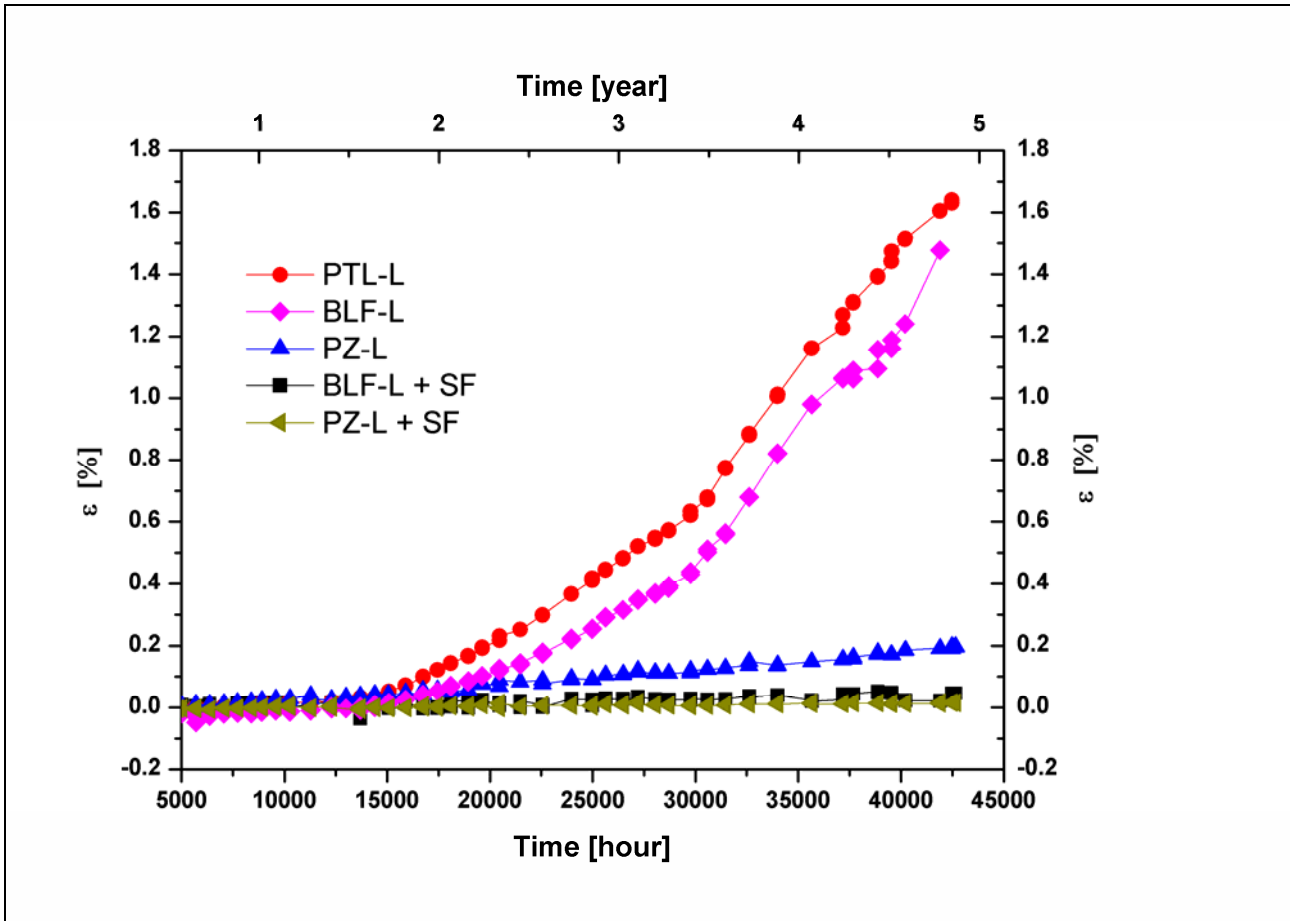


Figure 6 - Deformation [%] during the cyclic acid/sulphate attack.

The PZ-L shows a linear increase of expansion quicker than the same sample subjected only to sulphate attack. The specimens, prepared adding silica fume, don't show an increase of length and the rate of expansion is similar to the values recorded during the only sulphate attack.

Table 7 shows the rate of deformation during the cyclic acid/sulphate attack, which is calculated as the slope of the best linear interpolation of the experimental points. The PLT-L and the BLF-L show the highest deformation, compared with the two mixtures prepared adding silica fume and acrylic superplasticizer.

Table 7 - Slope of the straight line of the deformation during the cyclic acid/sulphate attacks. The value of the rates are in 10^{-7} %/hour.

Periods [hour]	5000-14000	14000-30000	30000-45000
PTL-L	38	396	780
BLF-L	28	294	810
PZ-L	45	53	62
BLF-L + SF	7	18	6
PZ-L + SF	15	4	3

The compression strengths of the cylindrical samples were measured and are reported in Table 8. The values of R_c meet the minimum requires strength class requested by the XA3 exposure class.

Table 8 – Concrete compression resistance

Cement	Additives (Typologies and quantity)	R_c (cubic sample) (MPa \pm 5)	R_c (cylindrical) (MPa \pm σ)
BLF-L + SF (30 kg/m³)	Superplasticizer (3 kg/m ³)	72	65.5 \pm 3.1
PTL-L	-	79	62.4 \pm 4.8
PZ-L	-	73	62.8 \pm 6.6
BLF-L	-	80	65.9 \pm 4.8
PZ-L + SF (30 kg/m³)	Superplasticizer (3 kg/m ³)	82	57.6 \pm 6.8

2.5.4 Characterization after 2000 hours of cyclic acid/sulphate attack

After 2000 hours of testing, a slice from each sample subjected to acid/sulphate attack, was cut and used for microstructural analysis. Using phenolphthalein test (EN 9944), the external cutting surface and the core were analyzed: there was an acceptable basic level (Figure 7).



Figure 7 – Phenolphthalein method results (EN 9944) on three mixtures (a) PTL-L, b) BLF-L and c) PZ-L+SF) after 2000 hour of acid/sulphate attack.

The core of all the specimens appeared basic during the phenolphthalein test. Moreover in the samples BLF-L and PZ-L + SF the basic response is high up to the border and even on the external surface. The BLF-L shows basic level on the cutting surface and on the external part after 2000 hours of testing. The basic reaction on the surface suggests a limited penetration of the sulphate and the acid solution into the materials, probably due to a low and not interconnected porosity of the samples. All this conclusions are confirmed by ESEM analysis of the cutting surfaces.

The micrographs of the same samples analysed with the phenolphthalein test are reported in Figure 8.

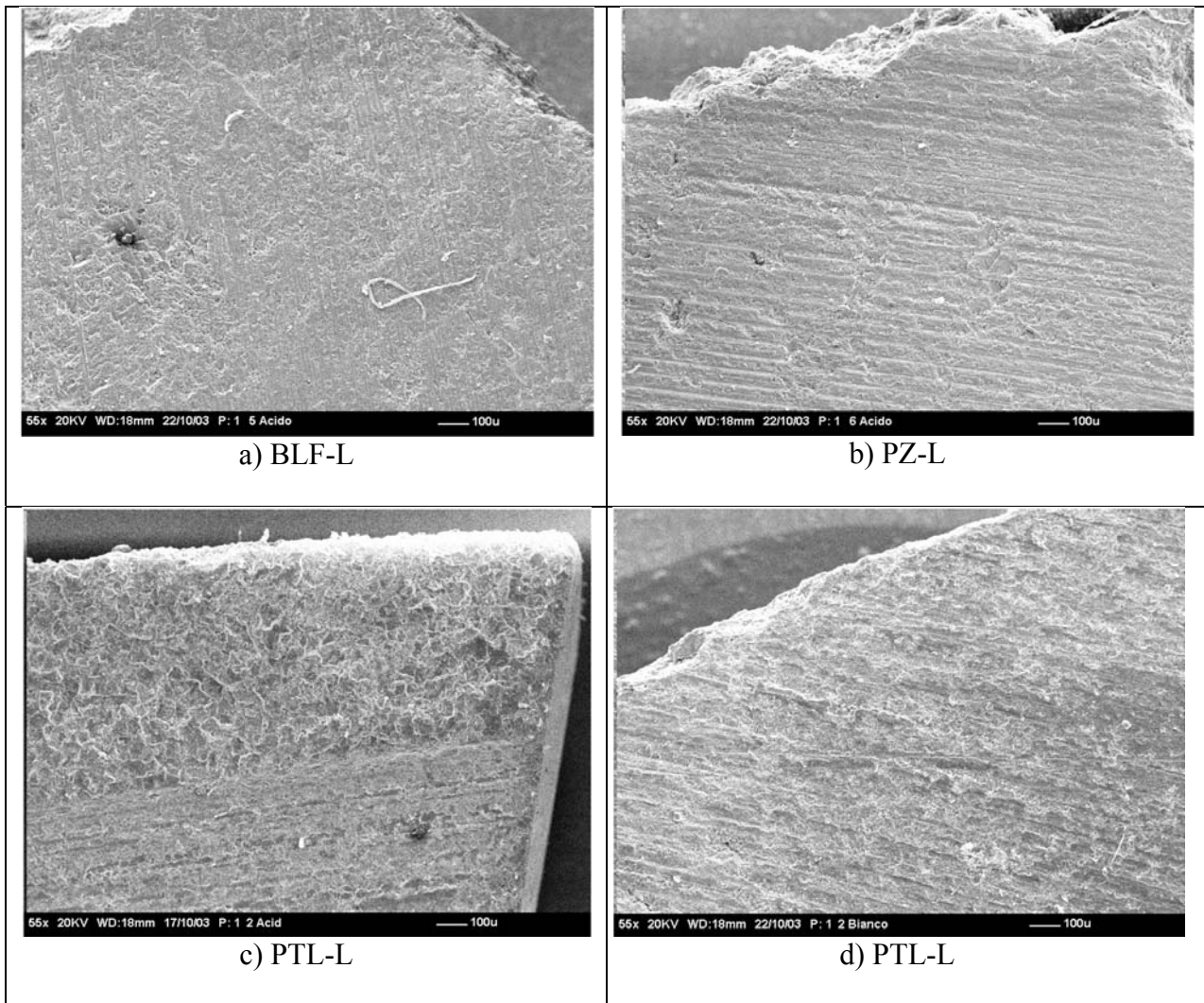


Figure 8 – Micrographs of the mixtures BLF-L, PZ-L + SF and PTL-L (a, b and c respectively) after 2000 hours of acid/sulphate attack and the PTL-L (d) after 2000 hours of only sulphate attack.

The cutting surface of the BLF-L (Figure 8 a) doesn't show any preferential path of the acid attack, which seems provide a general erosion of the surface. The acid erosion of the surface is consistent even in PZ-L + SF, which showed a rougher surface (Figure 8 b). On the PTL-L sample is visible a porous external layer of about 700 μm (Figure 8 c), consisting of a material without coherence. This suggests that the acid attack follows a preferential path. To make a comparison, Figure 8d shows PTL-L sample after immersion in only sodium sulphate solution, which lacks of the external incoherent part. Thus from ESEM observations, it can be deduced that the type of attack is depending on the type of cements.

The XRD analysis, after 2000 hours of testing, indicates only the presence of calcite and dolomite. This is attributable to the high fraction of fine aggregate, which peaks cover those of the hydrate compounds of cements or degradation products in XRD spectra.

2.5.5 Characterization after 45000 hours

A new series of microstructural analyses were performed in order to understand the degradation of all the concretes after about 45000 hours of test.

2.5.5.1 Phenolphthalein method (EN 9944)

Figure 9 shows the results of this analysis and an alkalinity level is recorded on all the samples. The samples d) and e) show a strong attack, whereas the best performance is showed by the PZ-L + SF (a) in both the type of attacks.

Sulphate attack		Cyclic acid/sulphate attack
 <p>Bianco 6</p>	<p>a) PZ-L + SF</p>	 <p>Sample 6</p>
 <p>Bianco 1</p>	<p>b) BLF-L + SF</p>	 <p>Sample 1</p>
 <p>Bianco 3</p>	<p>c) PZ-L</p>	 <p>Sample 3</p>
 <p>Bianco 5</p>	<p>d) BLF-L</p>	 <p>Sample 5</p>
 <p>Bianco 2</p>	<p>e) PTL-L</p>	 <p>Sample 2</p>

Figure 9 - Phenolphthalein method results (EN 9944) after 45000 hours of sulphate attack (on the left) and acid/sulphate attack (on the right).

2.5.5.2 Microstructural analysis

In order to analyse the thickness degradation, elements maps were recorded using the EDAX [18] instrument on all specimens subjected to the cyclic acid/sulphate attack. In Figure 10, the ESEM micrographs are shown of the left and on the right you can find the corresponding x-ray sulphur maps.

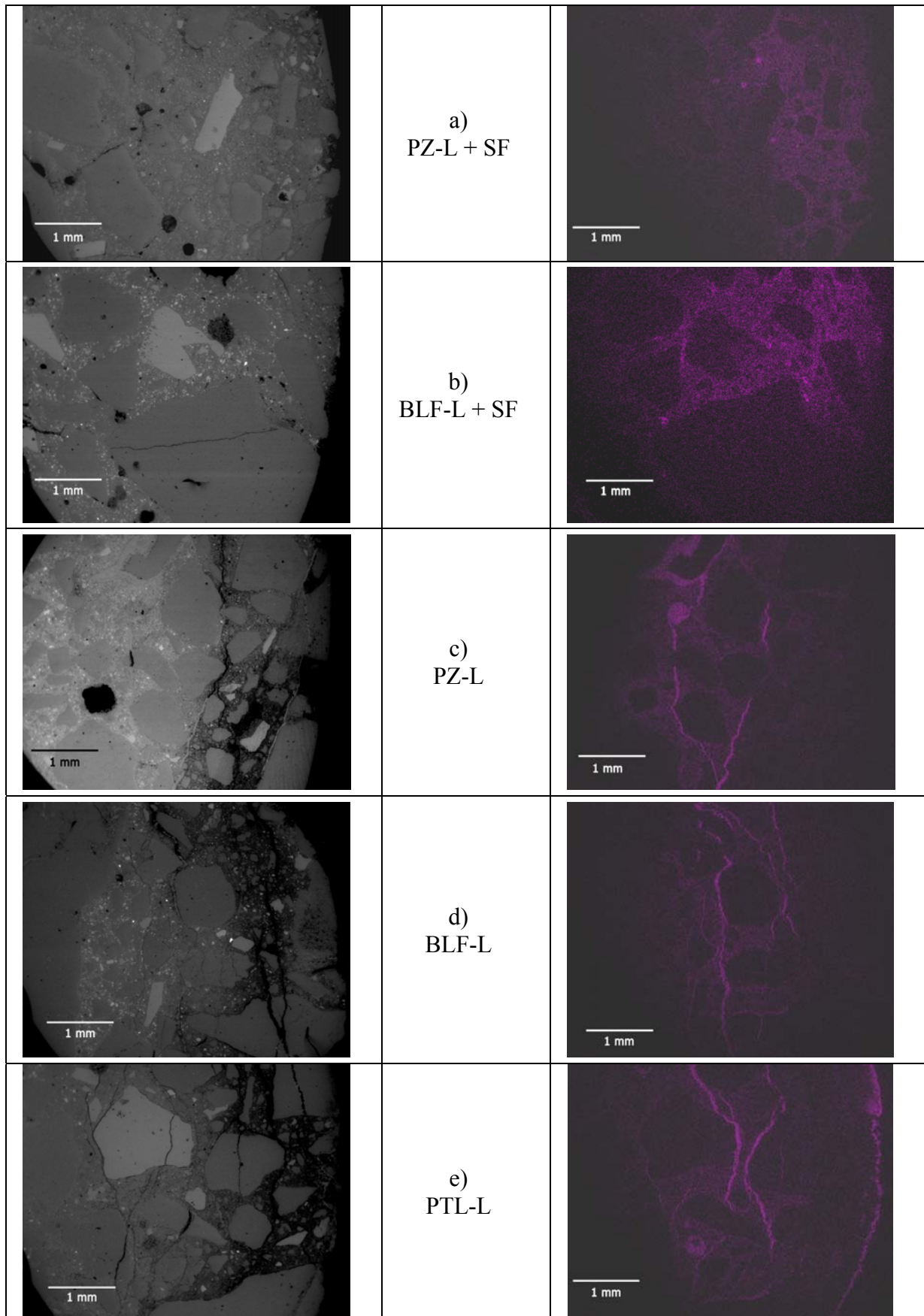


Figure 10 - ESEM images (on the left) and X-ray maps for sulphur (on the right) of polished surface subjected to cyclic acid/sulphate attack.

For the mixtures prepared adding silica fume (PZ-L + SF and BLF-L + SF, Figure 10a and Figure 10b respectively), the surface of the sample doesn't show cracks neither a preferential path of the acid attack, which seems instead to provide a general erosion of the surface. This is confirmed by the X-ray map for sulphur of the same sample; there is no evidence of cracks, the sulphur is present in the voids and entrained air bubbles.

In the cutting surface of the sample with pozzolanic cement (Figure 10c), which showed a greater expansion compared with the first two previous ones, a few cracks appears quite clearly in the cement paste. As it can be seen in the corresponding X-ray map for sulphur, the cracks are filled of columnar crystals.

The micrographs of the concretes with blast furnace and portland cement (Figure 10d and Figure 10e, respectively), which showed both the largest expansion values, show an extensive cracking, observed around aggregates and through the paste, with occasional cracking through aggregate particles. The most of cracks appear black, due to the loss of material during the cutting and polishing of samples. Many of the internal cracks were filled with columnar crystals. This is confirmed by the X-ray maps which suggest that the acid attacks through a preferential path and afterwards sulphate phases crystallize.

The concretes during cyclic acid/sulphate attack show a peculiar crack pattern, depending on the occurred mechanism. The PTL-L micrograph, after 45000 hours of cyclic acid/sulphate attack is reported in Figure 11a on the left, and shows a surface with three different zone: a zone with an high level of degradation (A), a zone of deposition of the attacks products (B) and an intact core (C). Details of the microstructure of the B zone are shown in Figure 11 b on the right.

In the internal part of the crack, there are crystals of the degradation products, which are grown perpendicular to the crack direction. EDAX analysis (reported in Figure 12) confirms the high content of sulphur in the columnar crystals embedded into cracks, in an atomic Ca/S ratio (36.69/35.84) compatible with that of calcium sulphate [33], rather than that of ettringite.

In Figure 13 the microstructures of the PTL-L of sulphate attack are reported. This specimen doesn't clearly show the three zones. Small cracks are present only in the external part of the section, where degradation products containing sulphur (as confirmed by the EDAX analysis) are visible (Figure 13 b).

In Figure 14a the microstructure of the BLF-L after 45000 hours of cyclic acid/sulphate attack (on the left) is reported: the surface is compromised to the presence of cracks due to the expansion of the degradation products (Figure 14b), similarly to the sample subjected only to the sulphate attack.

Figure 15 shows the micrographs of the BLF-L sample after 45000 hours of sulphate attack. The degradation is similar to that of the acid attack, but the crystals are thin with a needle form.

The concrete prepared with the PZ-L doesn't show a remarkable degradation but, only little cracks within expansion products in the cement matrix and in some aggregates, as reported in Figure 16a. The crystals in the crack are very large, in some cases over 40 microns (Figure 16b) and the EDAX analysis (reported in Figure 17) confirms the high content of sulphur in the columnar crystals embedded into cracks, in an atomic Ca/S ratio (32.72/32.29) compatible with that of calcium sulphate [33], rather than that of ettringite.

The micrographs related to the pozzolanic cement without silica fume during the sulphate attack, are reported in Figure 18a. The degradation is limited on the first 1 mm of depth from the external surface, with the presence of clear and thin crystals of gypsum (Figure 18b).

Figure 19 shows the microstructures of the sample produced with the BLF-L + SF during the cyclic acid/sulphate attack.

The combination of sulphate and acid attacks create only a few cracks in the external part of the section, differently from the sample subjected only to the sulphate attack, which doesn't show any sign of degradation (Figure 20). Only very thin and empty cracks are appeared on the section due to the cutting and polishing procedure.

The microstructure of the samples prepared with the PZ-L + SF (pozzolanic cement and silica fume) is reported in Figure 21, showing that no degradation is present under cyclic attack. The only cracks presence on the surface are empty, related to the cutting process.

In Figure 22 is reported the microstructure of the PZ-L + SF after 45000 hours of sulphate attack. This specimen doesn't present any signs of degradation.

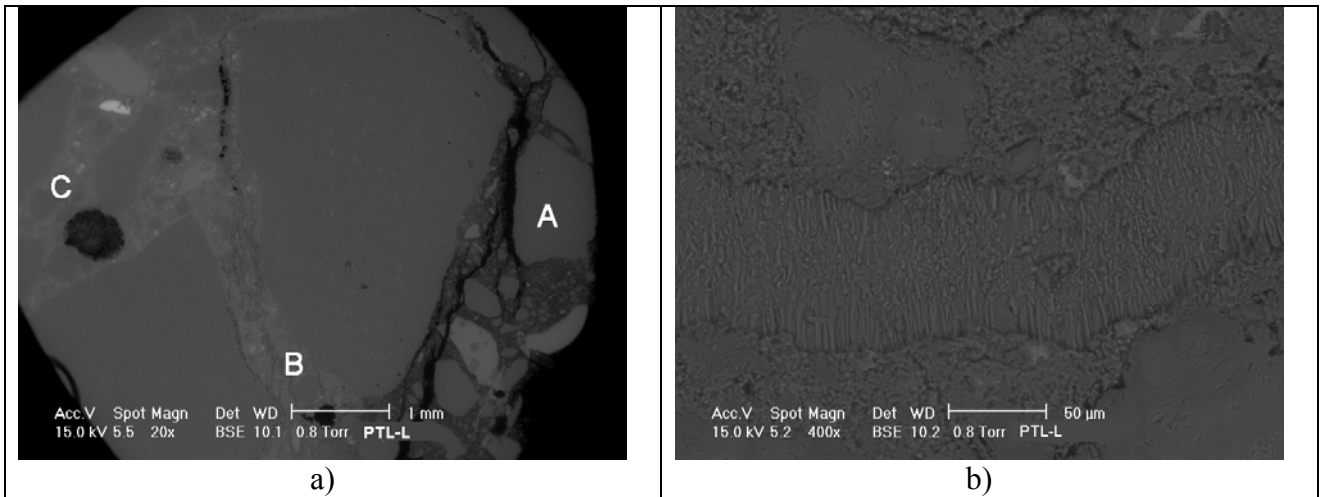


Figure 11 - Micrographs of the PTL-L after 45000 hours of cyclic acid/sulphate attack.

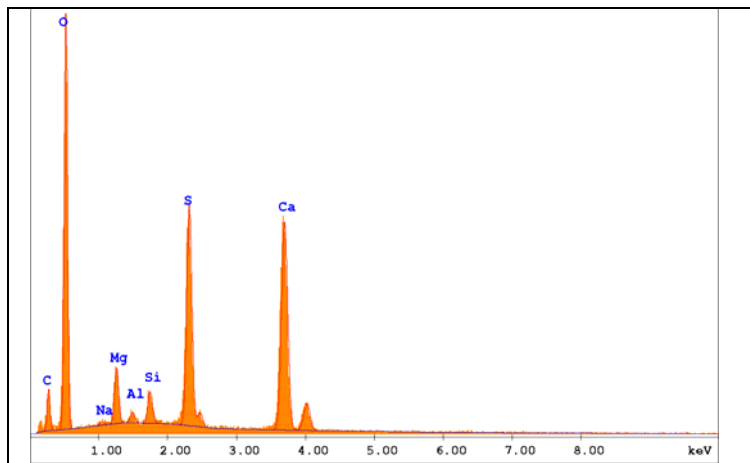


Figure 12 – EDAX results of the crystals in the crack reported in Figure 11b.

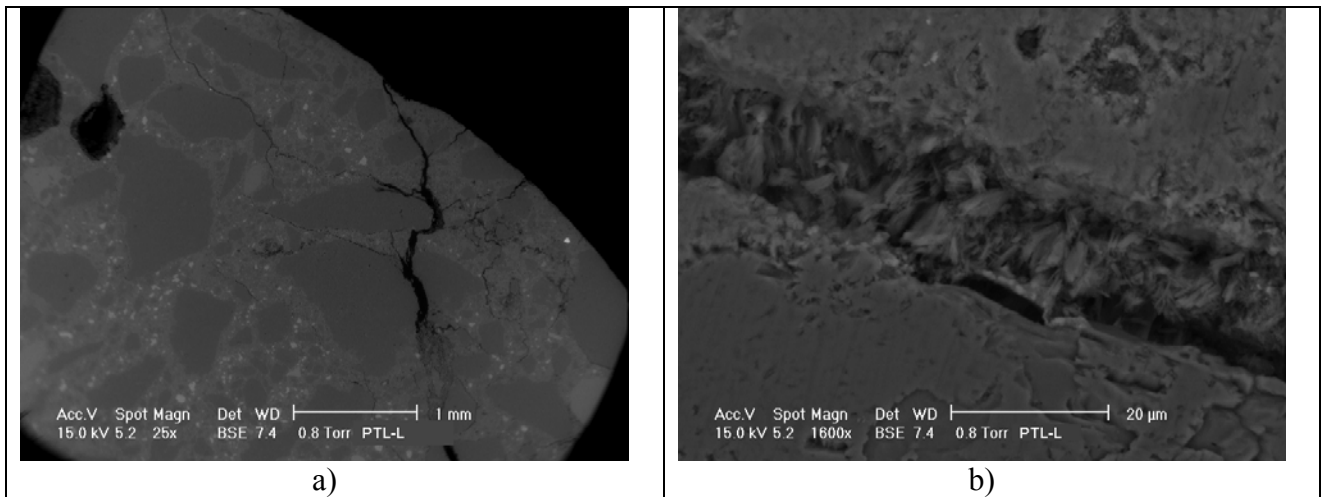


Figure 13 – Micrographs of the PTL-L after 45000 hours of sulphate attack.

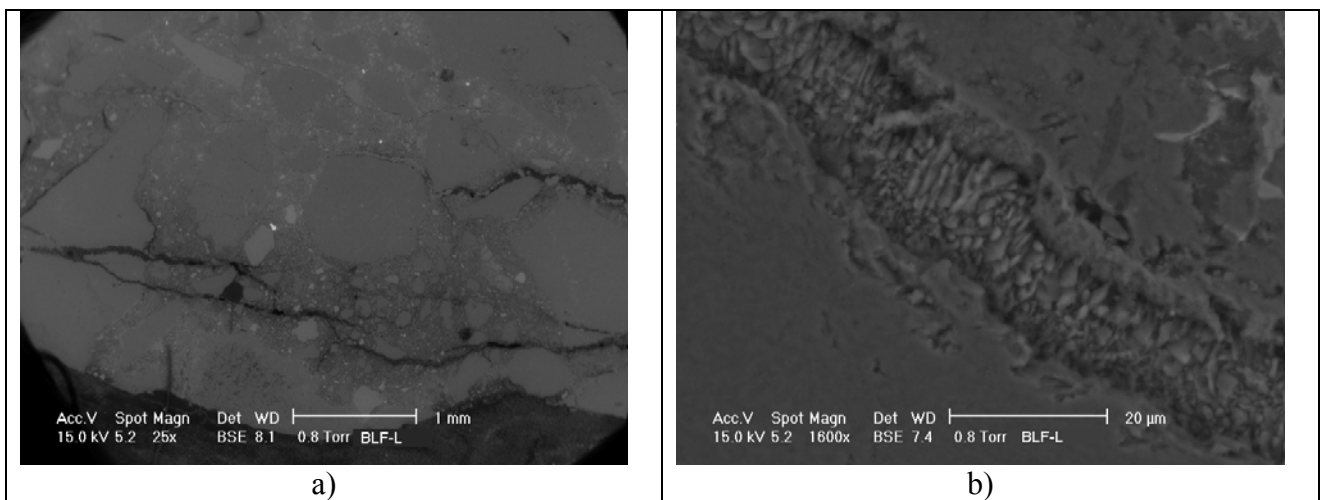


Figure 14 – Micrograph of the BLF-L after 45000 hours of cyclic acid/sulphate attack.

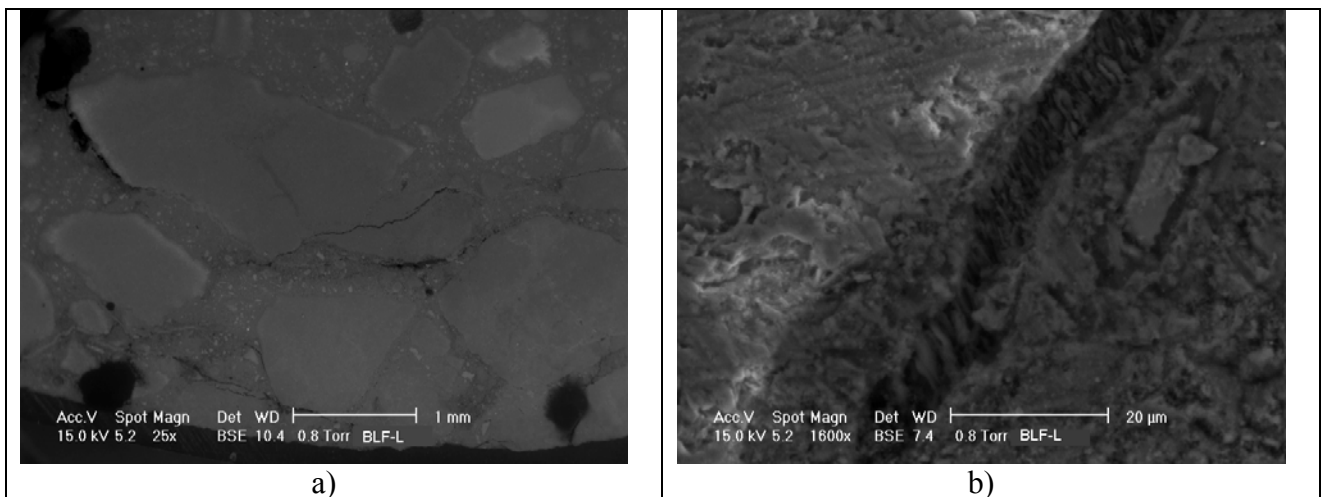


Figure 15 – Micrograph of the BLF-L after 45000 hours of sulphate attack.

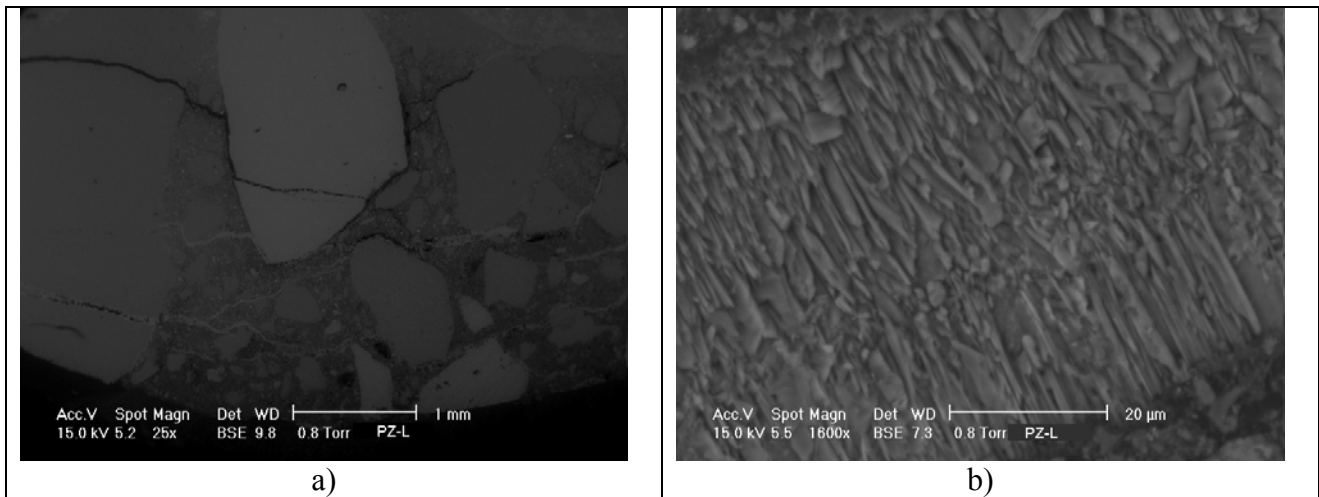


Figure 16 – Micrograph of the PZ-L after 45000 hours of cyclic acid/sulphate attack.

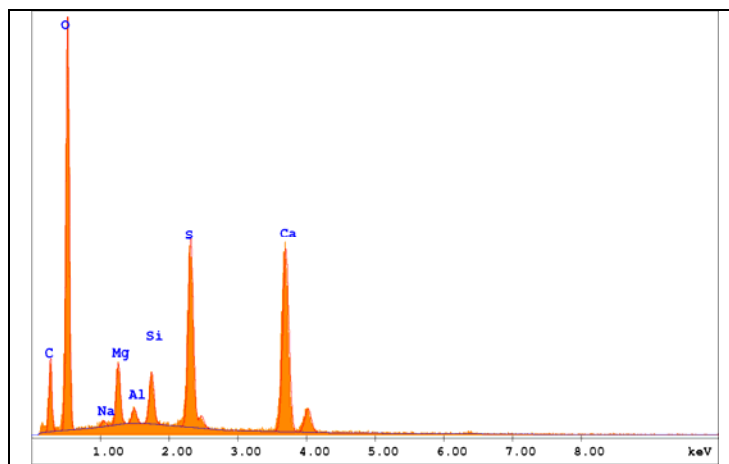


Figure 17 - EDAX results of the crystals in the crack reported in Figure 16b.

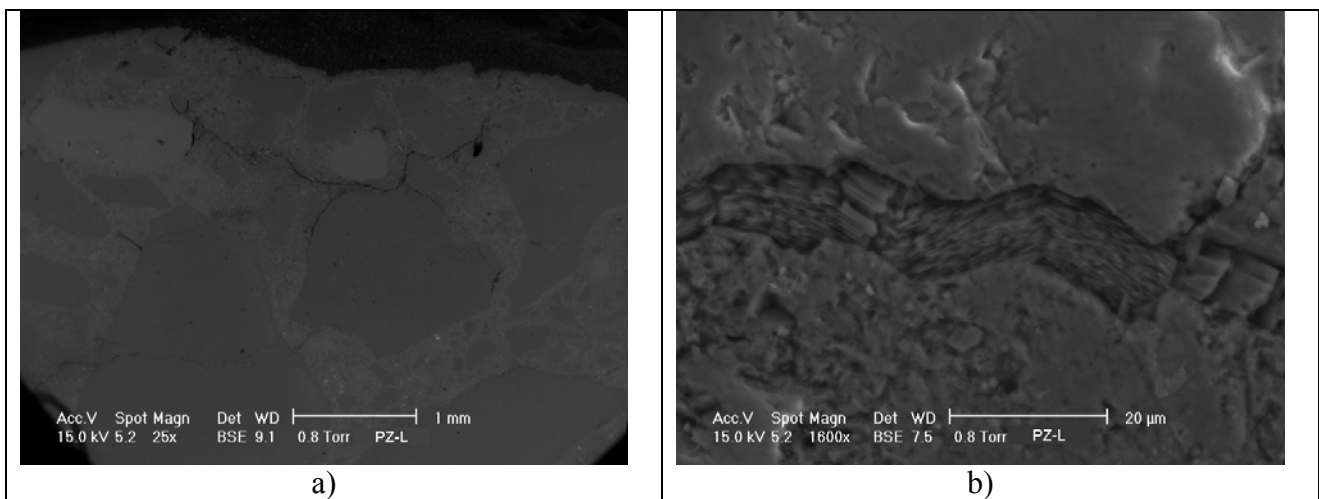


Figure 18- Micrograph of the PZ-L after 45000 hours of sulphate attack.

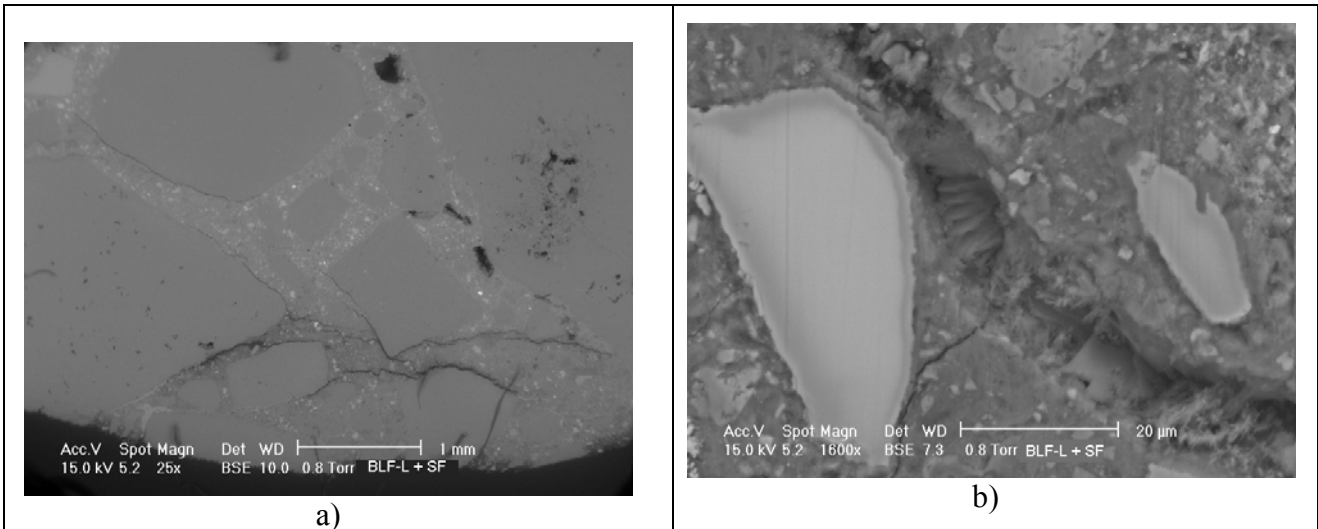


Figure 19 – Micrograph of the BLF-L + SF after 45000 hours of cyclic acid/sulphate attack.

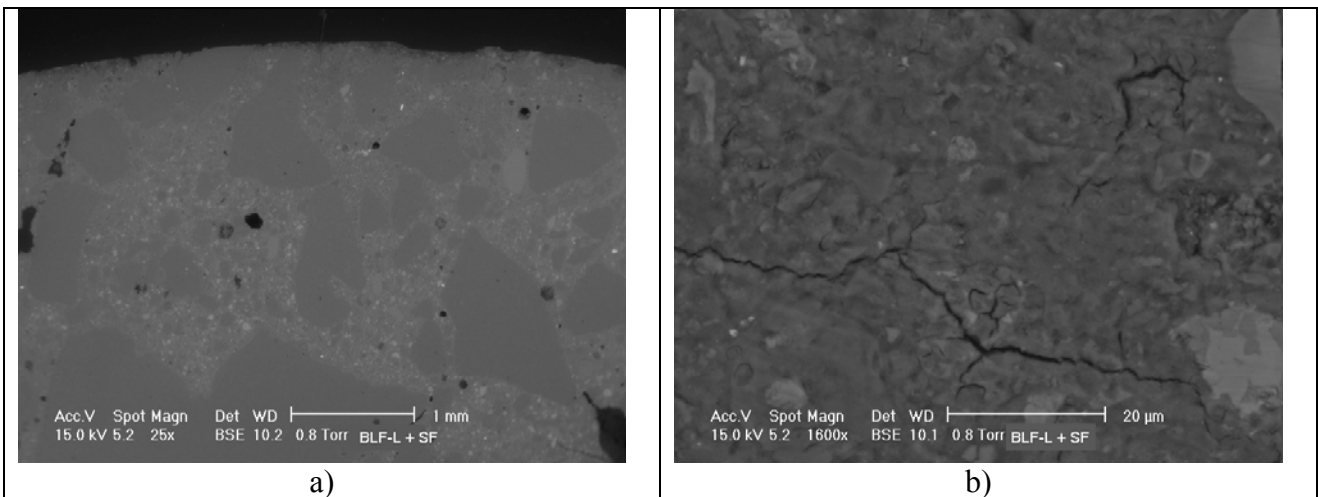


Figure 20 – Micrograph of the BLF-L + SF after 45000 hours of sulphate attack.

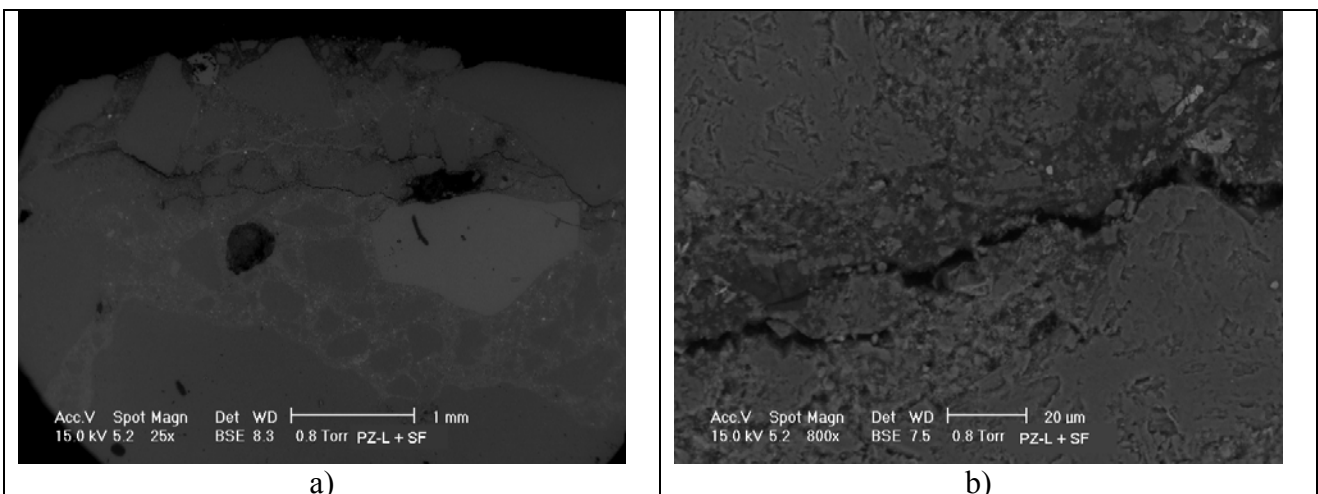


Figure 21 – Micrograph of the PZ-L + SF after 45000 hours of cyclic acid/sulphate attack.

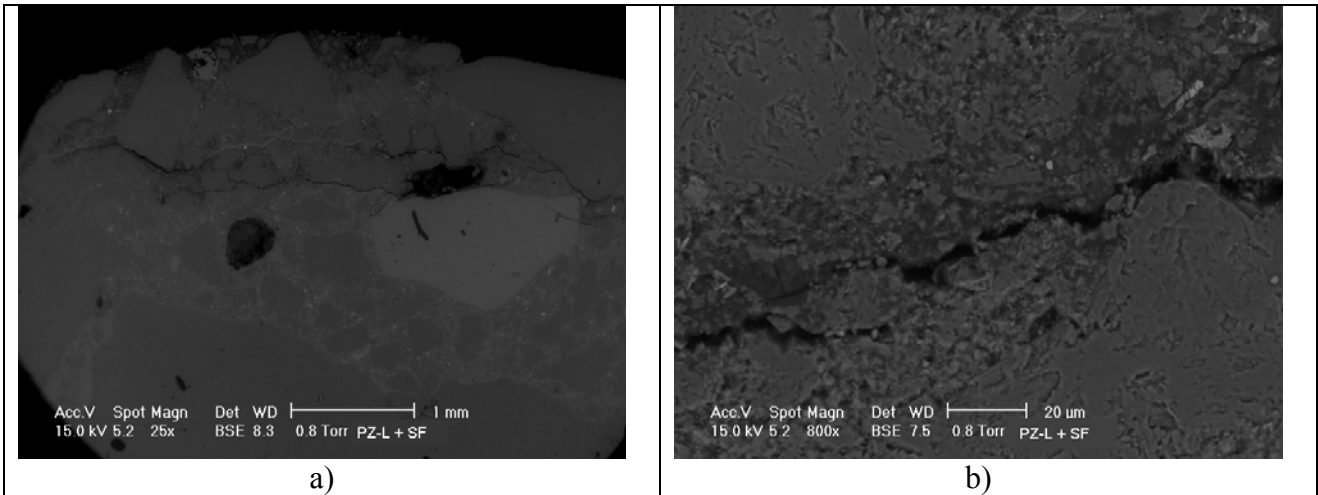


Figure 22 – Micrograph of the PZ-L + SF after 45000 hours of sulphate attack.

2.6 Discussion

Nowadays, there are no methods to evaluate the performance of hydraulic cements in both acid- and sulphate-rich environments. On the other hand, ASTM describes two test methods for assessing the performance in sulphate-rich environments (ASTM C452 and C012) and both of them have been subjected to criticism, because they seem to not adequately predict field performance [31]. Among the several critical aspects of the tests, it is worth noting they are performed on mortars and not on concretes, taking into account only expansion due to ettringite formation. The acid attack is generally ignored, though it could accelerate the degradation process.

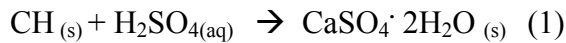
Accordingly, a reliable accelerated sulphate resistance test method represents a growing interest in production of concretes prepared with portland and non-portland cements. In this study, the sulphate resistance of concretes was assessed using an accelerated test based upon a method including a monthly acid attack. The evaluation of damage involves the measurements of both expansion and mass loss. The study involved the comparison with a test performed only in sodium sulphate, as it is required by ASTM C012 “Test Method for Length Changes of Hydraulic-Cement Mortars Exposed to a Sulphate Solution”.

In literature [9] [29] [30] it was found that the use of pozzolana or silica fume, which react with portlandite to produce C-S-H reducing meantime permeability, improves the resistance against the acid or sulphate attack, measured by mass variation, when they act apart. According to the data presented in this first part, the silica fume is helpful in preventing expansion, but not in reducing mass loss. The use of silica fume improves the resistance against sulphate attack and reduce the mass loss percentage when exposed to dilute acids during acid attack, but not to strong acids in high concentration. In this study an opposite behaviour with respect the concretes without SF, it must be a strong correlation between mass loss and expansion mechanisms, which reduce mass loss in concretes without SF.

The concrete degradation due to the exposure to a sulphate and acid ambient[20], can discuss on the base of two mechanisms: dissolution of components and expansive action of the

reaction products. The present study relates to both of them and evidences that silica fume is helpful in preventing expansion, but not in reducing mass loss during acid attack.

Dissolution is the loss of the portlandite and/or the calcite (present in the filler and in the calcareous aggregate) [22] as effect of the acid reaction (1)



The leaching of soluble NaOH decreases the pore solution alkalinity, resulting in loss of calcium silicate hydrate, the primary strength-giving component of the cement paste. The concrete permeability is a parameter for the degradation kinetics that depends on the diffusion of the aggressive and salt species. The geometry and the distribution of the porosity are more important than the only porosity value. When concrete is attacked by sulphuric acid, gypsum precipitates reducing the acid diffusion through the corroded layer, which in concretes without SF seems to promote more expansion than mass loss. Indeed, the quick formation of calcium sulphate limits acid could further react directly with calcite of aggregates or C-S-H, at least till portlandite is completely wasted. In the concretes with SF, there is not much portlandite available to reaction with acid, given that it has been already reacted with SF reducing meanwhile cement paste permeability. Accordingly, the acid attack is restricted to surface aggregate and C-S-H in more porous zone transition. Although the attack is presumably low, it is mainly focused on the calcium silicate hydrate, according the following reaction (2).



The decalcification of tobermorite bonding aggregates and cement paste causes the detachment of aggregate from the specimen surface. Indeed, the rate of mass loss of concretes with SF is not constant and increases with time. As a consequence, the specimen surface of the concretes with SF is generally consumed, even if the acid cannot penetrate the more internal and healthy regions.

Expansion may occur as a result of the formation of gypsum ($\text{CaSO}_4 \cdot 2\text{H}_2\text{O}$), the product of both the two reactions previously discussed for acid attack, and/or ettringite

(C₃A·3CaSO₄·32H₂O). [15][16] [21] [23] [28][32]. Also the following reaction (3) contributes to form and deposit gypsum.



The rate of degradation was found to depend on the concentration of aggressive substances. Indeed, if the concentration of SO₄²⁻ is high, gypsum will form, whereas if it is low ettringite will form. In this work, the accelerated test is performed with a high concentration of reagents (33800 ppm of SO₄²⁻) and a high specific area (the samples have a high area/volume ratio)[28]. Accordingly, calcium sulphate instead of ettringite is the main product and crystallizes into cracks. Furthermore, previous research results suggest that gypsum formation during sulphate attack is expansive [33]. However, ettringite could form afterwards, contributing to expansion. In this study the attention was focused on concretes and not mortars specimens, so that no X-ray powder diffraction analysis could be performed with the aim to individuate the phases of cement paste. Indeed, through EDXA it was found that the columnar crystals embedded into cracks show an atomic Ca/S ratio (36.69/35.84) compatible with that of calcium sulphate. Whatever the main reaction product, it nucleates during the induction period in the micro-cracks of cement paste or transition zone around aggregate, afterwards causing expansion due to the growth of the columnar crystal of the sulphate phase opening the cracks. In the concretes with SF, neither gypsum neither ettringite could be formed to a great extent in internal cement paste because of both the absence of free portlandite and restricted penetration of the attack. Accordingly, the induction period for nucleating crystals able to induce expansion is too long in the conditions chosen for this study. Indeed the expansion recorded for the concretes with SF is nearly the same in both the two tests: only sulphate or cyclic acid and sulphate attack.

2.7 Conclusions

The degradation of five concretes with different compositions were studied in a solution of sodium sulphate and for six hours per week/month in a solution of H_2SO_4 with $pH=2$. The damage extension was evaluated by measuring mass loss and expansion. The results of the test, performed for about five years, let the following conclusions be drawn.

The general trend is that the concretes with SF, which are less expansive, lose mass faster rate than those without SF, such as that prepared with PLT-L, which has the bad performance in terms of expansion. The concretes prepared with pozzolanic cement with SF have the best performance, taking into account both mass loss and expansion percentage. The concrete with blast furnace cement and SF showed a similar expansion, but a remarkable mass loss. The use of plain pozzolanic cement is not sufficient to minimize expansion in absence of SF. Finally the largest expansion and the most severe damage were recorded for BLF-L and PTL-L. In the last three cases, a two-stage process is evidenced in the expansion behaviour: the very low initial expansion is followed after about 10000 hours by a sudden increase of expansion rate, which continues nearly constant.

ESEM and EDAX analyses indicate that concretes with SF contain a few micro-cracks enclosing gypsum, whereas those without SF, especially PTL-L and BLF-L concretes, show a very damaged surface, a less deteriorated internal zone and the formation of cracks filled with gypsum around the aggregate particles and, where the damage was particularly severe, also in the cement paste and through the aggregate particles.

The behaviour of the concretes was also studied for comparison in sulphate solution. Of course, no mass loss was recorded and a continuous slow increase of weight was recorded as the effect of sulphate salt deposition. Although at the end of the test the classification of the deterioration of the five concretes is the same, the expansion percentage of the concretes without SF was remarkable lower than in the cyclic test. Indeed, the typical cracks filled with columnar crystals of gypsum can be observed in BLF-L and PTL-L concretes only at very high ESEM

magnification. Furthermore, the induction period is longer than that in cyclic test: the differences in expansion behaviour of the five concretes appeared almost 40000 hours in sulphate solution, whereas only 20000 hours in acid and sulphate solutions. At this regard the cyclic test set up in this study can be considered as an accelerated one.

It is a growing interest of concrete production to know the rate of deterioration, rather than its mechanism in order to predict life expectancy of concrete sewer pipes. Although, it cannot predict absolute life in quantitative terms, this test lets an evaluation of the behaviour and thickness reduction is obtained, surely quicker and more reliable than the present test based on simple sulphate attack. It was reported [14][21] that increasing temperature and concentration of attacking medium, the rate of deterioration is greater. At this regard an accelerated test could involve a weekly acid attack. On the other hand for sewage applications it could be of more interest to study the concrete behaviour at temperatures lower than room temperature, as adopted in this study. Moreover, the reliability of an accelerated test in this field could surely take advantage from using a complex solution including different salts. This will be the topic of next chapter.

Chapter 3 – Degradation of concr. with limestone/silicates aggregates in complex sulphate solution

3.1 Introduction

The first aim of this chapter is to understand the behaviour of the concrete when the sulphate attack is composed by different aggressive species, (not only sodium sulphate as in the case presented in the previous chapter). The role of this complex sulphate attack is to create an environment closer to the actual environment of a sewer. The second aim is to understand the behaviour of concrete prepared with the same cement but with two types of aggregates: limestone (samples-L) and silicates (samples-S).

3.2 Materials

Six concrete pipes were prepared at the industrial plant Eurobeton situated in Salerno (BZ), three with limestone aggregates and the others with siliceous aggregates. The pipes have the following dimensions: diameter 30 cm and height 200 cm. The chemical composition and the concrete mixtures are described in details in Table 9 (for more clarity in the text, the labels of the concretes are acronyms, where the first three letters indicate the type of cement, and the last the type of aggregate). The aggregates are ground limestone (dolomite) taken near Salerno and ground silicates taken near Piacenza, and both of them are regularly used in local plants for concrete preparation. Two mixtures were prepared with both silica fume and an acrylic superplasticizer admixture.

For comparing the chemical resistance of different cements, a portland limestone cement (CEM II-A/LL 42.5 R PTL-L), a pozzolanic cement with a low content of “aluminates” (CEM IV-A 42.5 PZ-L) and a blast furnace cement (CEM III-A 42.5 BLF-L) were chosen.

The pipes were removed from the mould after one day, then aged in open air. After 30 days, a series of cylindrical samples were extracted from the pipes with the following dimensions: diameter 30 mm and height 140 mm.

Table 9 – Concrete mixtures made with siliceous aggregates

Mixture	PTL-L	BLF-L	PZ-L + SF	Mixture	PTL-S	BLF-S	PZ-S + SF
Elements	Measuring kg/m³						
Aggregate	Limestone			Aggregate	Silicates		
Fine	722	722	720	Fine 0/2	460	460	460
Fine 0/4	412	412	410	Fine 0/5	460	460	460
Coarse 3/8	621	621	620	Coarse 3/6	400	400	400
Coarse 4/15	205	205	205	Coarse 9/14	680	680	680
Cement type	CEM II-A/LL	CEM III-A	CEM IV-A	Cement type	CEM II-A/LL	CEM III-A	CEM IV-A
Measuring	355	355	340	Measuring	400	400	400
Silica Fume (Meyco, MS610)	--	--	30	Silica Fume (Meyco, MS610)	-	-	30
Acrylic Superplasticizer (Glenium)	--	--	2.8	Acrylic Superplasticizer (Glenium)	--	--	2.8
Water	140	140	133	Water	155	155	155
w/c	0.39	0.39	0.39	w/c	0.39	0.39	0.39
Mass Volume Density (kg/dm³)	2.501	2.532	2.516	Mass Volume Density (kg/dm³)	2.303	2.309	2.349

N.B.: The measuring in the Table 9 is theoretical. The data are referred to weighting industrial plant

3.3 Chemical test

The chemical resistance was tested by the following types of attack:

- a) A cyclic immersion in a complex sulphate solution with an attack in acid solution at pH=2 by sulphuric acid for 6 hours weekly (until 3000 hours of test) and monthly (after 3000 hours test).
- b) Immersion in a complex sulphate solution, replenished weekly (until 3000 hours of test) and monthly (after 3000 hours of test).

For this experiment, a complex sulphate solution was used, and its composition is reported in Table 10.

Table 10 – Composition of attack sulphate solution

	g/l
Na₂SO₄	30
(NH₄)₂SO₄	15
MgSO₄	10
NaCl	10
KH₂PO₄	3
Glucose	1

For each composition of the samples-L, 3 specimens were immersed cyclically in the acid/sulphate solutions and 1 in the mixed sulphate attack. Two specimens for each composition of samples-S were studied with each type of attack.

In order to obtain reference data, a samples of each composition, was stored only in water, replenished every week or month, combined with the measures of the attacks a and b.

3.4 Testing program

Every week or month, the length and weight of each sample were measured. Before the weight measurement, the samples were dried with a cloth and was used a technical balance with 0.001 g of sensitivity. The sample length was measured with a digital comparator with 0.001 mm of accuracy. The alkalinity level was checked with the phenolphthalein method (EN 9944).

Morphological analyses were performed using an Environmental Scanning Electron Microscope (ESEM) (Philips XL30) and an Energy Dispersive X-ray (EDAX) detection system. The silicates aggregates were analyzed using XRD (40kV-22.5 mA). It was used an Imaging Plate diffractometer (Italstructure) in pure reflection geometry, with Cu-K α anode and Si multilayer monochromator on incident beam and a Ni filter on diffracted beam; the I.P. acquisition system

was a Perkin-Elmer Pico Cyclon scanner. A full-profile Rietveld refinement was performed using MAUD software (Material Analysis Using Diffraction). Thermal analyses were performed using a TG-DTA instrument (SETARAM) heating the samples from 25°C to 1000°C at the rate of 10°C/min, fluxing air.

3.5 Results

3.5.1 Analysis of samples-L

3.5.1.1 pH and permeability in water

The pH values of all the solutions were checked during every types of attack and in Figure 23 is reported the trend during the 6 hours of acid attack (a) and during the 28 days of mixed sulphate attack (b).

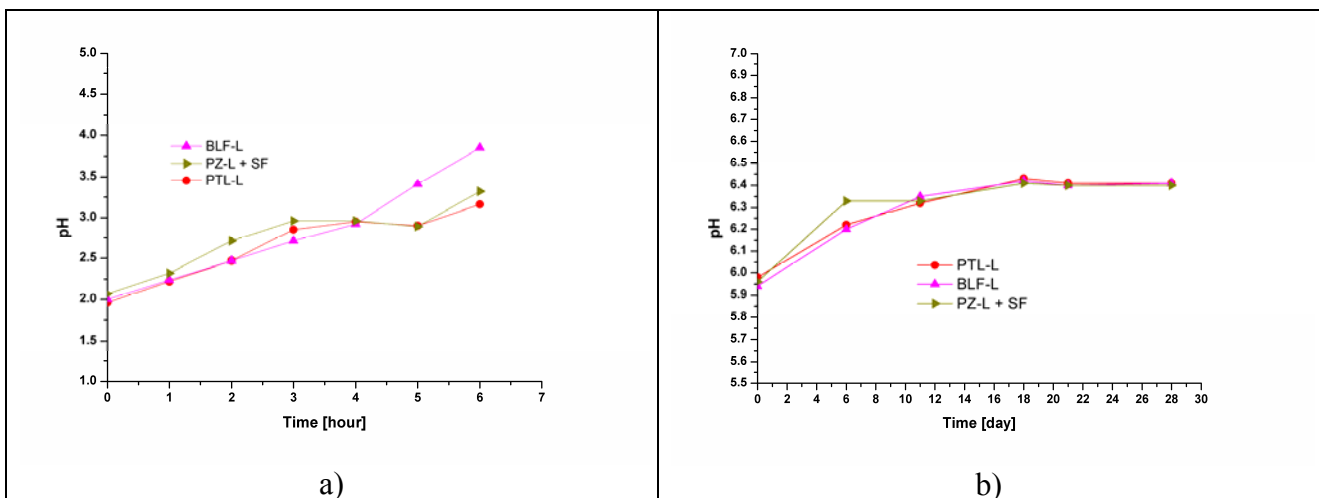


Figure 23 – pH values during acid attack (a) and during complex sulphate attack (b)

During the 6 hours of acid attack the pH increase from 2 to 3.5 because degradation products release into the solution. In the case of the sulphate attack during the first week, the pH increases from 5.8 to 6.1 and after one month the value is stable at 6.3.

The specimens stored in water show no signs of a degradation process occurs. No mass variation and no deformation appeared during the testing time, after the initial expansion and its change of mass is due only to the water absorption.

3.5.1.2 Mass variation

Three mixtures of concrete, prepared with three different types of cement and limestone aggregate, were analyzed using both a complex sulphate (the composition is reported in Table 10) and a cyclic test using acid sulphuric and a complex sulphate solution.

In Figure 24 the mass variation of the samples prepared with limestone aggregates during the sulphate attack is reported.

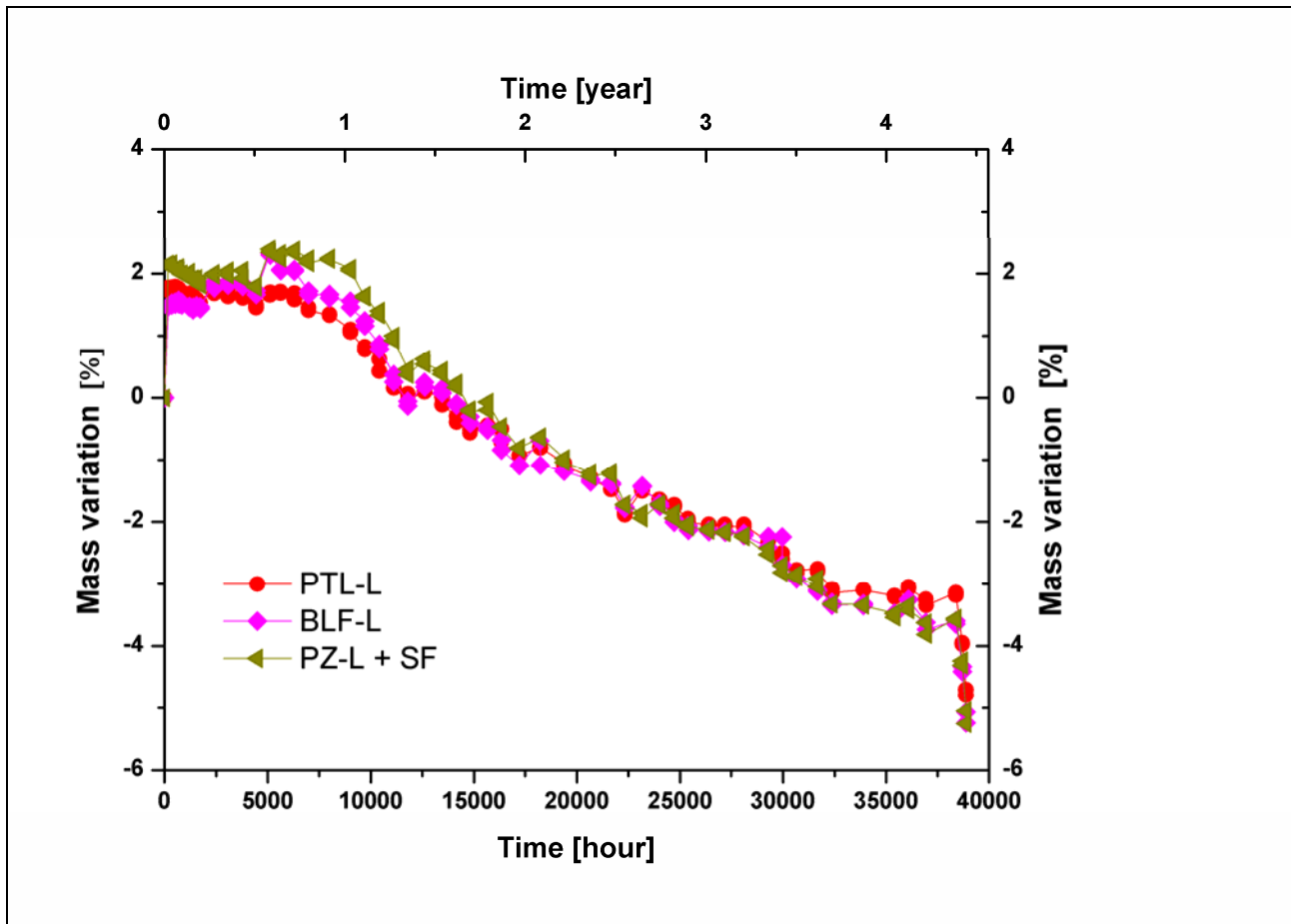


Figure 24 – Mass variation [%] during complex sulphate attack.

Different behaviours can be seen: the first, during the first week, consists of a large mass increase due to the absorption of the solution and the second consists of a loss of mass due to the effect of the sulphate attack. All the mixtures have a similar mass loss. After about 38000 hours, the sulphate attack produces only a change of mass between $\Delta m = -3.2\%$ and $\Delta m = -3.5\%$ for PTL-L and for sulphate resistance cements respectively. In order to check the mass variation, after 38000 hours, the frequency of the acid attack returns weekly, an increase of the mass loss was recorded.

In Table 11 the rates of the mass variation in the middle period (9000-33000 hours) and in the final period, when the frequency of the solution replenishment returns weekly, are reported.

Table 11 - Slope of the straight line of mass variation during the complex sulphate attack. The values of the rate are in 10^{-4} %/hour.

Periods [hours]	9000-33000	38000-39000
PTL-L	-1.52	-32.20
BLF-L	-1.68	-31.00
PZ-L + SF	-1.96	-32.50

The rate is the same for all the specimens, but in the final periods, in a range between 38000 and 39000 hours, the rates are one order higher than in the previous interval.

In Figure 25 the Δm of the samples during the cyclic acid/sulphate attack is reported. There are different behaviours: the first, for the first week, is a high incremental of the mass due to the absorption of the solution; the second, when the frequency of the attack is weekly, is a constant mass loss due to the effect of the acid attack; the third, is a quite mass loss, when the frequency of the attack is monthly, until 38000 hours.

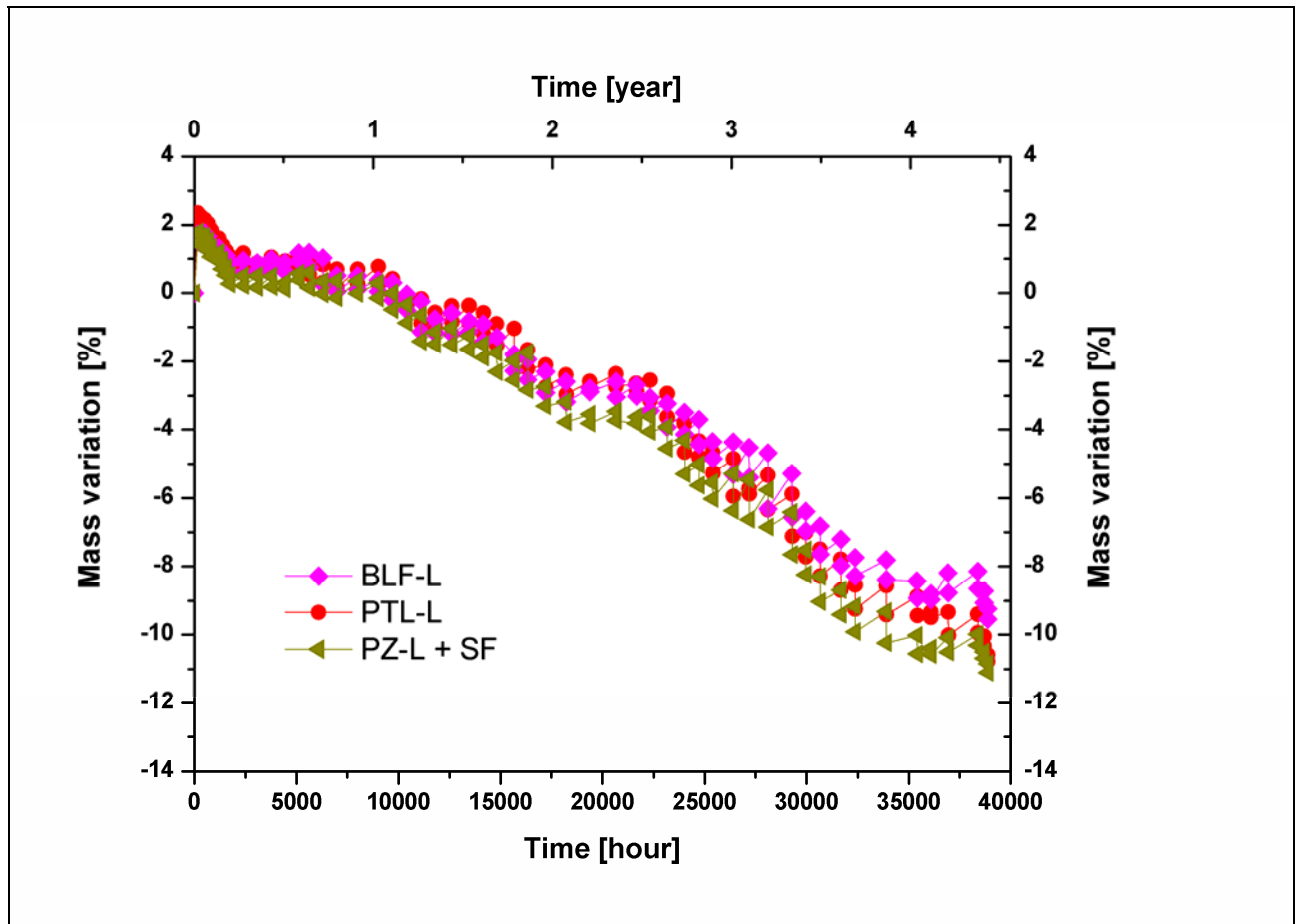


Figure 25 - Mass variation [%] (mean value of three samples for each typologies) during the cyclic acid/(complex)sulphate attack.

Although the trend of the curve of Δm vs. time is similar for every samples, after 38000 hours of testing, the BLF-L specimens prepared with blast furnace slag cement shows the lowest value of $\Delta m = -9.2\%$. The others two mixtures, PTL-L and PZ-L + SF, show Δm values of -10.7% and -11.3% , respectively.

Table 12 - Slope of the straight line of mass variation during the cyclic acid/(complex)sulphate attack. The values of the rate are in 10^{-4} %/hour.

Periods [hours]	200-2000	9000-35000	38000-39000
BLF-L	-5.25	-3.3	-16.9
PTL-L	-7.85	-3.7	-18.2
PZ-L + SF	-6.30	-4.1	-14.9

In Table 12 the values of the rate of mass loss are reported, after a linear regression of the experimental data in three different periods, corresponding to the different frequency of attack. After 38000 hours of accelerated test, when the frequency of the attack returns weekly, the rates of mass loss become one order higher than the velocities in the first periods (200-2000 hours) with the same type of attack.

3.5.1.3 Deformation

In Figure 26 the percentage deformation during the sulphate attack is reported. After the initial deformation due to the solution absorption, no expansion was recorded 20000 hours with no deformation for all the three mixtures.

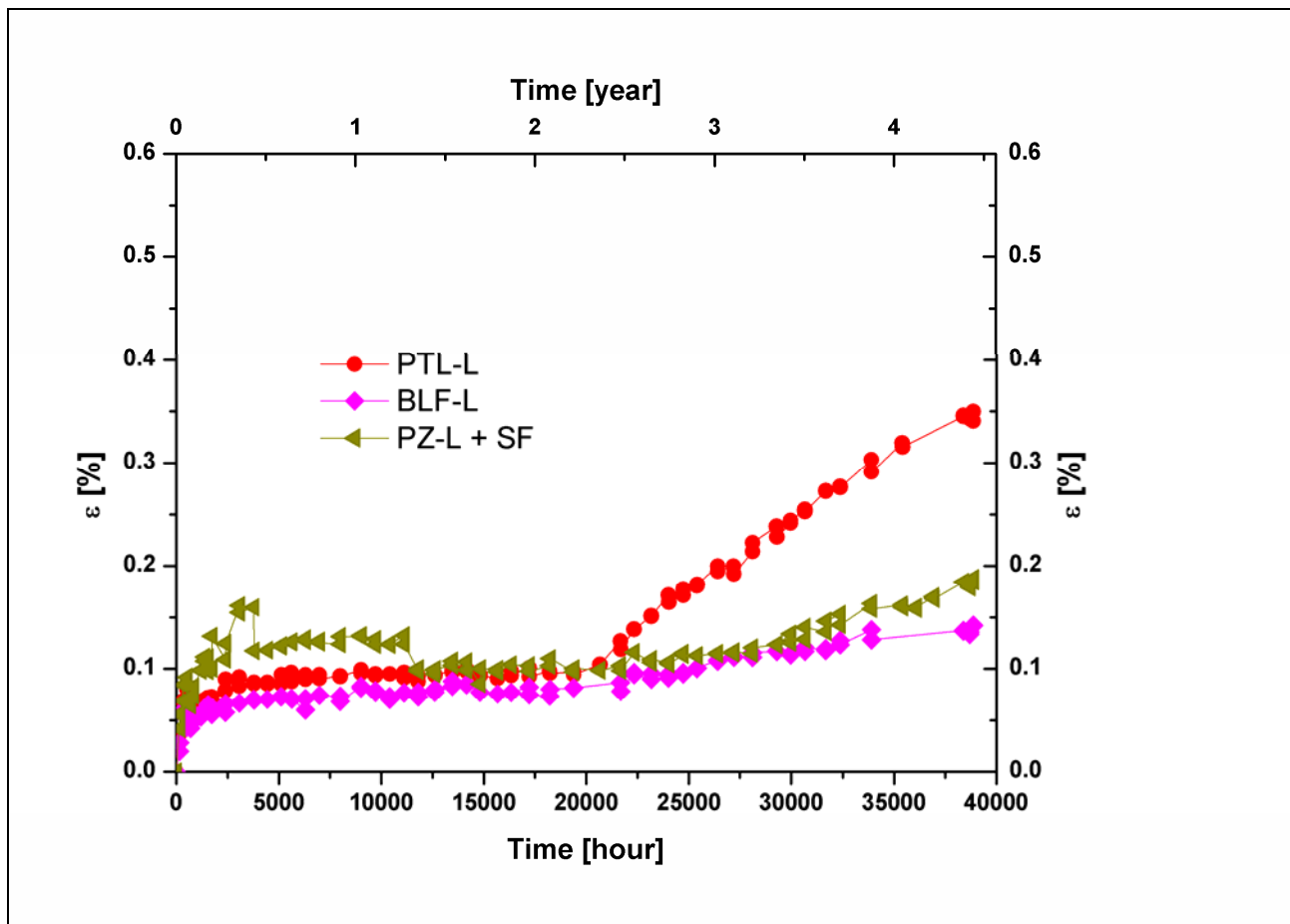


Figure 26 – Deformation [%] during the complex sulphate attack.

The PTL-L shows a deformation percentage higher than that of BLF-L and PZ-L + SF. In Table 13 the rates of expansion in two different periods are reported, before and after the start of the expansion phenomena of PTL-L.

Table 13 – Slope of the straight line of the deformation during the complex sulphate attack. The values of the rate are in 10^{-7} %/hour.

Periods [hours]	4000-20000	25000-40000
PTL-L	4.5	130
BLF-L	7.8	29
PZ-L + SF	2.5	47

In Figure 27 the expansion of the specimens subjected to the cyclic acid/sulphate attack is reported. Similarly to the sulphate attack, a deformation is recorded during the first weeks due to the solution absorption. Subsequently, no significant change of length occur until 20000 hours of analysis (induction period), unless PTL-L.

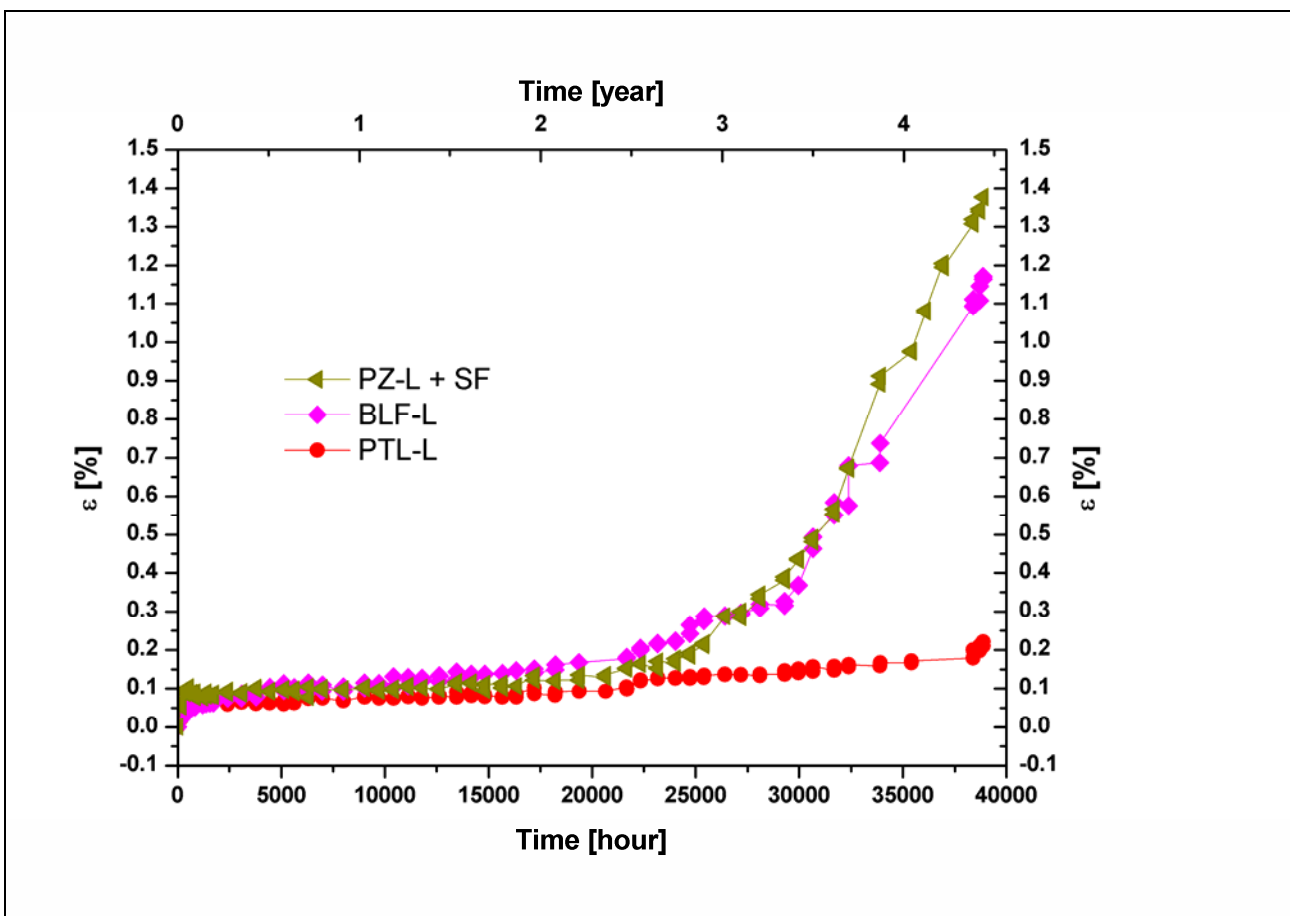


Figure 27 – Deformation [%] (mean value of three samples for each typologies) during cyclic acid/(complex) sulphate attack.

In this case, the PTL-L specimen shows an expansion of $\varepsilon = 0.2\%$ after 4.5 years of test. The other two mixtures, BLF-L and PZ-L +SF, show a final average deformation of $\varepsilon = 1.2\%$ and $\varepsilon = 1.35\%$, respectively.

In Table 14 the slope of the regression line that performs the best fit in two different interval are reported, before and after the start of the remarkable deformation for all the samples.

Table 14 – Slope of the straight line of the deformation during the cyclic acid/(complex)sulphate attack. The values of the rate are in 10^{-7} %/hour.

Periods [hours]	4000-20000	25000-40000
PZ-L + SF	18	900
BLF-L	42	890
PTL-L	16	52

During the first interval, the mixtures PTL and PZ-L + SF have similar rates. After 2.5 years the rates of the mixtures prepared with blast furnace slag and pozzolanic cement have an increase of deformation of two orders of magnitude.

3.5.1.4 Characterization after 40000 hours

A new series of microstructural analyses were performed in order to understand the degradation of all the concretes after about 40000 hours of test.

3.5.1.4.1 Phenolphthalein method (EN 9944)

Figure 28 shows the results of the phenolphthalein test. In the column on the left, there are the micrographs concerning the samples after the sulphate attack and on the right the micrographs regarding those subjected to the cyclic acid/sulphate attack. In the PTL-L (1a) alkalinity is acceptable after the sulphate attack, but in the other case an external layer of about 3 mm, doesn't show the pink colour. The same phenomena are obtained with the BLF-L (see 2a and 2b in the figure) and with the PZ-L + SF (3a and 3b in the figure). In this last case, only an area of the cutting section with about 10 mm of diameter has an acceptable response.

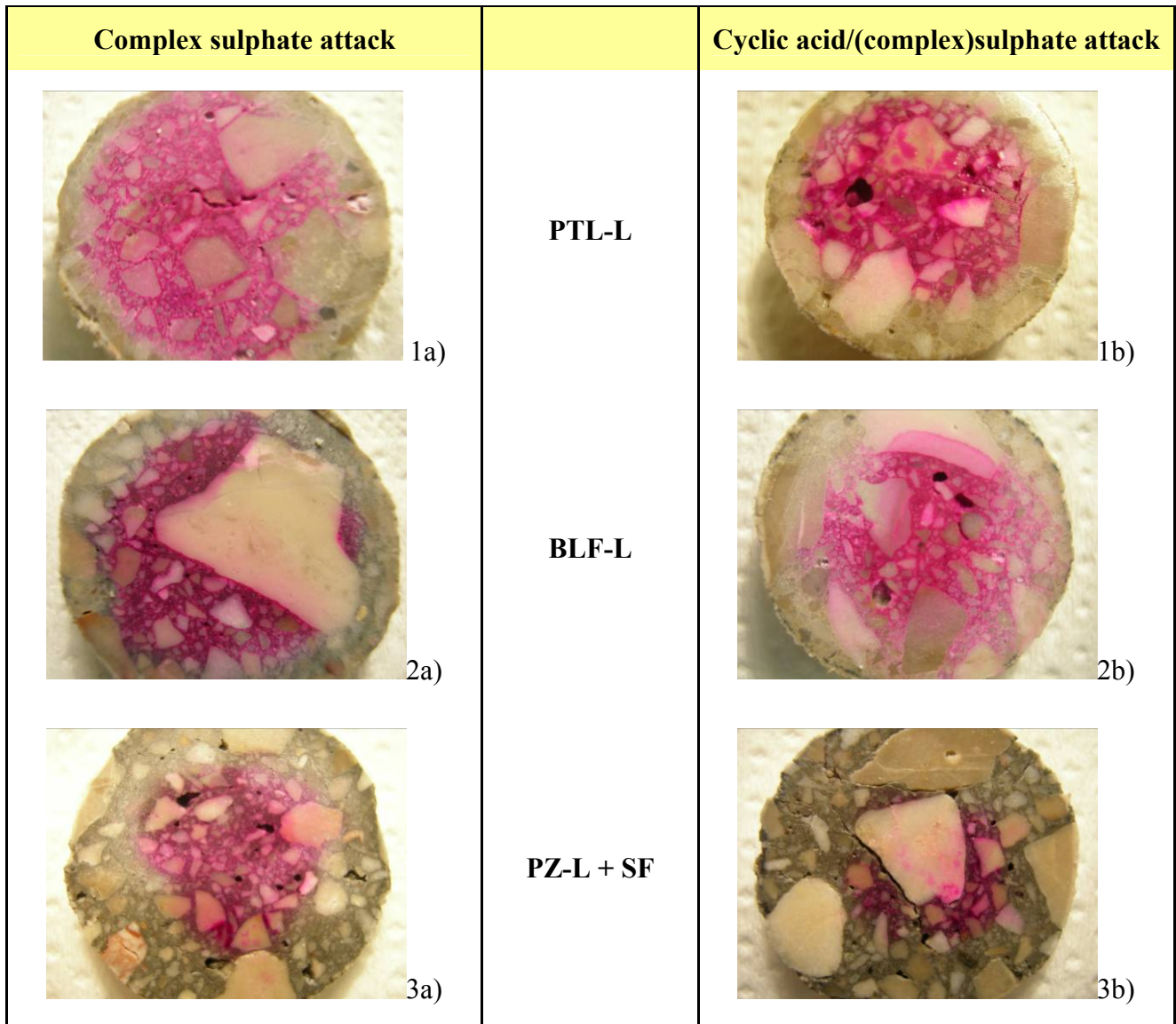


Figure 28 - Phenolphthalein methods results (EN 9944)

The micrographs of the samples stored only in water show no signs of degradation and carbonation and alkaline reaction is visible on the whole cutting section.

3.5.1.4.2 Microstructural analysis

In order to analyse the thickness degradation of an elements maps are recorded using the EDAX instrument on all specimens subjected to the cyclic acid/sulphate attack. In Figure 29, the ESEM micrographs are shown on the left and on the right you can find the corresponding x-ray sulphur maps.

The surface of the sample PTL-L (Figure 29a), doesn't show cracks neither a preferential path of the acid attack, which seems instead to provide a general erosion of the surface. This is

confirmed by the X-ray map for sulphur of the same sample. There is no evidence of cracks, the sulphur is present in the voids and entrained air bubbles.

In the cutting surface of the sample with blast furnace cement BLF-L (Figure 29b), which showed a greater expansion compared with the previous one, a few cracks appear quite clearly in the cement paste. As it can be seen in the corresponding X-ray map, the sulphur is present everywhere and some little the cracks are filled of columnar crystals.

The micrograph of the concretes with pozzolanic cement adding silica fume PZ-L + SF (Figure 29c), shows an extensive cracking, observed around aggregates and through the paste, with an occasional cracking through aggregate particles. The most of the cracks appears black, due to the loss of material during the cutting and polishing of samples.

Many of the internal cracks were filled with columnar crystals. The X-ray maps indicate sulphur in the cracks, so that after that the acid attack favours the microcracks formation afterwards sulphate phases crystallize.

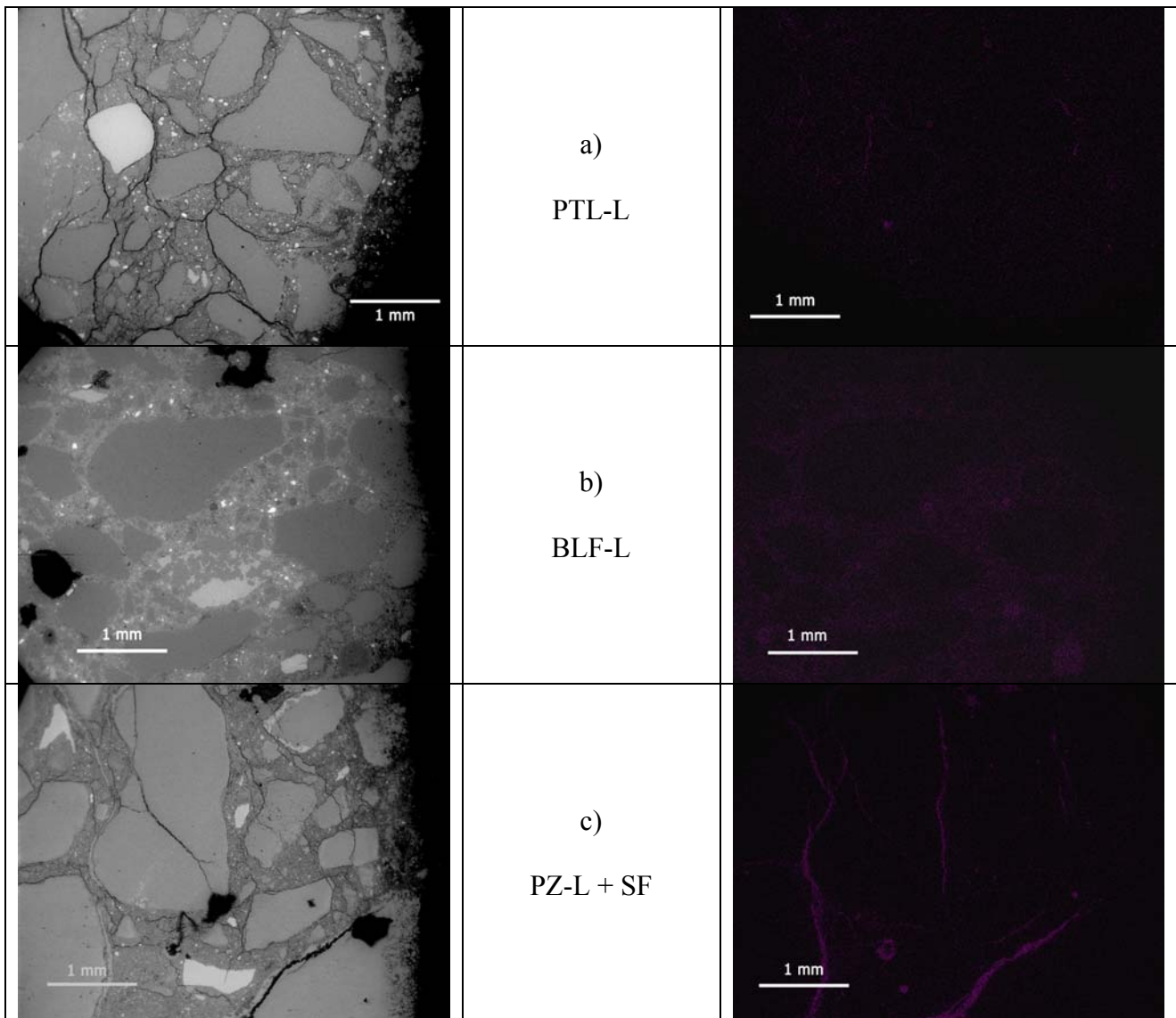


Figure 29 ESEM images (on the left) and X-ray maps for sulphur (on the right) of polished surface subjected to cyclic acid and complex sulphate attack.

Polished samples were prepared cutting a slice with 5 mm of thickness from every cylindrical specimen, and analyzed by Environmental Scanning Electron Microscope (ESEM).

In Figure 30a the micrographs of the mixture prepared with limestone portland cement after 40000 hours of cyclic acid/sulphate attack are reported. They exhibit a peculiar crack pattern, which occurs as a direct result of the degradation mechanism. The microstructure shows a disintegrated surface zone (A), followed by a zone of deposition of the attack products (B). The interior of the concrete doesn't show degradation (C). Extensive cracking is observed around aggregates and

through the cement paste. The Figure 30b shows a crack between cement paste and aggregates are filled by degradation products.

In Figure 31, the micrographs of the PTL-L after 40000 hours of sulphate attack are reported. The degradation is limited to the external part of the samples as reported in the picture on the left. The gypsum is found in some crack between the cement paste and aggregate in a needle form (Figure 31b) with a width of few microns.

In Figure 32a the micrograph of the BLF-L samples after 40000 hours of cyclic acid/sulphate attack is reported. The depth of the attack and the number of cracks, are higher than in the case of the mixture prepared with portland cement type CEM II-A/LL as reported in Figure 30a.

Large crystals of degradation products are present in all the cracks, especially in those formed between the aggregates and the cement paste. In some cases the aggregate is completely surrounded by degradation products (Figure 32b).

In Figure 33a the micrographs of the BLF-L after 40000 hours of sulphate attack are reported. The degradation is limited only in the external part of the specimens and the degradation products are needle like. In this case the crystals are very thin as in the micrograph reported in the Figure 33b.

Figure 34a shows the specimen PZ-L + SF after 40000 hours of cyclic acid/sulphate attack and a large number of cracks. Sometimes, the aggregates are directly affected by the attack as shown in Figure 34a. In the internal part of the crack, Figure 34b, there are crystals of the degradation products, which are grown perpendicular to the crack direction. EDAX analysis (reported in Figure 35) confirms the high content of sulphur in the columnar crystals embedded into cracks, and the atomic Ca/S ratio (38.57/28.90) is compatible with that of calcium sulphate [33], rather than that of ettringite.

In Figure 36a, the presence of an aggregate of large dimension shows that the deep degradation. The degradation products are crystals and filled the cracks as reported in Figure 36 on the right, for the PZ-L + SF after 40000 hours of sulphate attack.

In the Figure 37 the micrographs analysis of the specimens, stored in water for all the time are reported. The sample doesn't show signs of attack as cracks, but only a thin layer (light grey in the figure) on the external surface rich of Ca and C as measured by the EDAX analysis. This layer (30-40 μm) affected by carbonation. The microstructure is the same in all the analysed samples.

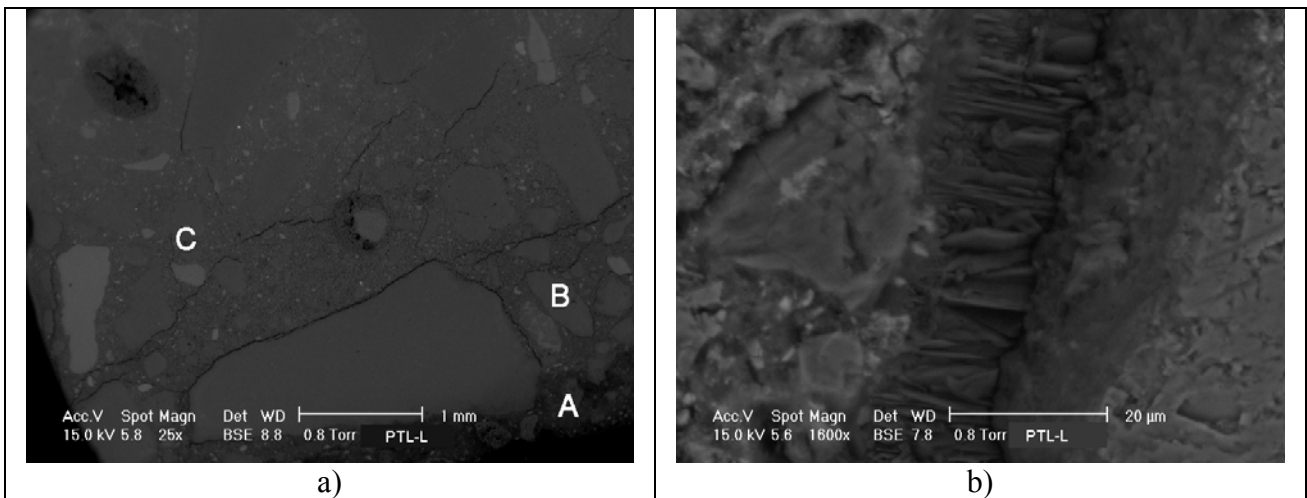


Figure 30 - Micrograph of PTL-L after 40000 hours of cyclic acid/(complex) sulphate attack.

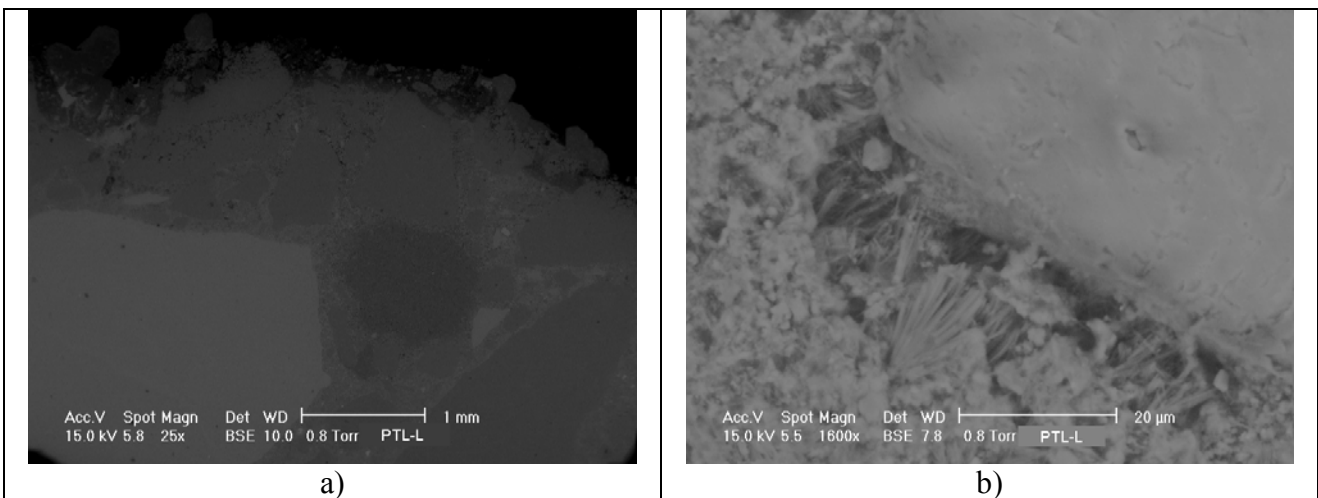


Figure 31 - Micrograph of PTL-L after 40000 hours of complex sulphate attack.

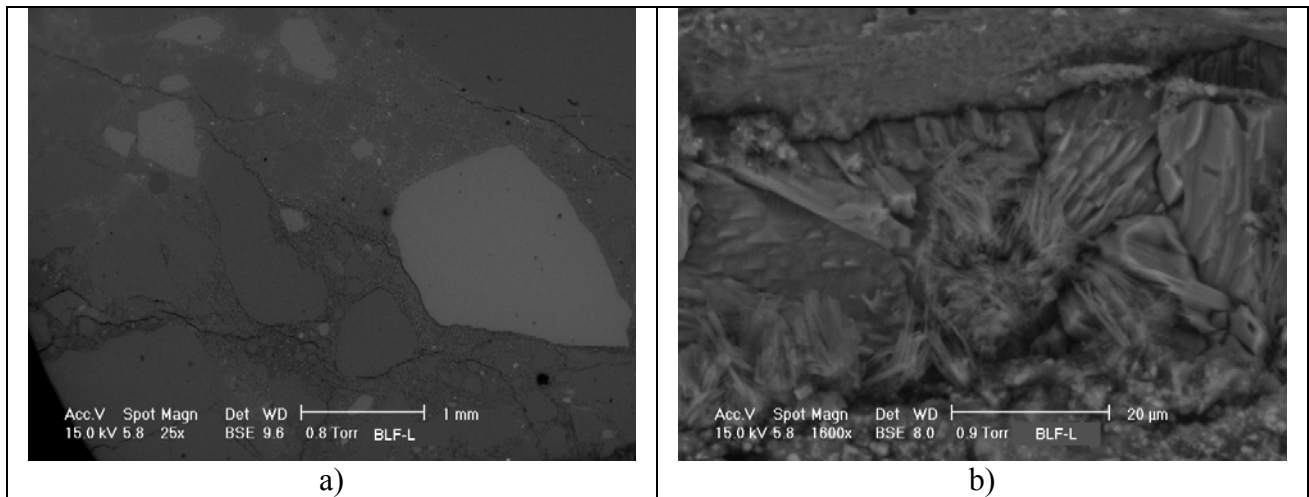


Figure 32 - Micrograph of BLF-L after 40000 hours of cyclic acid/(complex)sulphate attack.

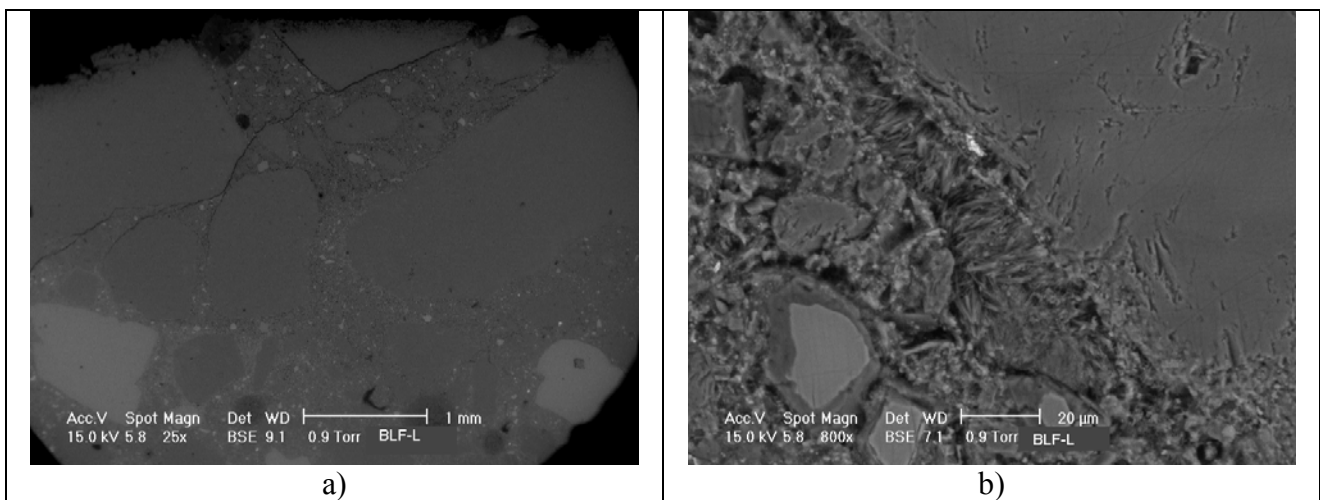


Figure 33 - Micrograph of BLF-L after 40000 hours of complex sulphate attack.

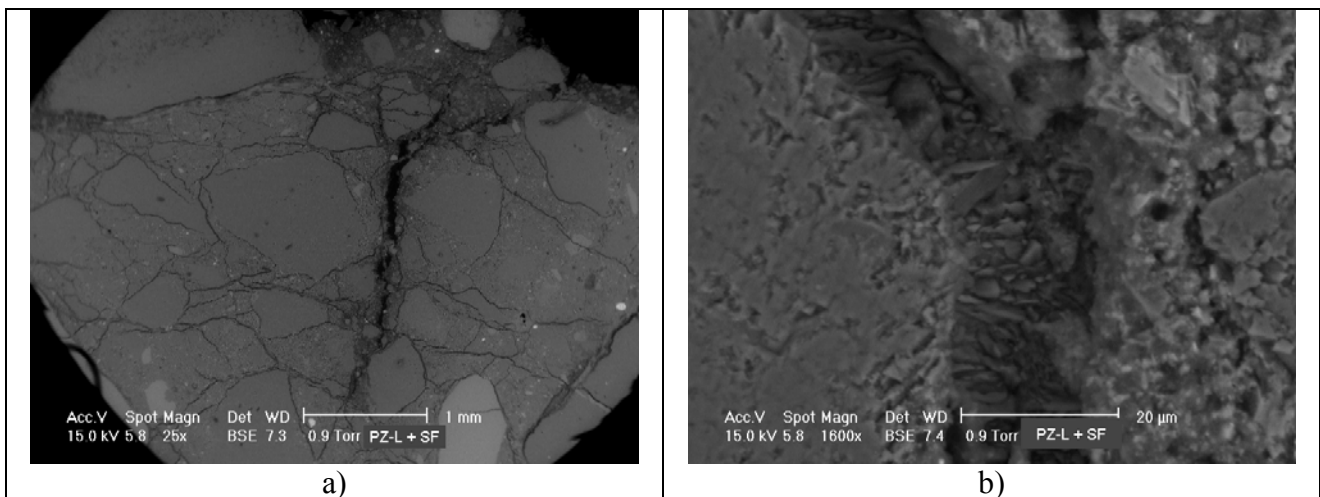


Figure 34 – Micrograph of the PZ-L + SF after 40000 hours of cyclic acid/(complex) sulphate attack.

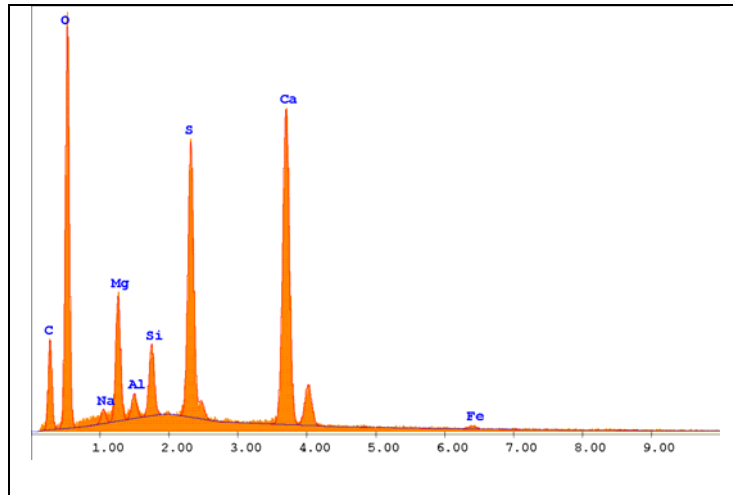


Figure 35 - EDAX results of the crystals in the crack reported Figure 34b.

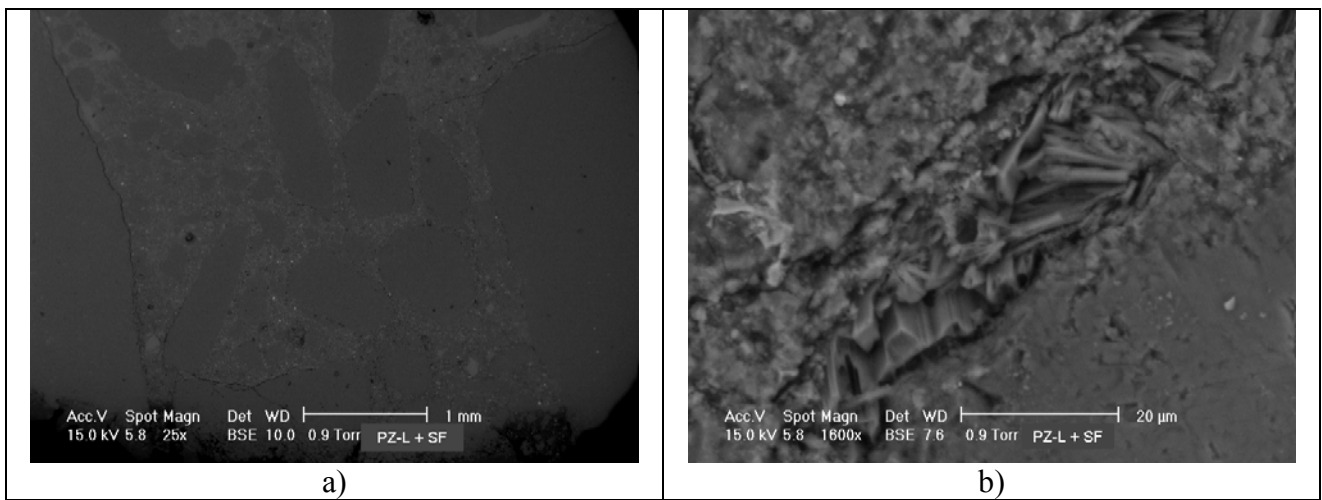


Figure 36 - Micrograph of PZ-L + SF after 40000 hours of complex sulphate attack.

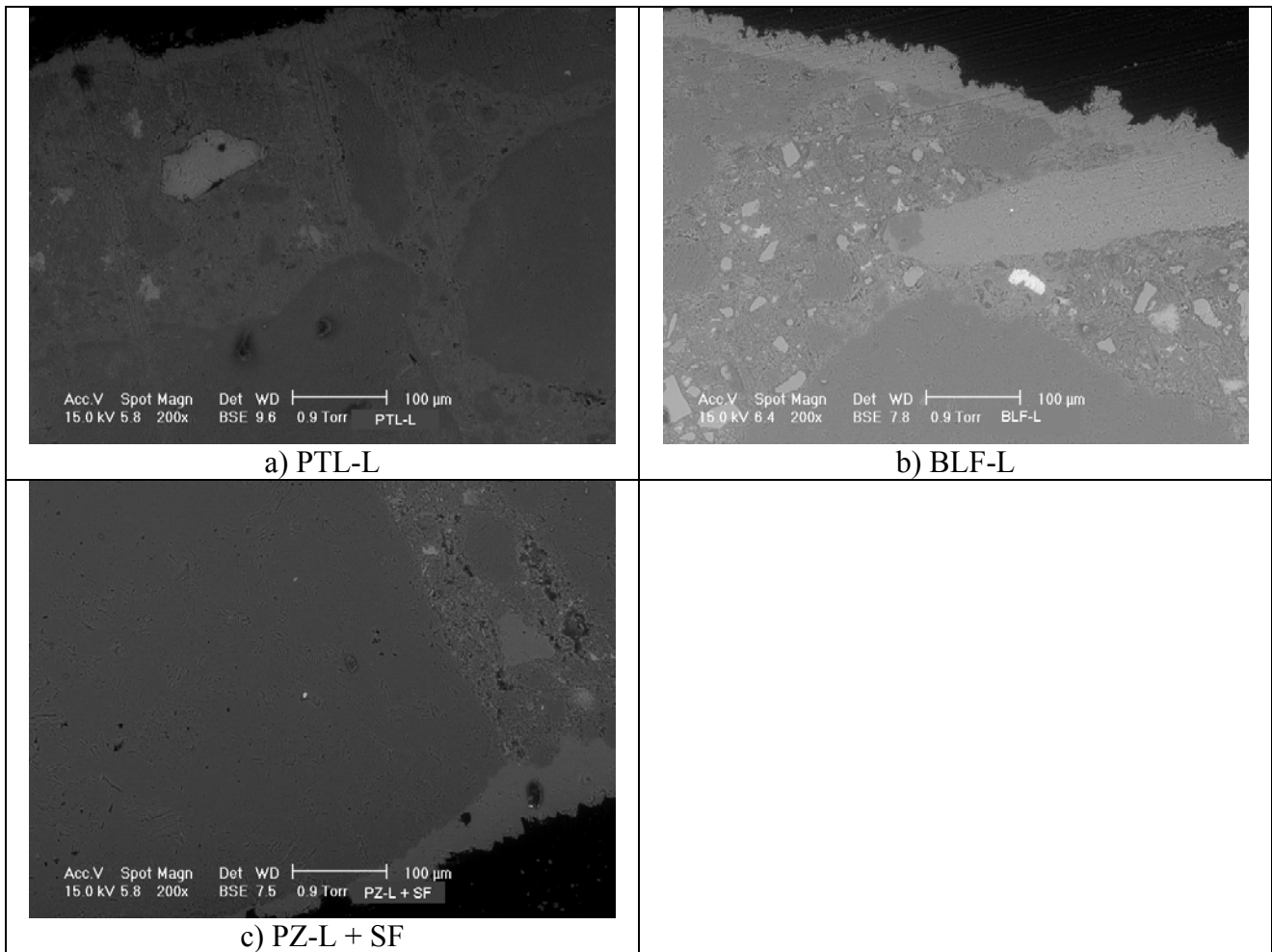


Figure 37 – Micrograph of the mixtures stored in water after 40000 hours.

3.5.2 Analysis of samples-S

3.5.2.1 pH and permeability in water

The pH values of all the solutions were checked during every types of attack and in Figure 23 is reported the trend during the 6 hours of acid attack (a) and during the 28 days of only sulphate attack (b).

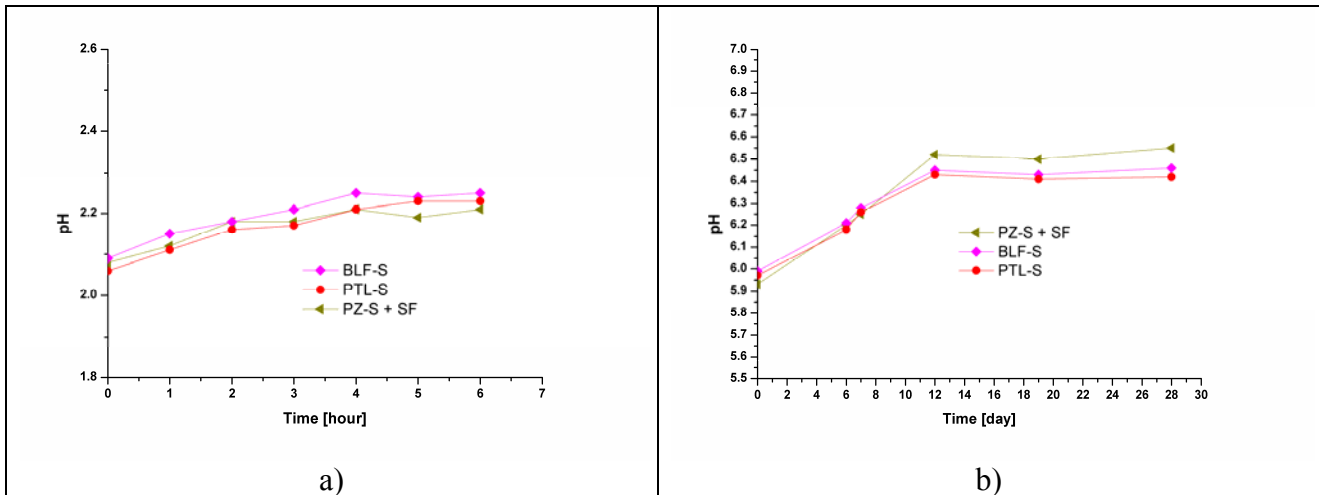


Figure 38 – pH values during acid attack (a) and during complex sulphate attack (b)

During the 6 hours of acid attack the pH increases from 2.1 to 2.2 because degradation products release into the solution. In the case of the sulphate attack during the first 2 weeks, the pH increases from 5.9 to 6.3 and after one month the value is stable at 6.4 .

The specimens stored in water, show no signs of degradation. No mass variation and no deformation appeared during the testing time, after the initial expansion and its change of mass is due only to the water absorption.

3.5.2.2 Aggregate analysis

In order to confirm and quantify the silicates nature of the aggregates, thermal analysis and powder XRD analysis were performed on the four fractions of the raw materials. In Table 15 the percentages of the calcium carbonate measured with the thermal analysis are reported.

Table 15 – TG results

	% CaCO₃
Sand 0/2	18.18
Sand 0/5	25.54
Gravel 3/6	54.12
Gravel 9/14	40.48

Calcium carbonate amount is around about the 20% in the sand fraction and increase with the size dimension of the aggregates.

Table 16 –XRD results - % in weight (± 1%)

	Quartz	Calcite	Feldspar
Sand 0/2	52	12	36
Sand 0/5	47	22	31
Gravel 3/6	32	51	17
Gravel 9/14	31	62	7

The XRD analyses, reported in Table 16, indicate nearly the 50%wt of quartz in the sand and 30%wt for the gravel.

3.5.2.3 Mass variation

In Figure 39 the mass variation vs. time of the samples during the sulphate attack is reported.

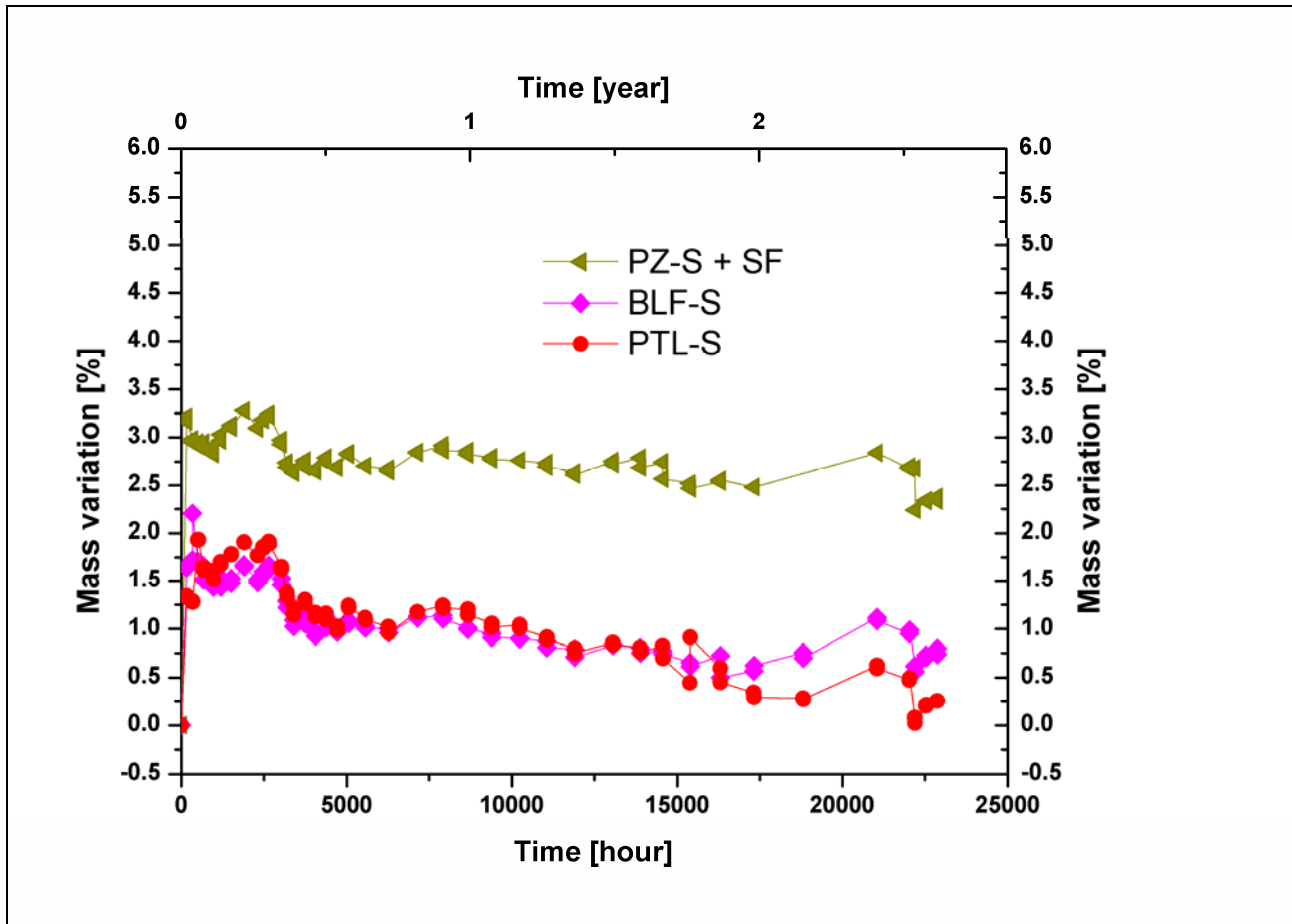


Figure 39 – Mass variation [%] during the complex sulphate attack (mean value of two samples).

There are different trends: the first, during the first week, is a large mass increase; its $\Delta m = 1.5\%$ for BLF-S and PTL-S and it's $\Delta m = 2.7\%$ for PZ-S + SF, due to the absorption of the sulphate solution; the second, is a low and constant loss of mass due to the effect of the sulphate attack. The trend of $\Delta m(\%)$ vs. time is similar for all the three mixtures. The rates of the mass variation after a linear fitting in an interval of 2.5 years are reported in Table 17. PZ-S + SF shows the lowest mass loss rate.

Table 17 - Slope of the straight line of mass variation during the complex sulphate attack. The values of the rate are in 10^{-4} %/hour.

Periods [hours]	400-22000
PZ-S + SF	-0.22
BLF-S	-0.36
PTL-S	-0.70

The Δm during the cyclic acid/sulphate attack is reported in Figure 40. After 2.5 years, all the typologies of mixtures have a high mass loss and, in particular, the mixture PZ-S + SF shows $\Delta m = -16\%$ whereas the others two show $\Delta m = -14\%$.

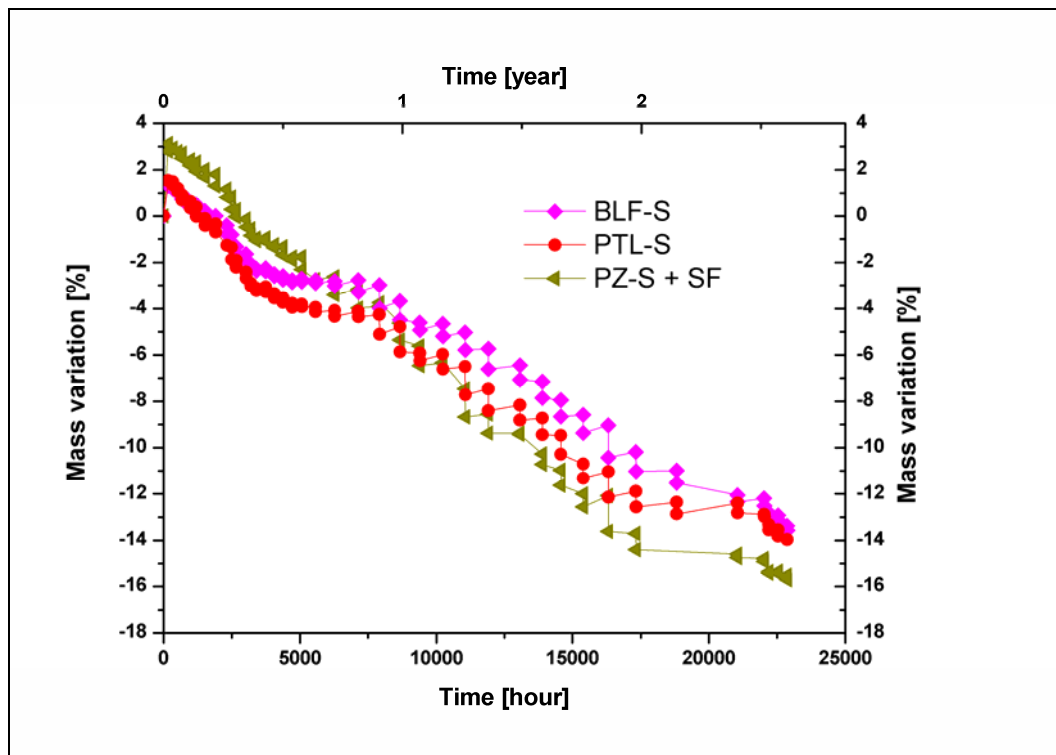


Figure 40 – Mass variation [%] during the cyclic acid/(complex) sulphate attack (mean value of two samples).

The rate of mass loss doesn't change in the sample PZ-S + SF changing the frequency of the acid attack and the initial increase of mass is higher than the others two. The rates of mass variation, measured in three different intervals, are reported in Table 18: in the first, the slopes are similar but in the others two intervals, the rates of the mixtures BLF-S and PTL-S increase of one order of magnitude.

Table 18 - Slope of the straight line of mass variation during the cyclic acid/(complex)sulphate attack. The values of the rate are in 10^{-4} %/hour.

Periods [hours]	200-3000	3000-8000	8000-18000
PZ-S + SF	-12.3	-6.9	-10.3
BLF-S	-11.1	-3.1	-7.3
PTL-S	-14.4	-3.1	-7.9

3.5.2.4 Deformation results

The deformation vs. time during the only sulphate attack is reported in Figure 41. The mixture PZ-S + SF started to expand already in the first week.

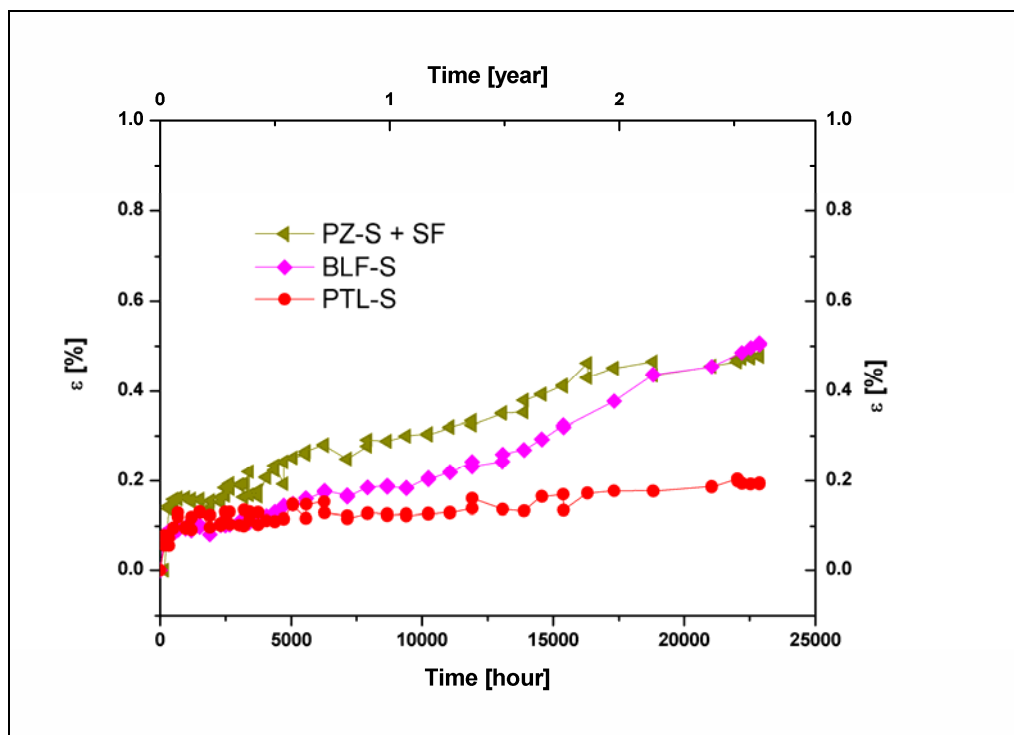


Figure 41 – Deformation [%] during the complex sulphate attack (mean value of two samples).

The PZ-S + SF and BLF-S samples show an increase of the deformation and after 2.8 years the value is $\epsilon = 0.5\%$. On the other hand, PTL-S sample expanded with a steady low increase. This is confirmed by the rates of deformation reported in Table 19.

Table 19 - Slope of the straight line of the deformation during the complex sulphate attack. The values of the rate are in 10^{-5} %/hour.

Periods [hours]	300-2000	2500-22000
PZ-S + SF	0.32	1.00
BLF-S	0.65	1.80
PTL-S	0.74	0.72

In Figure 42, the deformation during the cyclic acid/sulphate attack is reported. After the initial absorption of the solution, a period without any length variation followed.

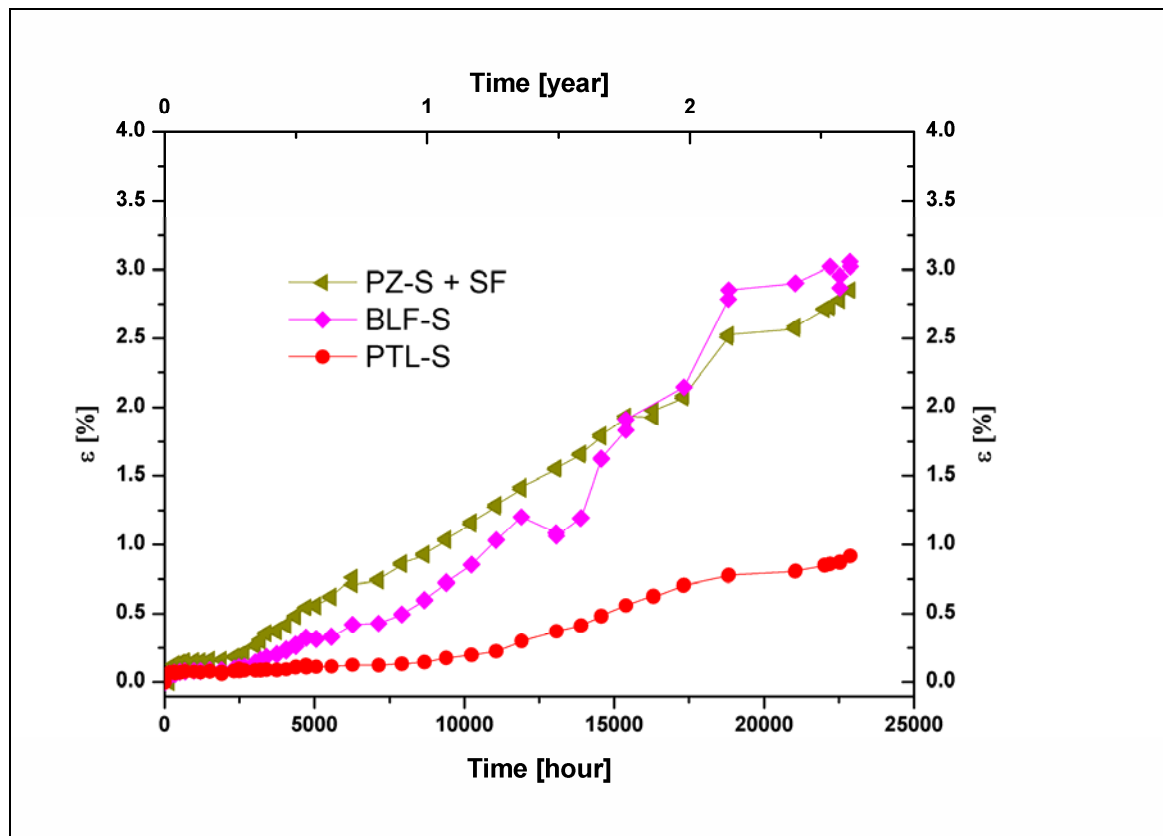


Figure 42 – Deformation [%] during the cyclic acid/(complex) sulphate attack (mean value of two samples).

The use of silicates aggregates decreases the induction time compared with the analysis performed on the concretes prepared with the same cements but limestone aggregate. Indeed, after only 2500 hours, the mixtures PZ-S + SF and BLF-S show a constant expansion until $\epsilon = 3\%$ in 25000 hours. ($\epsilon = 1\%$ was measured for PTL-L). In Table 20 the rates of deformation during the cyclic acid/sulphate attack are reported. In the first period the expansion of the PTL-S sample is

low. The others two mixtures show the same constant expansion rate. After the induction period, deformation occurs in all the specimens. However PZ-S + SF and BLF-S show a remarkable expansion.

Table 20 - Slope of the straight line of the deformation during cyclic acid/(complex)sulphate attack. The values of the rate are in 10^{-5} %/hour.

Periods [hours]	300-2000	2500-22000
PZ-S + SF	1.45	14.20
BLF-S	1.11	14.30
PTL-S	0.09	6.10

2.5.2.5 Characterization after 25000 hours

A new series of microstructural analyses were performed in order to understand the degradation of all the concretes after about 25000 hours of test.

2.5.2.5.1 Phenolphthalein method (EN 9944)

Figure 43 shows the results of the phenolphthalein test. On the column on the left, there are the micrographs concerning the samples after the sulphate attack and on the right the micrographs regarding those subjected to the cyclic acid/sulphate attack.

Complex sulphate attack		Cyclic acid/(complex)sulphate attack
 <p>3a)</p>	<p>PTL-S</p>	 <p>3b)</p>
 <p>2a)</p>	<p>BLF-S</p>	 <p>2b)</p>
 <p>1a)</p>	<p>PZ-S + SF</p>	 <p>1b)</p>

Figure 43 - Phenolphthalein methods (EN 9944) results on concretes prepared with silicates aggregate.

In the mixture PTL-S subjected to the sulphate attack (1a) the alkalinity level is acceptable, but the other case of the cyclic attack produces an increase of the degradation depth. The same results are obtained in the mixture BLF-S (2a and 2b) and in the mixture PZ-S +SF (3a and 3b). In the lat, the entire cutting section is compromised by the acid and the sulfatic attacks (3b), with no change of colour. The phenolphthalein test performed on the mixtures stored in water shows an acceptable alkalinity on the whole section.

3.5.2.5.2 Microstructural analyses

In order to analyse the thickness degradation, elements maps are recorded using the EDAX instrument on all specimens subjected to the cyclic acid/sulphate attack. In Figure 44 the ESEM

micrographs are shown on the left and on the right you can see the corresponding x-ray sulphur maps.

For the PTL-S sample (Figure 44a), the surface doesn't show cracks neither a preferential path of the acid attack, which seems instead to provide a general erosion of the surface. This is confirmed by the X-ray map for sulphur of the same sample: there is no evidence of cracks and the sulphur is present in the voids and entrained air bubbles and on the external surface. The cutting surface of the sample BLF-S (Figure 44b) a few cracks appear in the cement paste. As it can be seen in the corresponding X-ray map, the sulphur is present everywhere especially in the cracks. The micrograph of the PZ-S + SF sample (Figure 44c) shows an extensive cracking, observed around aggregates and through the paste, with occasional cracking through aggregate particles. The most of cracks appears black, due to the loss of material during the cutting and polishing of samples.

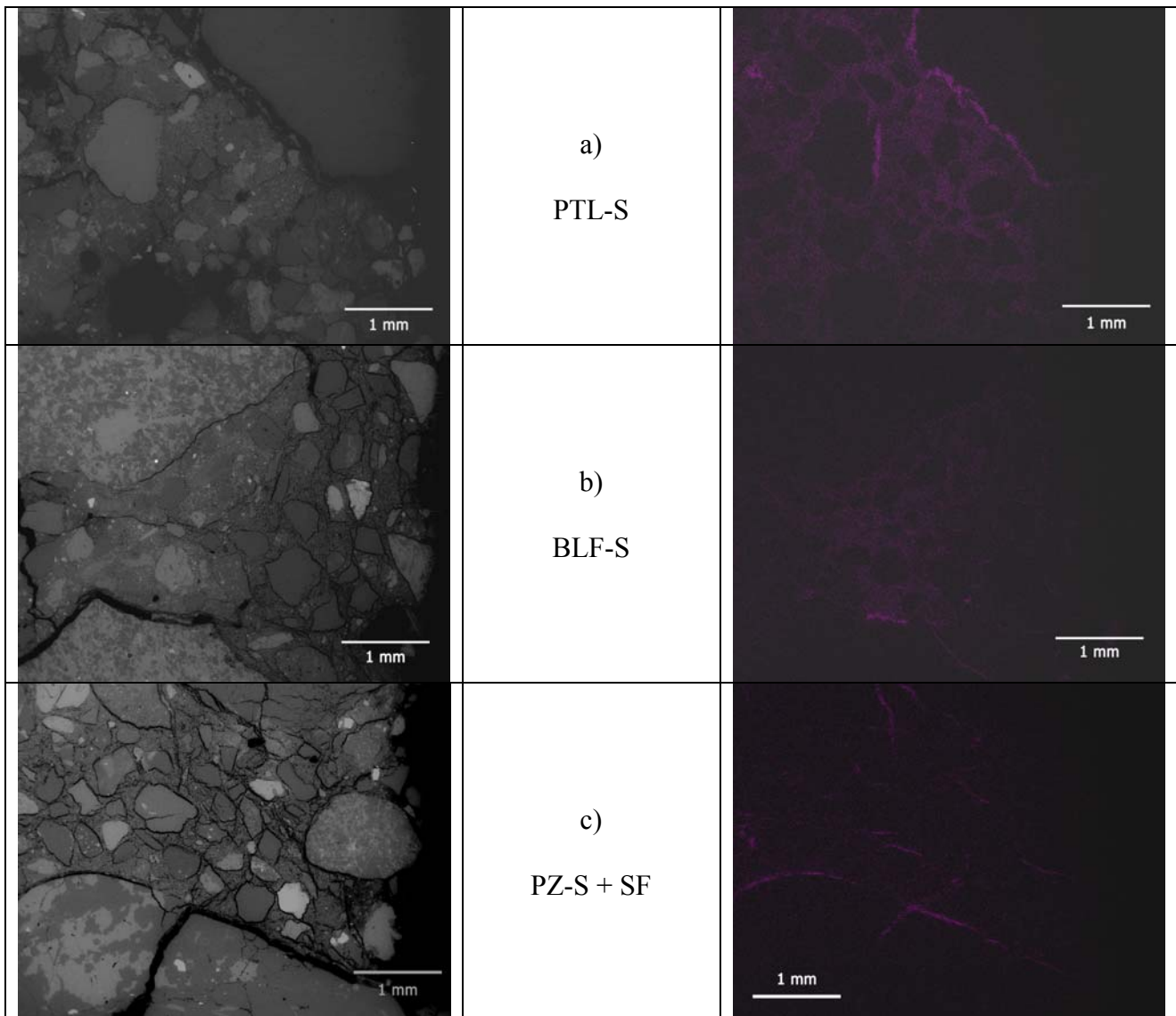


Figure 44 - ESEM images (on the left) and X-ray maps for sulphur (on the right) of polished surface subjected to cyclic acid and complex sulphate attack.

The micrographs of PTL-S sample subjected to the sulphate attack are reported in Figure 45a. The degradation is not clearly visible in the external part of the cylinder at low magnification, as reported on the left. The degradation products are founded in the cracks between the cement paste and aggregate in a needle form (Figure 45b).

Figure 46 shows the micrographs of the PTL-S subjected to the cyclic acid/sulphate attack: the surface is completely destroyed. The degradation products are presented in deep over 2-4 mm from the surface after 2.9 years of attack surrounding every aggregates. The gap between the aggregates and the cement matrix is over 40 μm , as reported in Figure 46. EDAX analysis (reported

in Figure 47) confirms the high content of sulphur in the columnar crystals embedded into cracks, and the atomic Ca/S ratio (30.75/26.14) compatible with that of calcium sulphate [33], rather than that of ettringite.

The micrographs of the mixture BLF-S subjected to the sulphate attack are reported in Figure 48.

The degradation is clearly visible in the external part of the section, even at low magnification. The attack affects the internal part of the aggregate and the cracks are filled by crystals (Figure 48b).

The micrographs of the BLF-S subjected cyclic acid/sulphate attack are reported in Figure 49. The degradation is clearly visible in the section of the sample, even at low magnification. The needle like crystal of gypsum is visible in the cracks between the cement paste and aggregate (Figure 49b). It is visible the void leaved by an aggregate and the crystals of gypsum.

The micrographs of PZ-S + SF during the sulphate attack are reported in Figure 50. A web of cracks is visible in the cross section, surrounding nearly every aggregates. In Figure 50b the crystals embedding in the cracks are visible.

The results of the microstructural analysis for the PZ-S + SF are reported in Figure 51. Also in this case the products of degradation are around every aggregate particles. The magnification of the gap between the cement matrix and the aggregate filled by crystals of large dimensions is shown in Figure 51b. EDAX analysis (reported in Figure 52) confirms the high content of sulphur in the columnar crystals embedded into cracks, and the atomic Ca/S ratio (31.22/29.65) compatible with that of calcium sulphate[33], rather than that of ettringite.

In Figure 53 the microstructural analysis of the mixtures stored only in water is reported. In every typologies of specimens, there are no signs that degradation processes occur after 2.9 years of testing.

Only a thin layer of a few microns of carbonation, is present in external part of the section of all the samples stored in water.

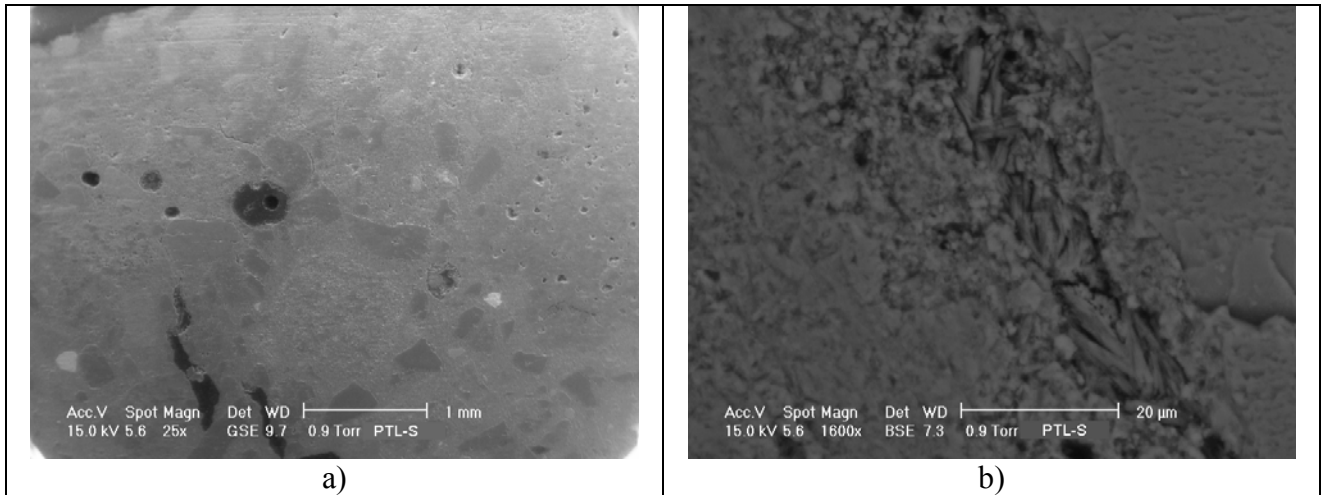


Figure 45 - Micrograph of PTL-S after 25000 hours of complex sulphate attack.

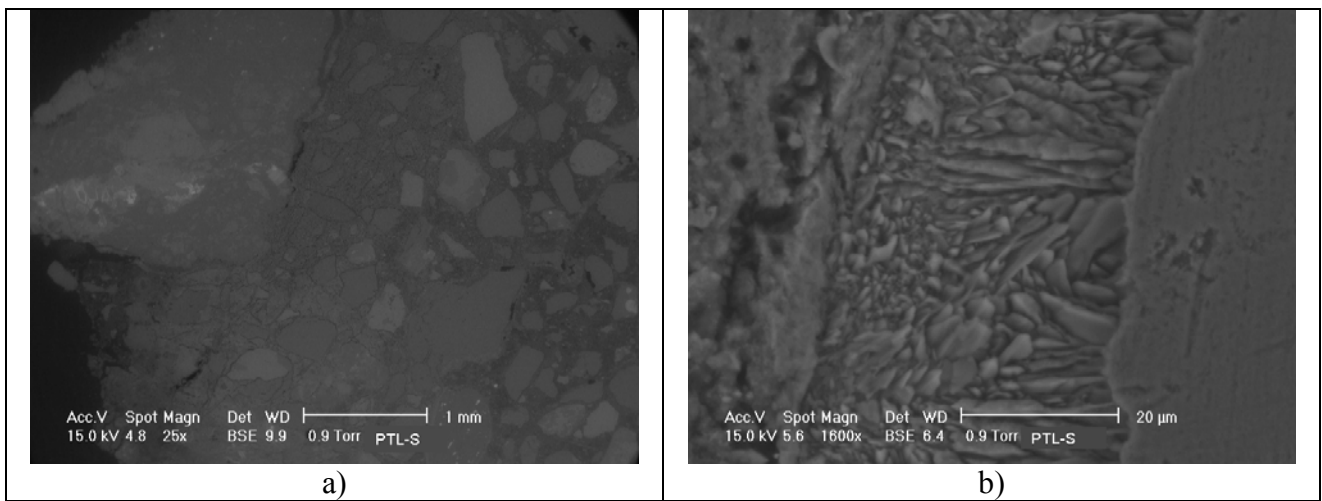


Figure 46 – Micrograph of PTL-S after 25000 hours of cyclic acid/(complex)sulphate attack.

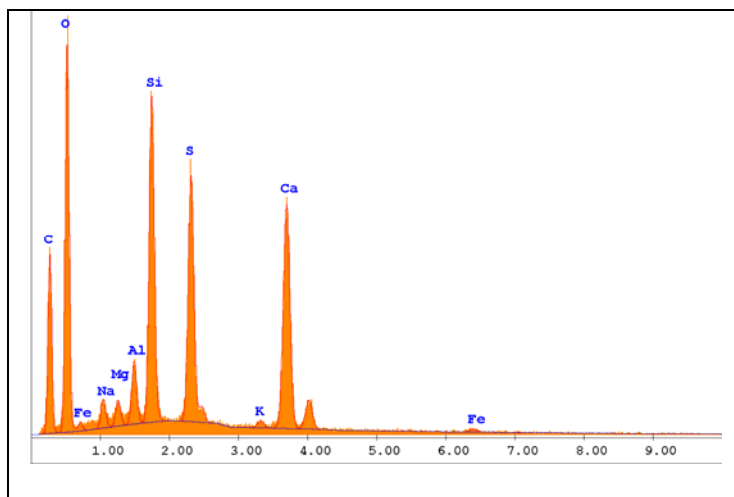


Figure 47 - EDAX results of the crystals in the crack reported Figure 46b.

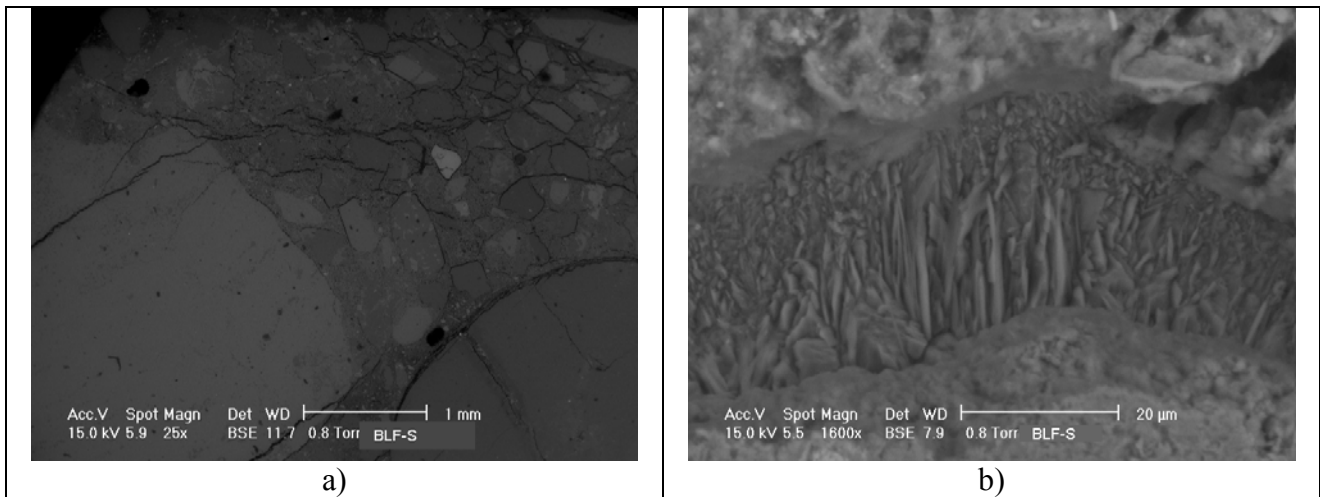


Figure 48 – Micrograph of the mixture BLF-S after 25000 hours of complex sulphate attack.

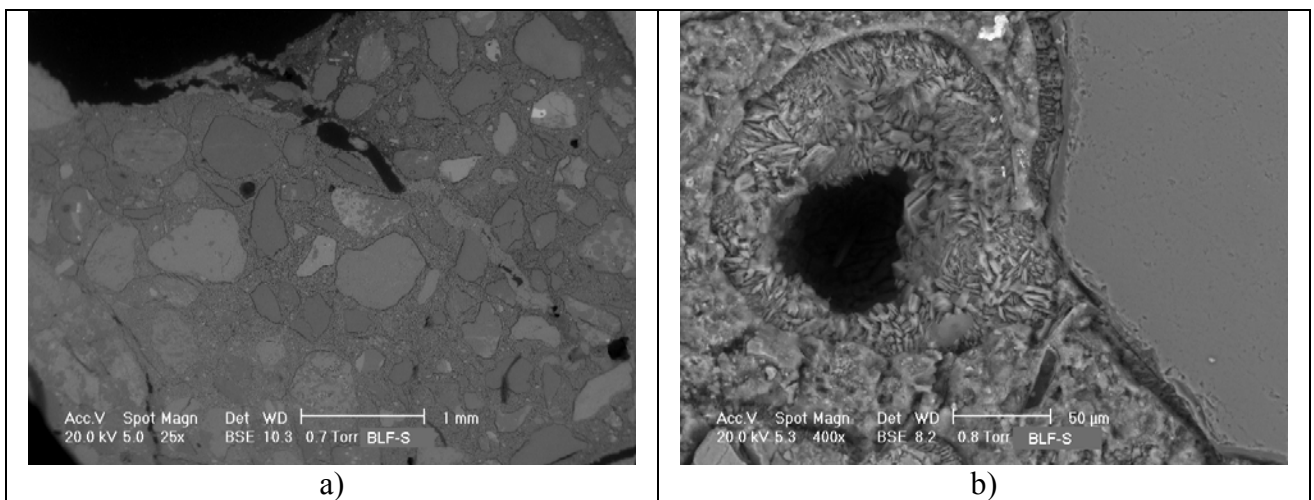


Figure 49 – Micrograph of the BLF-S after 25000 hours of cyclic acid/(complex)sulphate attack.

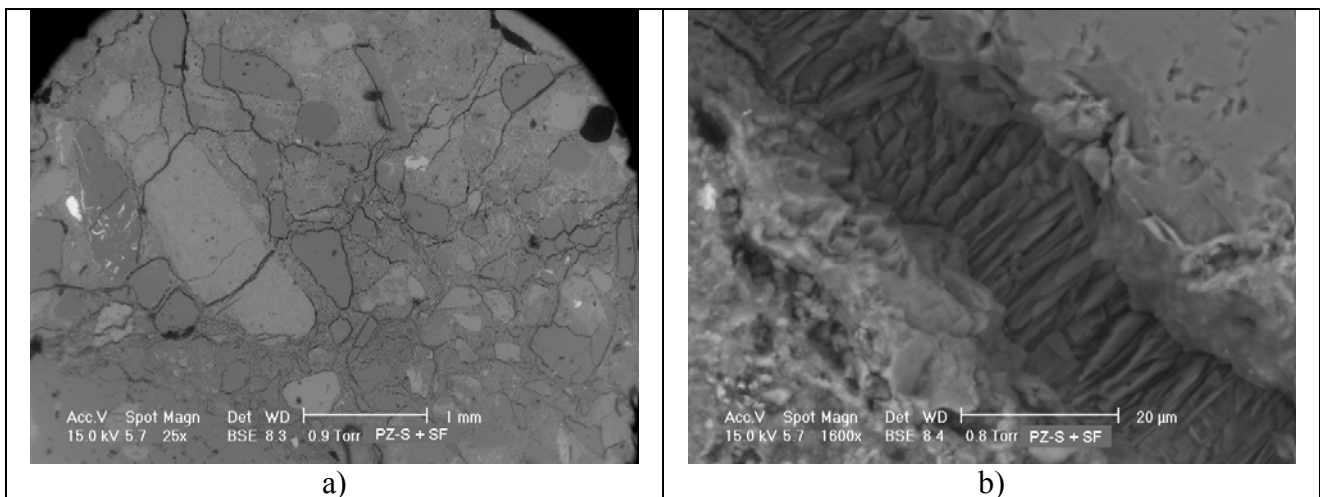


Figure 50 – Micrograph of PZ-S + SF after 25000 hours of complex sulphate attack.

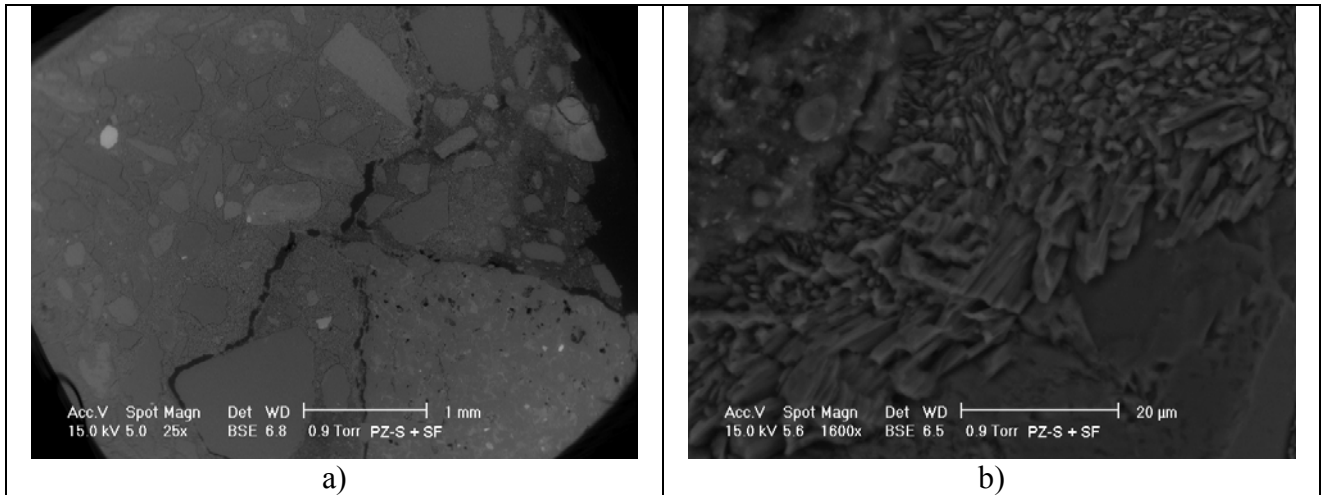


Figure 51 – Micrograph of the PZ-S + SF after 25000 hours of cyclic acid/(complex)sulphate attacks.

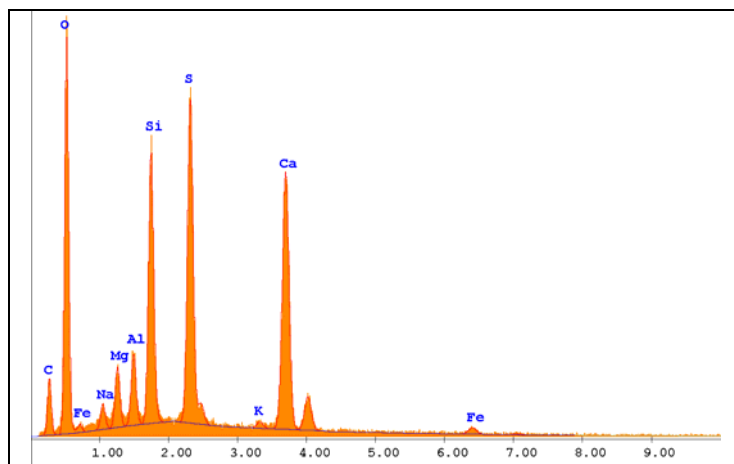


Figure 52 - EDAX results of the crystals in the crack reported Figure 51b

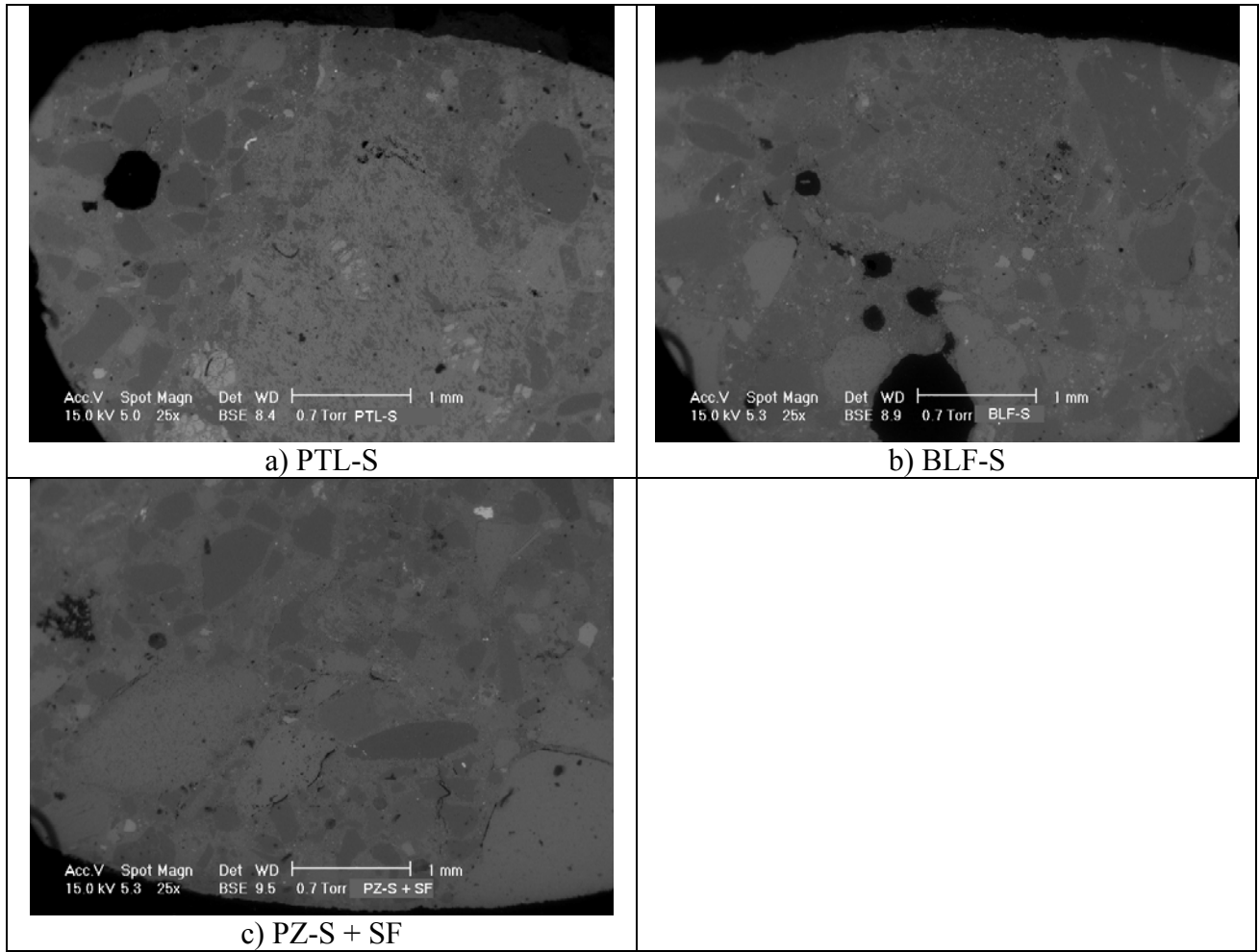


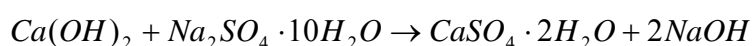
Figure 53 – Micrographs of the mixtures stored in water.

3.6 Discussion and conclusion

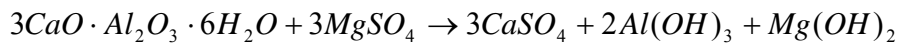
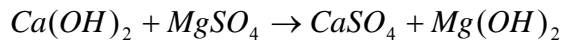
Currently, there are no methods to evaluate the performance of hydraulic cements in both acid- and sulphate-rich environments. On the other hand, ASTM describes two test methods for assessing the performance in sulphate-rich environments (ASTM C452 and C012) and both of them have been subjected to criticism, because they seem to not adequately predict field performance. Among the several critical aspects of the tests, it is worth noting they are performed on mortars and not on concretes immersed in sodium sulphate, as it is required by ASTM C012 “Test Method for Length Changes of Hydraulic-Cement Mortars Exposed to a Sulphate Solution”. They take into account only expansion due to ettringite formation, whereas the acid attack is generally ignored, though it causes mass loss and could accelerate the degradation process. Furthermore, one more critical aspect of the actual tests is that even considering also the acid attack alternating to that of sodium sulphate, the environment of a sewer pipe contains more than a single aggressive component.

Accordingly, a reliable accelerated sulphate resistance test method represents a growing interest in production of concretes prepared with Portland and non-portland cements. In this study, the sulphate resistance of concretes was assessed using an accelerated test based upon a method including a monthly acid attack. The evaluation of damage involved the measurements of both expansion and mass loss. Moreover, the study involved also the comparison with the results of samples of same composition immersed in a solution of mixed salts, among them sodium, ammonium and magnesium sulphate. In some recent studies the effect of each of those species have been studied and in this new test, both the presence of all the species and the sulphuric acid are taken into account.

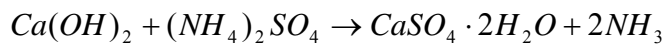
It is known that sodium sulphate reacts with the portlandite to forms expansive products like gypsum, which in the presence of aluminates forms ettringite [27].



It is also known that when the attacking solution contains just magnesium ions ($MgSO_4$), the formation of magnesium hydroxide are observed [14][17]. Magnesium sulphate reacts directly with the cement paste forming magnesium silicate hydrated (M-S-H) and gypsum, which after long time, could transform in ettringite .



Actually, the concrete deterioration by ammonium sulphate [27] overwhelms any other attack because only expansive products like gypsum are produced. An intensive dissolution occurs on the cement hydrates at the same time of the expansion.

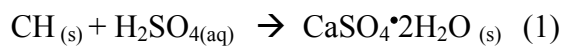


At this regard the complex solution modifies the rates of expansion with respect to the same mixtures reported chapter 2 by the only sodium sulphate attack. As reported in literature [28], for attack by sodium sulphate solution, at a low concentration of sulphates (<1000 ppm SO_4^{2-}), the primary product deposited is ettringite, while at high concentrations (>8000 ppm SO_4^{2-}), gypsum is the main product. In the intermediate range ($1000-8000$ ppm SO_4^{2-}), both gypsum and ettringite are observed. In magnesium sulphate attack, ettringite production is observed at a low concentration (<4000 ppm SO_4^{2-}), a mixture of ettringite and gypsum forms at an intermediate concentration (between 4000 and 7500 ppm SO_4^{2-}), and magnesium corrosion dominates at high concentrations (>7500 ppm SO_4^{2-}). In this work, the accelerated test is conducted with a high concentration of reagents (see Table 10) and with a high area/volume ratio.

In the previous chapter, [F. Girardi, W. Vaona, R. Di Maggio, Accelerated test for measuring sulphate resistance of concrete pipe prepared with different hydraulic cements, 2009, Cement and Concrete Research, submitted.][9][29][30], it has been reported that the use of silica fume with the pozzolanic or blast furnace cements is able to reduce expansion to negligible values, even if a monthly attack with sulphuric acid determines a certain mass loss. In that

experiment with cyclic immersion of the samples in acid sulphuric and sodium sulphate solutions, PTL concretes were found to expand to a remarkable extent, although with a lower mass loss. Accordingly to these results, PZ+SF, BFL and PTL cements have been chosen for this study along with two different aggregate, limestone- or silicate-rich as typically available in many regions of Italy. Generally, the degradation of S-samples is much greater than that of the L-samples, confirming that silicate-rich aggregate is not the most suited choice for concretes, which have to be used in a very aggressive environment. Finally, all the samples lose mass, even in absence of acid sulphuric attack. This phenomenon is attributable to the acidity, even if low, of the mixed sulphate solution, which favours dissolution of portlandite. The pH of the solutions of attack increases with time similarly for all the samples. Indeed, degradation during the concrete exposure to both acid and mixed sulphate environment, can be discussed on the base of two mechanisms: dissolution of components and expansive action of the reaction products.

Actually, the larger phenomenon of dissolution occurs during the immersion in sulphuric acid, mainly due to the reaction portlandite with acid [22] according the following reaction (1):



Gypsum precipitates reducing the acid diffusion through the corroded layer, at least till portlandite is completely wasted. In the concretes containing a minor amount of portlandite, there is not much of it available to the reaction with acid, given that it has been already reacted with SF or slag, the acid attack is restricted to surface aggregate and secondary calcium silicate hydrate (CSH) according the following reaction (2).



The decalcification of tobermorite, which bonds aggregates and cement paste, causes the detachment of aggregate from the specimen surface. As a consequence, the surface of the concretes with SF is generally consumed and even the acid can penetrate the more internal zones.

Expansion may occur as a result of the formation of gypsum ($\text{CaSO}_4 \cdot 2\text{H}_2\text{O}$), the product of both the two reactions previously discussed for acid attack, and/or ettringite

(C₃A:3CaSO₄:32H₂O).[15-16,21-23,28,32] However, the following reaction (3) contributes to form and deposit gypsum during ammonium sulphate exposure:



The NH₃ is leached, decreasing the pore solution alkalinity and resulting in loss of calcium silicate hydrate, the primary strength-giving component of the cement paste.

The concrete permeability is an important parameter for the degradation kinetics, which depend by the diffusion of the aggressive species. The geometry and the distribution of the porosity are more important than the whole porosity volume. The rate of degradation depends also on the concentration of aggressive substances. Indeed, if the concentration of SO₄²⁻ is high, gypsum will form, whereas if it is low, ettringite will form. In this work, the test is performed with a high concentration of reagents (33800 ppm of SO₄²⁻) exposing a high specific area (the samples have high area/volume ratio)[28]. However, the analysis EDXA of the columnar crystals embedded into cracks indicated an atomic Ca/S ratio (36.69/35.84), compatible with that of calcium sulphate, rather than that of ettringite. Accordingly, calcium sulphate instead of ettringite is the main product. In this study the attention was focused on concretes and not mortars specimens, so that no X-ray powder diffraction analysis could be performed with the aim to individuate the phases of cement paste in a very accurate way. Whatever the main reaction product, it nucleates in the micro-cracks of cement paste or in transition zone around aggregate. Afterwards, the growth of the columnar crystals enlarges the cracks and causes expansion, in agreement with the research results of Tian et al. suggest that gypsum formation during sulphate attack is expansive [33].

The cyclic immersion in sulphuric acid solution has the effect to bring the attack through the depassivation layer, so that the gypsum forms in more internal zone. The final effect is to reduce the dormant period, necessary to observe macroscopic expansion.

As regards expansion, PTL samples showed always the opposite behaviour with respect to the other composition: they expand less than the others, unless in the mixed sulphate solution when containing limestone-rich aggregates.

Indeed, ammonium sulphate produces a concrete deterioration: only expansive gypsum is formed. There are little data available concerning ammonium sulphate attack; however, some of it indicates that this salt is very harmful to concrete [3][4][6]. There occurs not only expansion due to the formation of gypsum and ettringite [3], but also intensive dissolution of cement hydrates. In PTL concretes, this generalized deterioration is comparable with acid attack, indeed the expansion values don't change significantly.

Differently, the role of admixtures such as silica fume or blast furnace slag on the improvement in the ammonium sulphate resistance of concrete is negative. Indeed, they react with portlandite producing C-S-H. The low presence of free portlandite focuses the acid attack on CSH.

In order to predict life expectancy of concrete sewer pipes, it is a growing interest of concrete production to have a tool, even phenomenological, to compare the resistance and the behaviour of different concrete mixtures in cyclic contact with sulphuric acid and sodium sulphate. Although, it cannot predict absolute life in quantitative terms, the results of the cyclic test of this study let an evaluation of the behaviour and thickness reduction be obtained, surely in a quicker and more reliable way than the test based on simple sulphate attack. It was reported that increasing temperature and concentration of attacking medium, the rate of deterioration is greater [14][21][28]. At this regard this accelerated test could be improved for example using a weekly acid attack. On the other hand for sewage applications it could be of more interest to study the concrete behaviour at temperatures lower than room temperature [28]. Moreover, the reliability of an accelerated test in this field could surely take advantage from using a complex solution prepared mixing different salts.

Part 2

Development of a protective system

Chapter 4 – Silica coating

4.1 Introduction

In order to reduce the degradation on concrete sewer pipe, different sets of experiments were performed on one type of concrete with different coatings. In this chapter the study of a new coating based on a silica sol is presented..

4.2 Materials

A typical concrete for sewer pipes was prepared at the industrial plant Eurobeton S.p.a. situated in Salerno (BZ) using limestone aggregates and portland limestone cement (CEM II-B/LL 32.5 R). The chemical composition and the concrete mixture are described in details in Table 21. The aggregate is ground limestone (dolomite) taken near Salerno (BZ). The cement choice (CEM II-B/LL 32.5 R) is the same to compare the different chemical resistance between concretes protected with two different amount of coating (labelled HC for High amount of Coating and LC for Low amount of Coating) and concretes protected with an additional hydrophobic layer (labelled LCP: Low amount of Coating and hydroPhobic component). In order to obtain reference data a sample was analyzed without coating (labelled WC).

Table 21 - Concrete mixture and for silica coating.

	Concrete	Label	WC	HC	LC	LCP
Elements	Measuring kg/m ³	Silica Sol	-	70.3 g/m ²	7.3 g/m ²	7.3 g/m ²
Aggregate	Limestone	Hydrophobic component	-	-	-	2.0 g/m ²
Fine 0/2	700	Notes	Without Coating	High amount of Coating	Low amount of coating	Low amount of coating + hydrophobic component
Fine 0/4	400					
Coarse 3/15	800					
Cement type	CEM II- B/LL 32.5 R					
Measuring	300					
Water	100					
w/c	0.43					
Mass Volume Density (kg/dm³)	2.383					

N.B.: The measuring in the Table 21 is theoretical. The data are referred to weighting industrial plant

The concrete samples have the following dimensions: diameter 36 mm and height 102 mm and were extruded from a cylindrical mould few minutes after the forming process. The samples HC, LC and LCP were coated by spraying directly on the wet concrete after the de-moulding.

The coating is a silica sol, applied on the external surface of the cylindrical specimens by a spray system on wet concretes. Commercially available reagents were used without further purification. Tetraethyl orthosilicate (TEOS), ethanol and water were mixed under air atmosphere, adding some drops of hydrochloric acid (HCl) and the final composition of the sol are reported in Table 22. The silica sol is stable and long lasting, with high time of gelification.

Table 22 – Silica sol composition

Components	Mass (g)
H₂O	52.5
TEOS	86.9
Ethanol	287.3
HCl	drops

The hydrophobic layer was prepared adding an hydrophobic component (Fluorine alkyl silane - FAS) to the TEOS in order to produce a layer that reduce the wettability.

4.3 Chemical test

The chemical resistance was tested by the following types of attack:

- c) A cyclic immersion in a complex sulphate solution with an attack in acid solution at pH=2 by sulphuric acid for 6 hours weekly (until 3000 hours of test) and monthly (after 3000 hours test).
- d) Immersion in a complex sulphate solution, replenished weekly (until 3000 hours of test) and monthly (after 3000 hours of test).

For this experiment a complex sulphate solution was used, and its composition is reported in Figure 23.

Table 23 – Composition of attack sulphate solution

	g/l
Na₂SO₄	30
(NH₄)₂SO₄	15
MgSO₄	10
NaCl	10
KH₂PO₄	3
Glucose	1

Two specimens for each composition were studied with each type of attack. In order to obtain reference data, two samples of each composition were stored only in water, replenished every week or month, combined with the measures of the attacks a and b.

4.4 Testing program

Every week or month, the length and weight of each sample were measured. Before the weight measurement, the samples were dried with a cloth and was used a technical balance with 0.001 g of sensitivity. The sample length was measured with a digital comparator with 0.001 mm of accuracy. The alkalinity level was checked with the phenolphthalein method (EN 9944).

4.5 Results

4.5.1 Mass variation

In the second part of this thesis, the development of a protective system that increase the durability of the concrete pipes is presented. With this aim, a pozzolanic coating, like colloidal silica, is applied on the concrete surface and analyzed by the same chemical test used in the previous chapters. The concretes, for sewers or aggressive ambient in accordance with EN 206 for the XA3 class, have the following parameter: $w/c \leq 0.45$, $R_{ck} \geq 45$ MPa. The concretes are in the XA3 exposition class. The concrete were analyzed with a new accelerated test using a complex sulphate (the composition is reported in Figure 23).

The mass variation vs. time during the sulphate attack is reported in Figure 54. The Δm vs. time trend is similar for every typologies and it is composed by an high incremental of the mass due to the adsorption of the solution during the first week, followed by a strongly decrease until 3000 hour when the replenishment of the sulphate solution is weekly. When the frequency becomes monthly the $\Delta m(\%)$ is weakly. After 20000 hours of sulphate attack, the samples WC and HC, show the lowest mass variation. The others two typologies of samples, LC and LCP, show the highest mass variation.

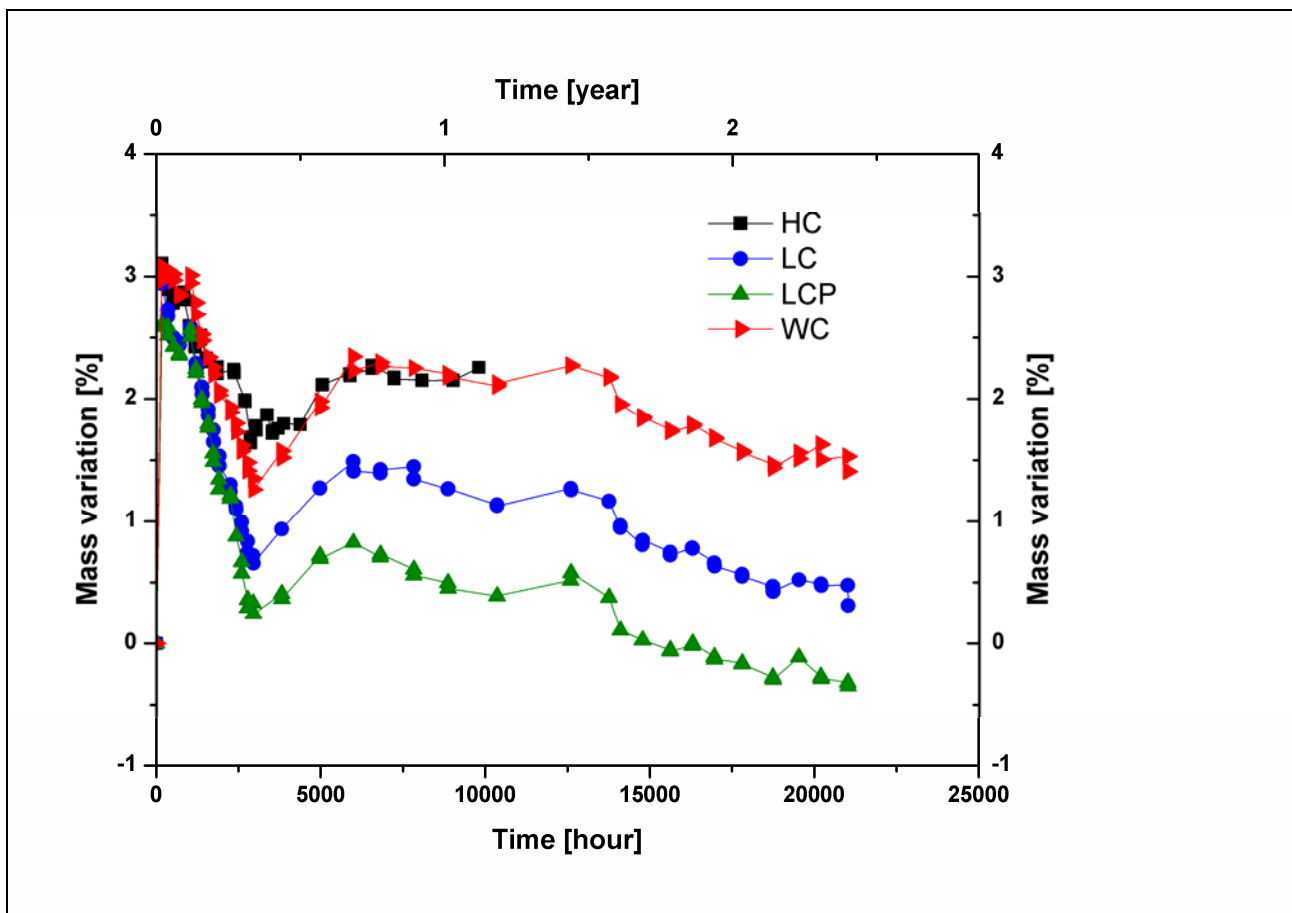


Figure 54 – Mass variation [%] during the complex sulphate attack (mean value of two samples).

The mass variation during the cyclic acid/sulphate attack is reported in Figure 55. The Δm trend is similar for every samples, and after about 20000 hours of testing, the WC sample shows a $\Delta m = -13\%$, LC and LCP samples show the same $\Delta m = -12\%$ and the HC sample shows the lowest mass loss ($\Delta m = -3\%$). The trend of $\Delta m(\%)$ vs. time, is that the coating reduces the mass loss, especially when acid attack is monthly.

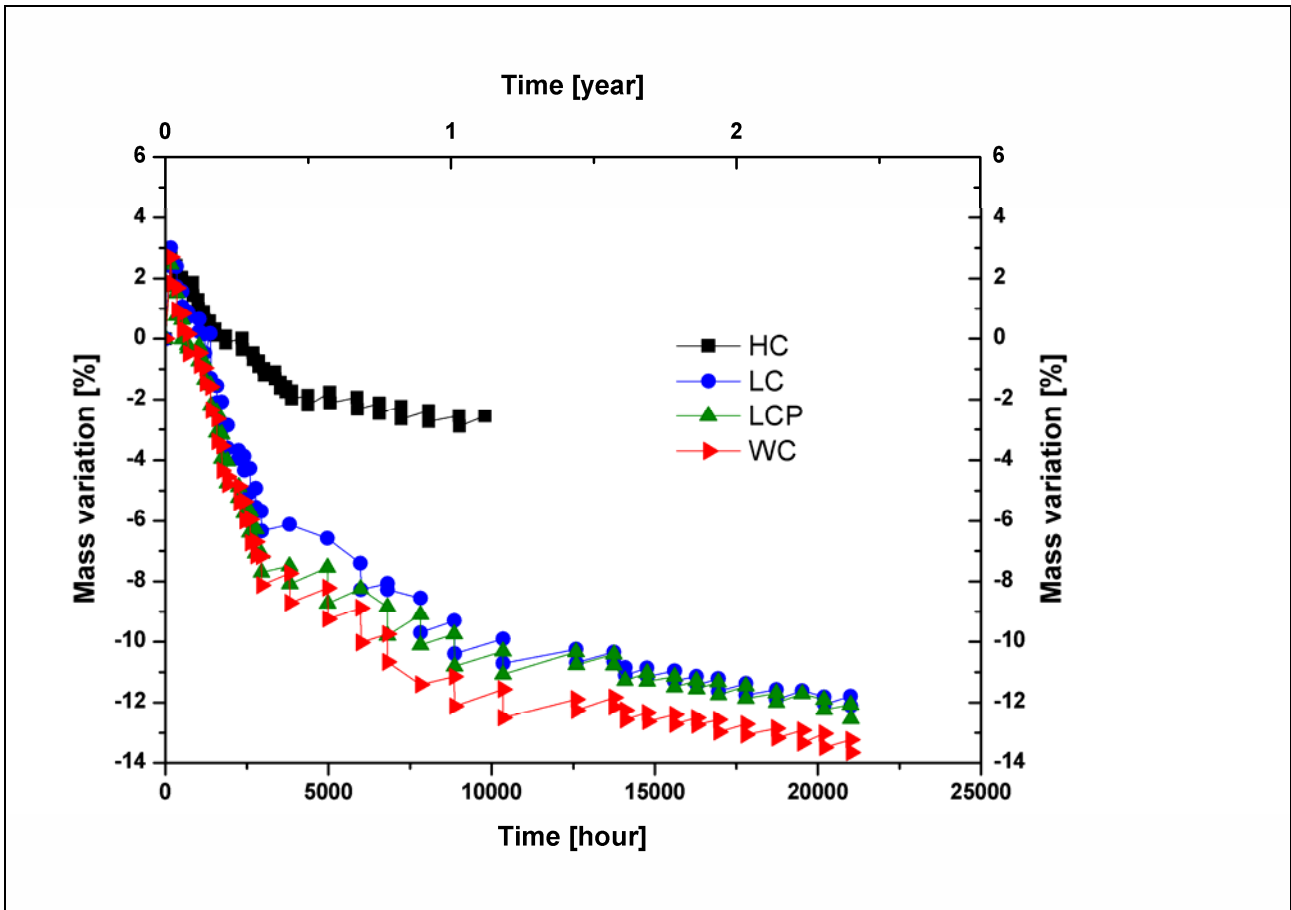


Figure 55 - Mass variation [%] during the acid/(complex)sulphate attack.

The specimens stored only in water show no signs that a degradation process occurs. No mass variation appears during the testing time, after the initial Δm due to the water absorption.

4.3.1 Deformation

The deformation during the sulphate attack is reported in Figure 56. The behaviour of the expansion is similar for all the samples in analysis, but in the LCP specimen the initial deformation arrives to $\varepsilon = 0.16\%$ after 2000 hours. The others typologies show an initial deformation of $\varepsilon = 0.08\%$, $\varepsilon = 0.09\%$ and $\varepsilon = 0.1\%$ for the LC, WC and HC, respectively and after 2000 hours the value is constant. As evidenced in chapter 3 the induction period occurs at times more larger then those 20000 hours.

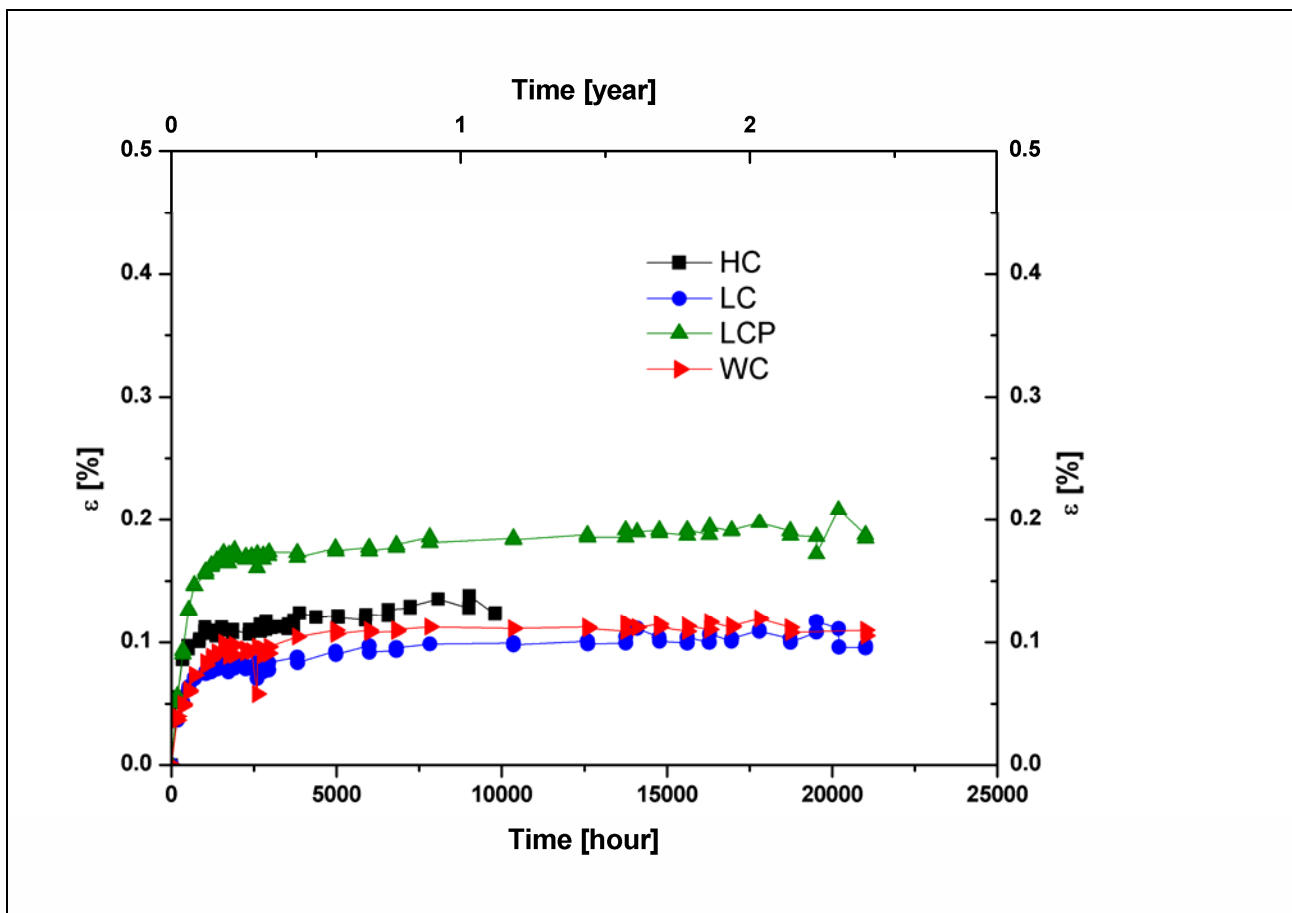


Figure 56 – Deformation [%] during the complex sulphate attack.

Figure 57 shows the deformation during the cyclic acid/sulphate attack. When the attack is cyclic, there aren't remarkable differences with the corresponding sample subjected to the only sulphate attack during the first 10000 hours. In the range between 10000 and 15000 hours, the WC sample shows an expansion and after 20000 hours is $\varepsilon = 0.22\%$. The others typologies of samples have similar trend, a initial expansion due to the solution absorption followed by no significant deformation until the end of the periods of analysis. In particular the LC shows the same initial deformation of the WC ($\varepsilon = 0.1\%$) and for HC and LCP $\varepsilon = 0.13\%$ and 0.18% respectively.

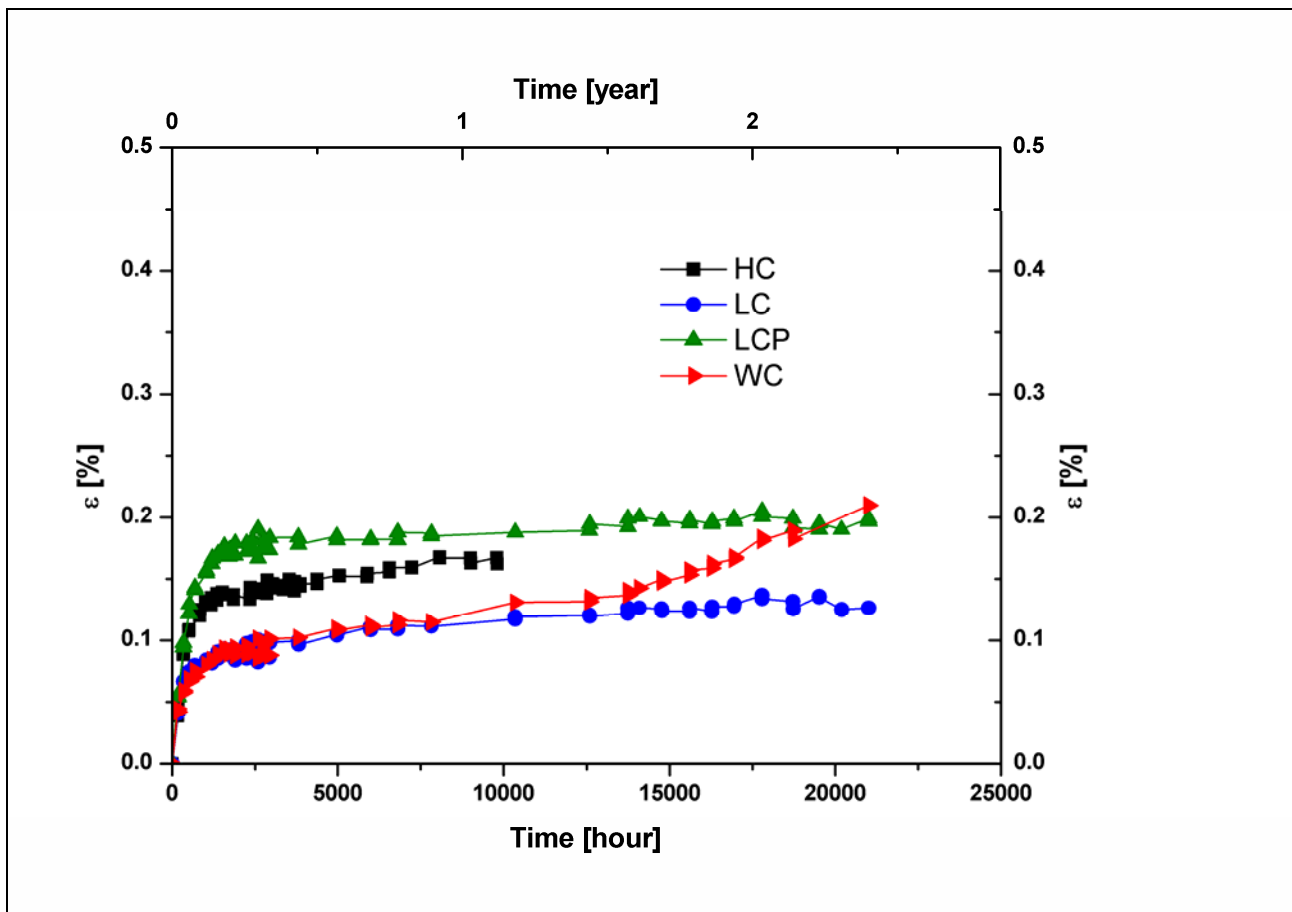


Figure 57 – Deformation [%] during the cyclic acid/(complex)sulphate attack.

The specimens stored only in water, show no signs that a degradation process occurs. No deformation appear during the testing time, after the initial expansion due to the water absorption.

The presence of glucose in the complex sulphate solution is the cause of the formation of algae and weed on the surface of the solution during the time. This formation starts few days after the renewing of the complex sulphate solution. After 5000 hours, the algae appear directly on the surface of the specimens, and they are green if the samples are stored on the sun light or they are black if the specimens are stored in a closet. The presence of the silica coating reduce the formation of this biological elements on the coated surface. In Figure 58 pictures of three different typologies of samples are reported. On the surface of the WC sample are present a lot of grey/black stain, but in the coated specimens this number decrease, specially for the LC.

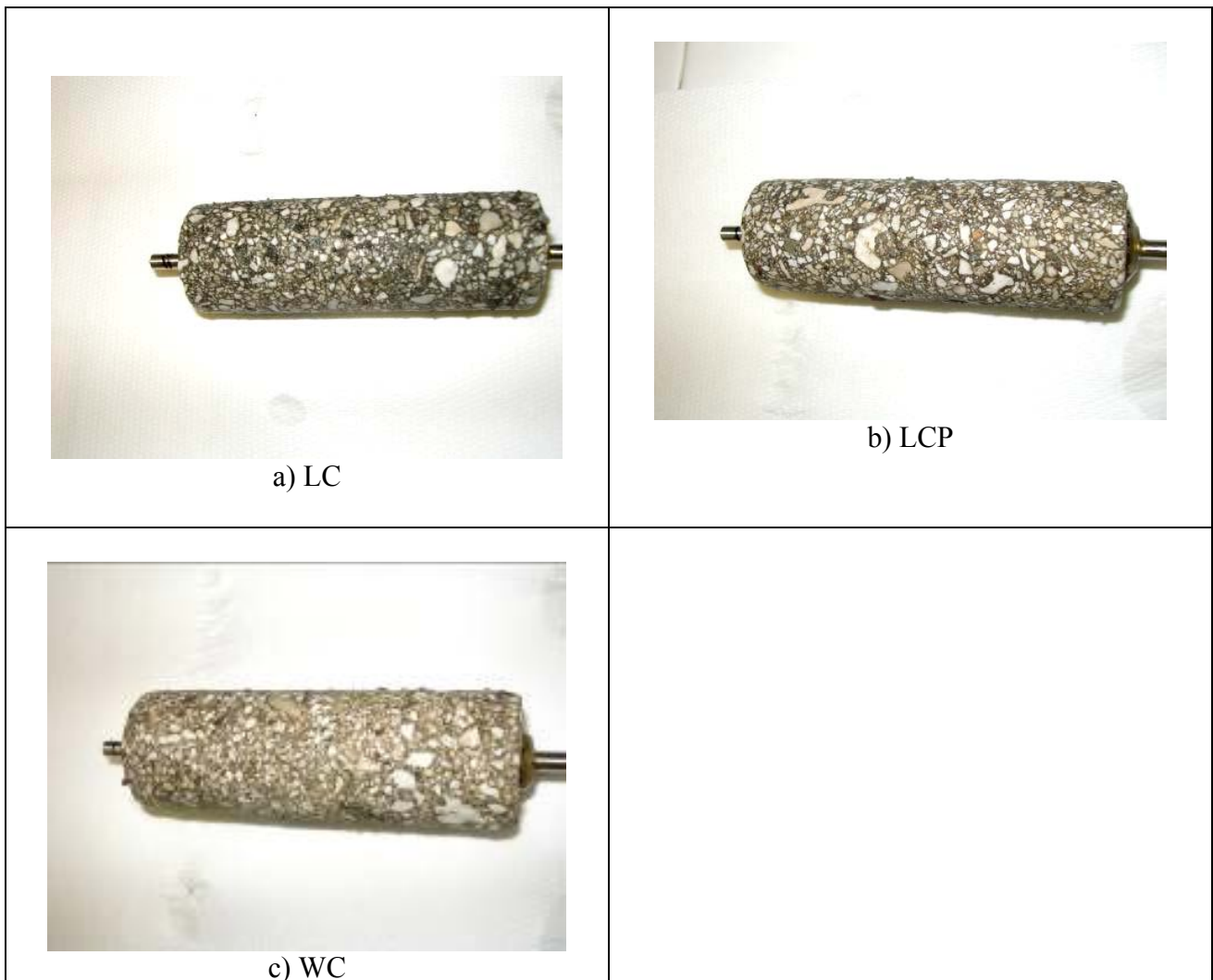


Figure 58 – Effect of the silica coating on the grow of algae.

4.5.2 Test on hardened concrete

For a preliminary test, the coating were applied directly on the hardened concrete. The silica sol has a good wettability on the surface, as reported in Figure 59a, but after 1 hour different flakes appear on the external surface. Some of these pieces of the silica coating are reported in Figure 59b.

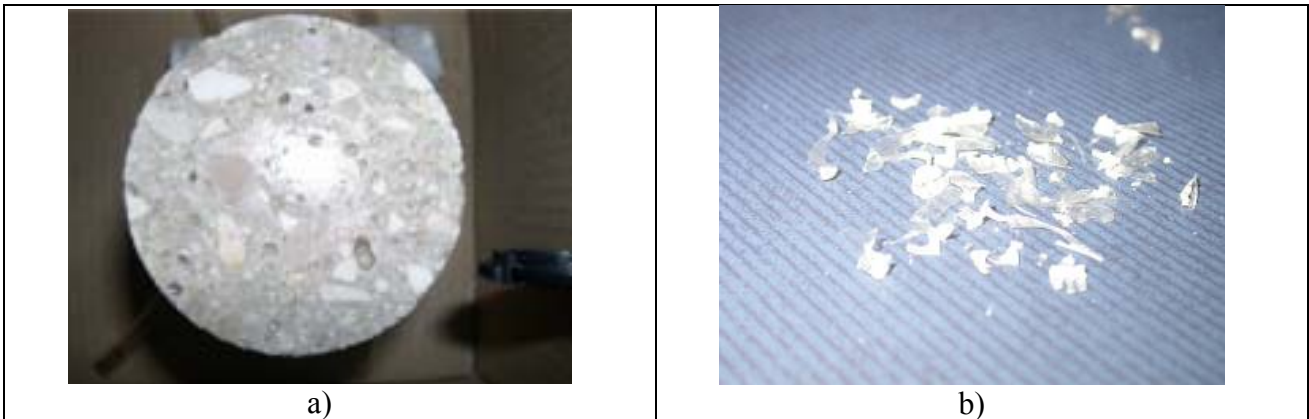


Figure 59 – Silica coating applied on hardened concrete.

On the base of this results, the coating were applied by spraying directly on the wet specimens, few minutes after the extrusion process.

4.5.3 Phenolphthalein and wettability tests

In order to evaluate the alkalinity level on the concretes, phenolphthalein testes were performed on the surface after the hardened periods of 28 days at 20°C and 95% R.H., according to the EN 9944. The results regarding the specimens covered with 7.3 g/m² of silica coating (LC) are reported in Figure 60. The purple stains appear on the surface only after 30 seconds.

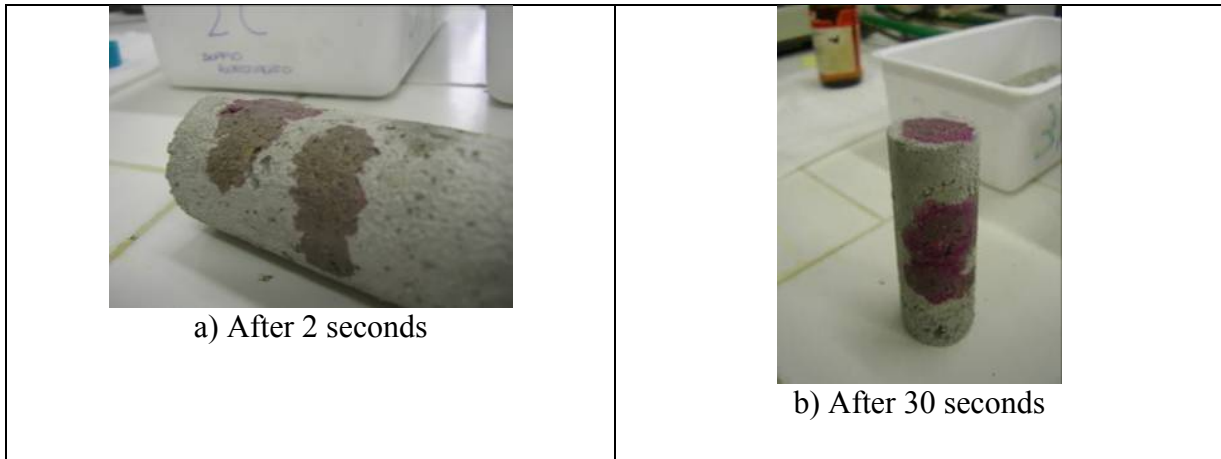


Figure 60 - Phenolphthalein methods (EN 9944) results on LC sample.

A wettability test was performed in order to understand the behaviour of the coating in contact with the water. The results of this test are reported in Figure 61. The WC sample (Figure 61a) shows a good wettability; in fact the drop of water has a low contact angle, typical of an hydrophilic surface. The specimen LCP (Figure 61b and Figure 61c) shows an opposite behaviour, with an high contact angle, and the water drop is resistance to the gravity, if the surface is rotated of 90 degrees.

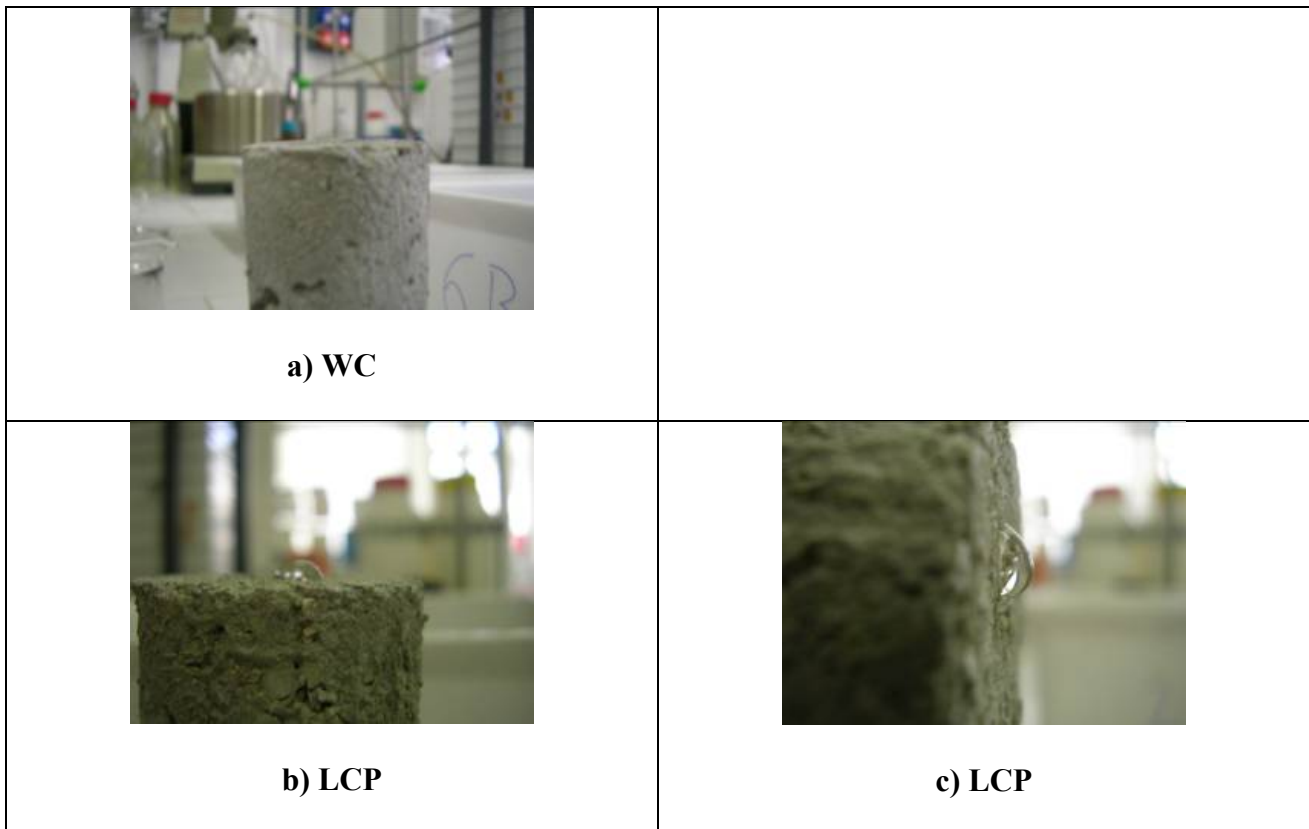


Figure 61 - Wettability test of WC (a) and LCP (b, c).

4.6 Discussion

Nowadays, there are different commercially solutions and methods to protect the concrete in aggressive environments. The use of co-axial PVC pipes introduces some problems, like debonding phenomena between the polymer and the concrete. Moreover, the production of this type of pipes is more complex and the system of vibro-compression is not suitable.

In order to obtain a long durability, various parameters are take into account, like the type of the cement and the possibility to use a protective coating. An appropriate selection of the cement is based on the results of the previous part of this work, showing that the use of a portland limestone cement is very recommended.

A potential protective system is coating the pipes with materials resistant to acid attack, as reactive silica. The role of this components is to induce a pozzolanic reaction in the layer directly in contact with the aggressive fluids. The good stability of the starting solution (high time of gelification) and the feasibility increase the industrial implementation, with automatic spraying system.

The application immediately after the de-moulding process is in agreement with the typical production time. In fact after the de-moulding, the pipes are stored in open air for few days before the commercialization.

The analysis of the rate of the mass loss, during the sulphate attack, shows a similar change trend in all the samples, with a weak Δm due to the dissolution processes involved by the magnesium and the ammonium sulphate of the complex sulphate solution. The WC and HC show the same behaviour.

When the samples are subjected to a cyclic acid/sulphate attack, the mass loss increases, especially for the WC. The silica coating reduces this trend especially when the concrete is protected with 70.3 g/m^2 of silica sol (HC). In fact, after 10000 hours, the HC sample shows a $\Delta m = -2\%$ and at the same time, WC shows $\Delta m = -12\%$ and the others two, LC and LCP, $\Delta m = -10\%$

and $\Delta m = -11\%$ respectively. As the results reported in the chapter 3, the behaviour depends on the frequency of the acid attack, and all the coated samples show the best trend.

During the only sulphate attack, every specimens don't show signs that an expansion occurs. But the concrete degradation due to the exposure to a sulphate and acid ambient, as the results presented in the chapter 3, can be discuss on the base of two mechanisms: dissolution of components and expansive action of the reaction products.

After about 15000 hours, an expansion phenomenon appears in the sample without coating and confirms that the acid-sulphate attack is a two-stage process also for the limestone portland cement type CEM II-B/LL 32.5R. The samples coated with the silica layer seems to increase the induction periods of the first stage. In fact, after over 20000 hours of testing, there are no signs that a degradation process occurs.

When the sulphate attack is monthly, the silica coating reduce the formation of algae due to the presence of glucose in the complex sulphate solution. This is clear when the samples are stored in a closed, without the presence of the sun light.

An increase of the silica coating amount is good, because decrease the severity of the acid attack. In fact comparing the data for the mass variation in the samples prepared with 7.3 g/m^2 (LC) and 70.3 g/m^2 (HC), the increase of silica sol sprayed on the concrete surface reduces Δm from -12% to -2.5% .

4.7 Conclusions

The degradation of a concrete covered with different silica coatings, prepared with limestone portland cement (CEM II-B/LL) and limestone aggregates were studied in a complex sulphate solution and for six hours weekly/monthly in a solution of H_2SO_4 with $pH=2$. The damage extension was evaluated by measuring mass loss and expansion. The results of the test, performed for about 20000 hours, let the following conclusions be drawn.

The concretes coated with the silica sol show the best performance, taking into account both mass loss and deformation percentage when subjected to a cyclic acid and sulphate attack. The concrete without coating shows an expansion after 15000 hours with a two stage process. The amount of the coating is important, and an increase of this coating reduces the mass loss but increases the initial expansion.

The behaviour of the concretes was also studied to comparison in only a complex sulphate solution. A little mass loss was recorded due to the attack produces by the aggressive ions of the complex sulphate solution. At the end of the test after about 20000 hours, the classification of the concretes in terms of damage resistance is the same and the expansion percentage is remarkable lower than in the acid and sulphate solutions. The mixtures stored only in water show a continuous and slow increase of weight as the effect of the water absorption.

The use of a silica coating increase the life of a sewer pipe and for the easy use is good candidate for an industrial implementation, such as a spray system.

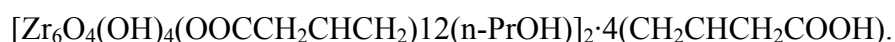
Chapter 5 – Hybrid coating

5.1 Hybrid coating

This last chapter shows preliminary results regarding the development of a new hybrid coating, which, contains also zirconium oxide, could have a protective effect without the drawbacks evidenced upon using pozzolanic addition or coating.

5.2 Materials

Commercially available reagents were used without further purification. Vinylacetic acid (VAA) and zirconium n-propoxide were mixed in the molar ratio of 4:1, at the aim to substitute each alkoxy group, under inert atmosphere and left aside until precipitation of crystals. After that, the precipitate product, labelled ZrNBB, was separated and dried. Elemental analysis (C, 36.74; H, 4.14; Zr, 25.20 wt%) suggests the following theoretical formula:



Crystals have been dissolved in tetrahydrofurane (THF) and stirred with vinyl trimethoxysilane (VTMS) in different Zr:Si molar ratio (1:1, 1:2, 1:4, 1:10) in air at room temperature with the addition of benzoyl peroxide (BPO, 1 wt% with respect to VTMS).

The solution was evaporated to dryness under vacuum, leaving a yellowish transparent xerogel (ZrNBB/VTMS). Differential Scanning Calorimetry analyses were performed by a DSC92 SETARAM, from 30°C to 200°C in N₂ with a heating rate of 10°C/min. Thermo-Gravimetric Analysis (TGA) was performed from 30°C to 1000°C in air with a heating rate of 10°C/min, using a Labsys SETARAM thermobalance. Dynamic mechanical spectroscopy (DMS) was performed in shear mode on cured prism having planar and parallel faces 12 mm² large and 3.5 mm thick, by using a Seiko DMS 6100 instrument at a frequency of 1 Hz, with a displacement 0.005 mm along the diameter direction. The scan maximum temperature was 200°C with heating rate 2°C/min. Shear storage modulus (G'), loss modulus (G'') and tan δ were measured. FT-IR spectra were recorded in transmission mode in the range 4000–400 cm⁻¹ on KBr pellets (64 scans and 2 cm⁻¹

resolution), using a Thermo Optics Avatar 330 FTIR instrument. Solid state NMR analyses were carried out with a Bruker 400 WB instrument applying a carrier frequency of 400.13 MHz (1H). 1D experiments were based on single pulse sequence under the following conditions: ^{29}Si at 79.50 MHz with $p/2$ 4.3 μs at -2 dB and 10 s delay time; ^{13}C at 100.07 MHz, $p/2$ 3.5 μs at -1.7 dB, 5.3 μs decoupling pulse and 10 s delay time; 2D ^{13}C - ^1H hetero experiments with LG-RF 73529 Hz, delay time 2.5 s, contact time 200 μs , decoupling & excitation pulse -4.2 μs . Samples were packed in 4 mm-zirconia rotors, which were spun at 9.5 kHz under air flow.

5.3 Result and discussion

The zirconium oxo-cluster was prepared according to previous studies of Schubert et al. [34] [35] and it can be described as a dimer of Zr_6 clusters, having chelating, bridging and terminal vinylacetate ligands. Each mer consists of a zirconia core containing six zirconium atoms. ZrNBB appears colourless and does not swell in water. The reaction between ZrNBB and vinyltrimethoxy silane (VTMS) leads to a gel which polymerizes upon heating, in the presence of a thermal polymerisation initiator, such as benzoyl peroxide. The polymerisation of the gel was followed by differential scanning calorimetry. Figure 62, on the left, presents the recorded curve, for the 1:4 Zr:Si ratio, featuring a large exothermic peak. The T_{onset} is 98°C and the maximum of the peak is 140°C.

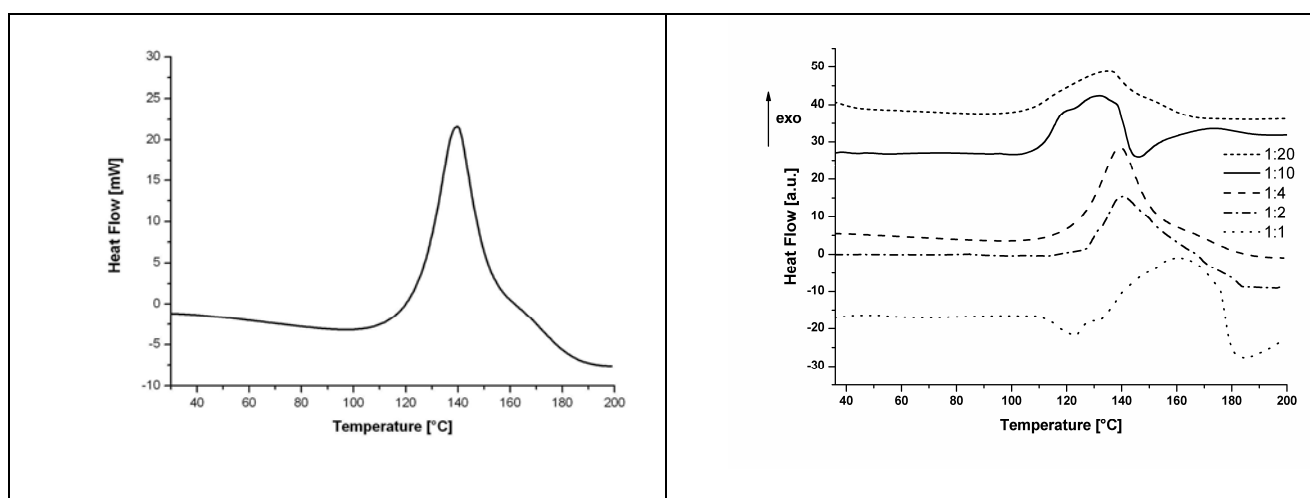


Figure 62 - DSC curve of the solution VTMS/ZrNBB/BPO; Zr:Si 1:4 on the left; different ratio on the right.

The polymerization heat, calculated including the shoulder, was 214 J/g and the mass loss was 9%. The absence of an endothermic peak at low temperature due to the evaporation of VMTS indicates that the vinylalkoxysilane should have reacted with the zirconium oxocluster through a condensation process.

Moreover, a high temperature shoulder is present on the main polymerization peak in the DSC curve, indicating that two separate thermal events of polymerization occurred. The shoulder is attributed to the polymerization of steric hindered vinyl groups of the zirconium oxocluster. This has been already observed, in a preliminary study on polymerization of organic methacrylate monomer and zirconium oxocluster. In Figure 62 on the right are reported the DSC curves of the other Zr:Si ratios. Increasing the content of oxocluster, the polymerization peaks shift from lower to higher temperatures, becoming meantime quite sharp. A shoulder at higher temperature is always present and relies on the polymerization of vinyl groups, less available to radical reaction, such as those on ZrNBB. DSC curve of the Zr:Si molar ratio 1:1 shows an endothermic peak due to the decomposition of zirconium oxo-clusters.

As a consequence, the choice of polymerization parameters, such as the temperature or time, can affect the polymerization degree and accordingly the final properties of the hybrid polymer. In this chapter, bulk samples were obtained heating the xerogel up to 130°C, after an isothermal step at 90°C. This thermal treatment produces a glassy dense hybrid material as presented in Figure 63, where the typical cylinder used for the thermo-mechanical test is shown.



Figure 63 – Bulk sample obtained heating the xerogel up to 130°C for 1 h

The FT-IR spectra of the reagents and of the hybrid ZrNBB/VTMS xerogel are reported in Figure 64 on the left. The spectrum of the hybrid sample shows the features of the reagents VTMS and ZrNBB, along with the peaks relating to siloxane bonds and the signals due to Zr–OH and Zr–O bonds (ν_{OH} 3400 cm^{-1} , $\nu_{\text{Zr-O}}$ 653 cm^{-1}).

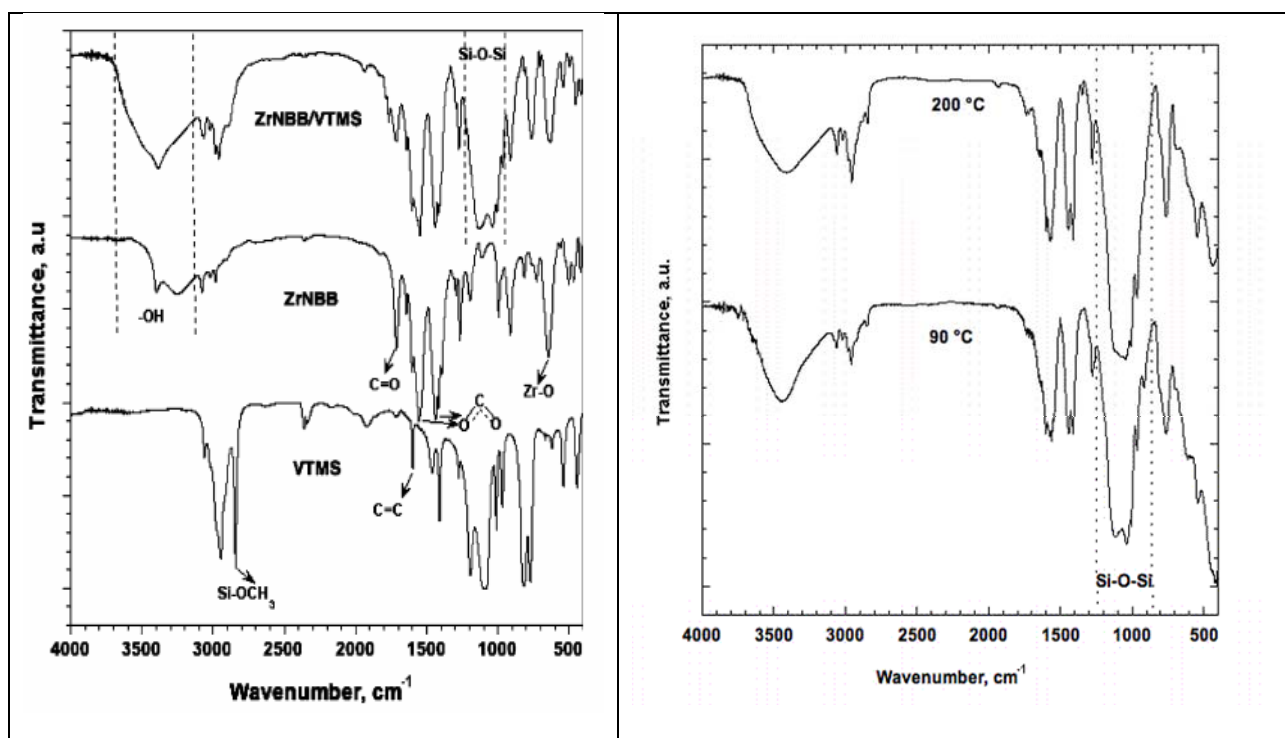


Figure 64 - FTIR spectra of reagents (ZrNBB and VTMS) and hybrid gel

Moreover, the complexity of the spectrum of the hybrid material is due to the different vinylacetate species, as reported above. Finally, the typical peaks of zirconium oxocluster are still visible in the FT-IR spectra of hybrid material recorded after thermal treatments, reported in Figure 64 on the right, indicating the ZrNBB are stable, at least up to 200°C. The ^{29}Si MAS spectra, reported in Figure 65 on the left, and recorded after different thermal treatments, indicate that the condensation degree of the siloxane counterpart is low and the main species are T2 units $\{\text{RSi}(\text{OSi})_2\text{OR}(\text{O})\}$. ^{13}C MAS spectra, reported in Figure 65 on the right, confirm the low condensation of the vinyltrimethoxy silane, given that the peak of methoxy groups are still present in the hybrid material even at high temperature

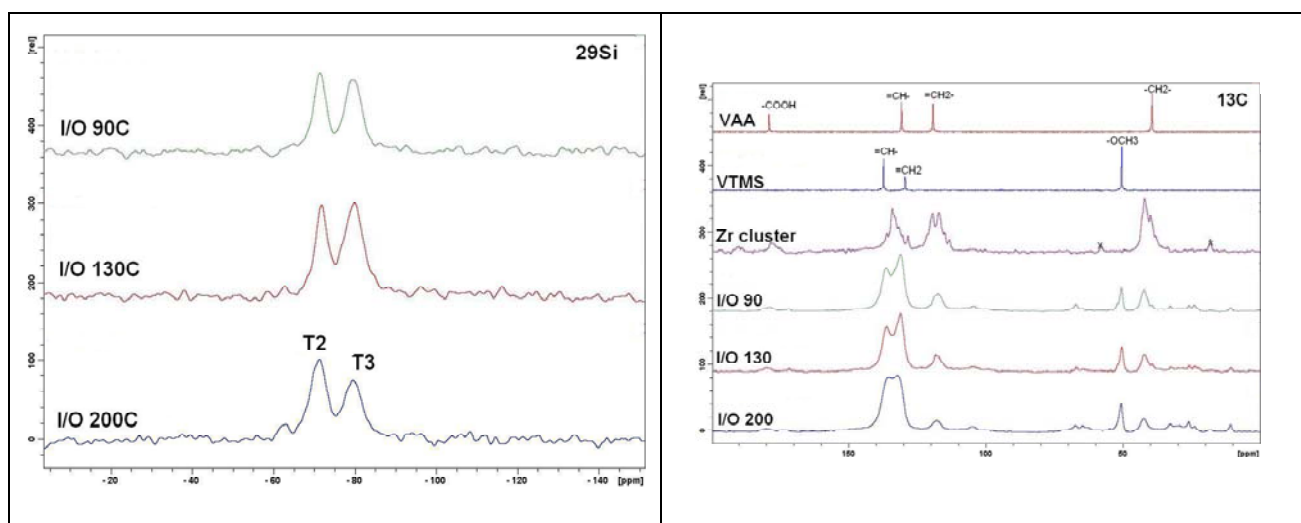


Figure 65 - Evolution with temperature of ^{29}Si MAS spectra of ZrNBB/VTMS hybrid materials on the left - ^{13}C spectra of VAA and VTMS in d_8 -THF and ^{13}C MAS spectra of ZrNBB and ZrNBB/VTMS hybrid material treated at different temperatures on the right.

The complexity of CH_2 and COOH regions in the spectrum of ZrNBB suggests the presence of different vinylacetate species, probably due to different isomeric species. A decrease of the intensity of $=\text{CH}$ and $=\text{CH}_2$ signals derived from VTMS and ZrNBB is observed with increasing temperature, along with an increase in the intensity and broadening of the aliphatic region, indicating an advancement of the polymerization process with double bond breaking and growth of longer carbon chains. In Figure 66 are reported the curves of $\tan \delta$, storage and loss moduli (G' and G'' , respectively) for the materials with Zr:Si 1:4 molar ratio. A very slight increase of modulus is observed from room temperature up to the glass transition temperature. This is measured as the temperature of the maximum of the peak of the loss modulus curve and is 180°C .

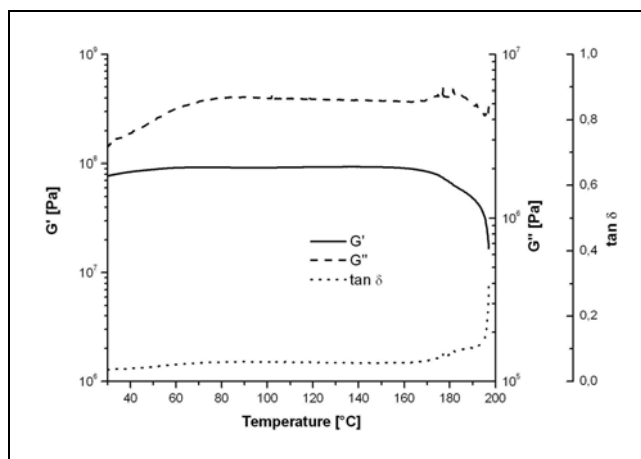


Figure 66 - Viscoelastic properties of sample ZrNBB/VTMS (Zr:Si 1:4) hybrid material vs. temperature

Correspondingly, the value of $\tan \delta$ is quite low, indicating a strong interconnectivity of the network, so that there is no viscous flow [36]. Moreover, the specimens underwent to other runs as shown in Figure 67: the increase of the storage modulus is clear from the first to fifth run due to the occurrence of further polymerization. For the sake of clarity, the 3rd curve was The last run was performed in a larger temperature range just in order to measure the new T_g , which exceeds the previous temperature range. Indeed the new T_g increases up to 240°C . At this regard, it is worth noting that the dynamical-mechanical test, using shear configuration, requires two specimens of the same size. Both of them were recovered after the runs without failure and presented a whole mass loss of 8.3%.

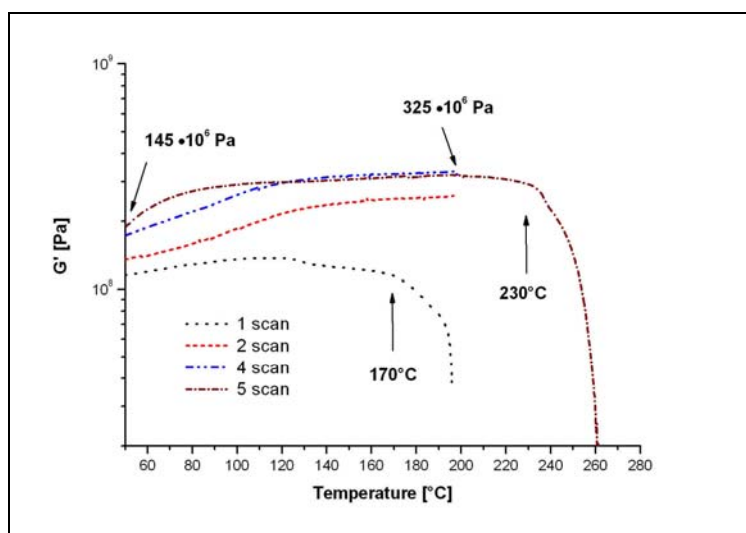


Figure 67 - Storage modulus (Zr:Si 1:4) vs. temperature of the same samples, subjected to five consecutive DMS tests

5.4 Conclusions

A hybrid polymer composite has been obtained by co-polymerization of vinylacetate zirconium oxocluster and vinyltrimethoxy silane. The hybrid inorganic–organic polymer contains high amount of $\text{SiO}_2\text{--ZrO}_2$ and bulk specimens were prepared in order to evaluate their structure and thermo-mechanical properties. The Zr–Si ratio can be modified and the final samples could be films or bulk specimens, with the desired size and shape. The structural characterization has indicated a low extent of the inorganic condensation and of the polymerization of vinyl groups, particularly those belonging to the pristine VMTS.

The materials showed high stiffness (G') and glass transition temperature (T_g). These properties are even improved increasing temperature or repeating the thermal tests: 145 MPa and 240°C for G' and T_g , respectively. This result is interesting because it was recorded in absence of a remarkable mass loss. The polymer has the potentiality for applications requiring high thermal stability and aggressive environment, and the Zr–Si molar ratio can be varied, tailoring the final architectures and properties of hybrid polymer.

References

- [1] A. Delagrave, M. Pigeon, E. Revertégat, , “Influence of chloride ions and pH level on the durability of high performance cement pastes” *Cement and Concrete Research* 24 (1994) 1433-1443
- [2] V. Pavlík, S. Unčák, “The rate of corrosion of hardened cement pastes and mortars with additive of Silica Fume in acids” *Cement and Concrete Research* 27 (1997) 1731– 1745
- [3] V. Pavlík, “Corrosion of hardened cement paste by acetic and nitric acid part I: Calculation of corrosion depth” *Cement and Concrete Research*, 1994, Vol. 24, pp. 551– 562
- [4] V. Pavlík, “Corrosion of hardened cement paste by acetic and nitric acid part II: Formulation and chemical composition of the corrosion products layer”, *Cement and Concrete Research*, 1994, Vol. 24, pp. 1495–1508.
- [5] C. D. Parker, “The corrosion of Concrete”, *Australian Journal of Experimental Biology Medicine Science*, 23 (1945) 91-98
- [6] V. Pavlík, “Effect of carbonates on the corrosion rate if cement mortars in nitric acid” *Cement and Concrete Research*, 2000, Vol. 30, pp. 481– 489.
- [7] K. Milde, W. Sand, W. Wolf, E. Bock, “Thiobacilli of the corroded concrete wall of the hamburg sewer” *Journal of General Microbiology*, 123 (1988) 1327-1333
- [8] N.I. Fattuhi, B. P. Hughes, “The performance of cement paste and concrete subjected to sulphuric acid attack” *Cement and Concrete Research* 18 (1988) 545-553
- [9] T.A. Durning, M. C. Hicks, “Using microsilica to increase concrete's resistance to aggressive chemicals”, *Concrete International*, 13 (1991) 42-48
- [10] A. Attal, M. Brigodiot, P. Camacho, J. Manem, “Biological mechanisms of H₂S formation in sewer pipes.”, *Water Science Technology*, 26 (1992) 907-914
- [11] N. A. Padival, J. S. Weiss, R.G. Arnold, “Control of Thiobacillus by means of microbial competition: implications for corrosion of concrete sewers”, *Water Environmental*

Research, 67 (1995) 201-205

[12] F. Jahani, J. Devinny, F. Mansfeld, I. G. Rosen, Z. Sun, C. Wang, "Investigations of sulfuric acid corrosion of concrete. I: modelling and chemical observations" *Journal of Environment Engineering*, 127 (2001) 572-579

[13] F. Jahani, J. Devinny, F. Mansfeld, I. G. Rosen, Z. Sun, C. Wang, "Investigations of sulfuric acid corrosion of concrete. II: electrochemical and visual observations" *Journal of Environment Engineering*, 127 (2001) 580-584

[14] M. Santhanam, M. D. Cohen, J. Olek, "Mechanism of sulfate attack: a fresh look. Part 1: Summary of experimental results" *Cement and Concrete Research* 32 (2002) 915-921

[15] J. M. Tulliani, L. Montanaro, A. Negro, M. Collepardi, "Sulfate attack of concrete building foundations induced by sewage waters", *Cement and Concrete Research*, 32 (2002) 843-849

[16] A. Borsoi, S. Collepardi, L. Coppola, R. Troli, and M. Collepardi, "Sulphate Attack on Blended Portland Cements", *Proceedings del Fifth CANMET/ACI International Conference on "Durability of Concrete"*, Barcellona, Spain, 4-9 Giugno 2000, pp. 417-432.

[17] M. Collepardi, "A state of the art review on delayed ettringite attack on concrete" *Cement and Concrete Composites*, 25 (2003) pp. 401-407

[18] F. Tittarelli, G. Moriconi, A. Bonazza "Atmospheric deterioration of cement plaster in a building exposed to a urban environment" *Journal of Cultural Heritage* 9 (2008) 203-206

[19] C. Vipulanandan, Jie Liu, "Glass-fiber mat-reinforced epoxy coating for concrete in sulfuric acid environment" *Cement and Concrete Research*, 32 (2002) 205-210

[20] R. E. Beddoe, H. W. Dorner, "Modelling acid attack on concrete: Part I. The essential mechanism" *Cement and Concrete Research* 35 (2005) pp. 2333-2339

[21] M. Santhanam, M. D. Cohen, J. Olek, "Modelling the effects of solution temperature and concentration during sulphate attack on cements mortars" *Cement and Concrete Research* 32 (2002) pp. 585-592

- [22] J. Hill, E. A. Byars, J. H. Sharp, C. J. Lynsdale, J. C. Cripps, Q. Zhou, “An experimental study of combined acid and sulfate attack of concrete”, *Cement and Concrete Composites* 25 (2003) 997–1003.
- [23] M. Thomas, K. Folliard, T. Drimalas, T. Ramlochan, “Diagnosing delayed ettringite formation in concrete structures” *Cement and Concrete Research* 38 (2008) pp. 841-847
- [24] K. L. Scrivener, J-L. Cabiron, R. Letourneux, “High-performance concretes from calcium aluminate cements” *Cement and Concrete Research*, 29 (1999) 1215-1223
- [25] J. Liu, C. Vipulanandan, *Tunnelling and Underground Space Technology*, 2001, Vol. 16, pp. 311-321
- [26] J.M. Tulliani, L. Montanaro, A. Negro, M. Collepardi, “Sulphate attack of concrete building foundations induced by sewage waters” *Cement and Concrete Research* 32 (2002) pp. 843–849
- [27] M. Mbessa, J. Péra, “Durability of high-strength concrete in ammonium sulphate solution” *Cement and Concrete Research* 31 (2001), pp. 1227–1231
- [28] M. Santhanam, M. D. Cohen, J. Olek, “Modelling the effects of solution temperature and concentration during sulphate attack on cements mortars” *Cement and Concrete Research* 32 (2002), pp. 585–592
- [29] J. Monteny, E. Vincke, A. Beeldens, N. De Belie, L. Taerwe, D. Van Gemert, W. Verstraete, “Chemical, microbiological, and in situ test methods for biogenic sulphuric acid corrosion of concrete” *Cement and Concrete Research* 30 (2000) pp. 623-634
- [30] T. Bakharev, J.G. Sanjayan, Y.-B. Cheng, “Resistance of alkali-activated slag concrete to acid attack” *Cement and Concrete Research* 33 (2003) pp. 1607– 1611
- [31] P.K. Mehta, D. Pirtz, M. Polivka, “Properties of alite cements” *Cement and Concrete Research* 9 (1979) pp. 439-450.
- [32] P.K. Mehta, *Materials Science of Concrete III*, American Ceramic Society, Westerville, OH, 1992.

- [33] B. Tian, M. D. Cohen, "Does gypsum formation during sulphate attack on concrete lead to expansion?" *Cement and Concrete Research* 30 (2000) pp. 117-123
- [34] U. Schubert, "Organofunctional metal oxide clusters as building blocks for inorganic-organic hybrids materials" *Journal of Sol–Gel Science and Technology* 31 (2004) pp. 19-24
- [35] U. Schubert, "Silica-based and transition metal-based inorganic-organic hybrids materials – a comparison" *Journal of Sol–Gel Science and Technology* 26 (2003) pp. 47-55
- [36] F.R. Kogler, T. Koch, H. Peterlik, S. Seidler, U. Schubert, "Mechanical, thermomechanical, and thermal properties of polystyrene crosslinked with a multifunctional zirconium oxo-cluster" *Journal of Polymer Science Part B: Polymer Physics* 45 (2007) pp. 2215–2231

Acknowledgements

Publicemento and ASSOBETON “Sezione Tubi” are greatly acknowledged for funding the study. The author would like to express his gratitude to S. Cossalter and Eurobeton, who gave a remarkable support to the research work. For their interest and valuable hints, the author would like to thank C. Bonfanti, P. Bonora, U. Ursella, M. Soraruf, F. Cona, A. Giacalone, A. Tofani, E. D’Alessandro, M. Appoloni, M. Santolin, F. Zorzi and W. Vaona.

Publications

- F. Girardi, W. Vaona, R. Di Maggio, Accelerated test for measuring sulphate resistance of concrete pipe prepared with different hydraulic cements, 2009, Cement and Concrete Research, submitted.
- F. Girardi, F. Graziola, P. Aldighieri, L. Fedrizzi, S. Gross, R. Di Maggio, Inorganic-organic hybrid materials with zirconium oxoclusters as protective coatings on aluminium alloys, Progress in organic coatings, 2008, Vol. 62, pp. 376-381.
- F. Graziola, F. Girardi, M. Bauer, R. Di Maggio, M. Rovezzi, H. Bertagnolli, C. Sada, G. Rossetto, S. Gross, UV-photopolymerisation of poly(methyl methacrylate)-based inorganic-organic hybrids coatings and bulk samples reinforced with methacrylate-modified zirconium oxocluster, Polymer : the international journal for the science and technology of polymers, 2008, Vol. 49, pp. 4332-4342
- R. Di Maggio, S. Dirè, E. Callone, F. Girardi, G. Kickelbick, Si and Zr based NBBs for hybrid O/I macromolecular materials starting by preformed zirconium oxo-clusters, Journal of sol-gel science and technology, 2008, Vol. 48, pp. 168-171

Proceeding:

- Graziola F., Girardi F., Bauer M., Bertagnolli H., Sada C., Di Maggio R., Gross S., UV-PHOTOPOLYMERISATION OF PMMA-BASED INORGANIC-ORGANIC HYBRID COATINGS AND BULK SAMPLES REINFORCED WITH METHACRYLATE-MODIFIED ZIRCONIUM OXOCLUSTER. In: VII Research Course on New X-Ray Sciences, : , 2008, Published in proceedings of the workshop "VII Research Course on New X-Ray Sciences" Hamburg, 5-7 March 2008
- Girardi F., Di Maggio R., Dire' S., Callone E., Kickelbick G., "Zr and Si based hybrid I/O macromolecular materials with zirconium oxoclusters". In: Atti del Convegno, x:x, 2008. Atti del convegno: "VI Workshop Sol-Gel Italiano", Lecce , 21/22 Giugno 2008
- Di Maggio R., Ischia M., Girardi F., Fambri L., "Polymerization of 2-hydroxyethyl-methacrylate (HEMA) with titanium and zirconium alcoxides". In: XIV International Sol-Gel Conference: Book of abstracts , Montpellier:ENSCM Communication, 2007. p. 223-223. . Atti del convegno: "Sol-Gel 2007", Montpellier, 2nd-7th September 2007, URL : <http://www.enscm.fr/sol-gel2007.html>
- Girardi F., Di Maggio R., Fambri L., "Poly-Hydroxyethyl-Methacrylate (PHEMA) reinforced by preformed zirconium oxo-cluster". In: Trento Innovation Conferences in Materials Engineering: Advances in Polymers, Composites and Biomaterials, Trento:Università degli Studi di Trento, 2007. p. 106-. Atti del convegno: "1st Meeting-Advances in Polymers, Composites and Biomaterials (TICME 2007)", Trento, 16th-19th December 2007, URL : <http://www.ticme.ing.unitn.it/>. Note: ISBN 978-88-8443-209-4.
- Di Maggio R., Fambri L., Girardi F., "Polymerization of 2-hydroxyethyl-methacrylate (HEMA) with zirconium oxoclusters". In: XIV International Sol-Gel Conference: Book of abstracts , Montpellier:ENSCM Communication, 2007. p. 185-185. . Atti del convegno: "Sol-Gel 2007", Montpellier, 2nd-7th September 2007, URL : <http://www.enscm.fr/sol-gel2007.html>
- Graziola F., Girardi F., Fambri L., Di Maggio R., "UV-photopolymerisation of PMMA-based inorganic-organic hybrid coatings and bulk samples reinforced with methacrylate-modified zirconium oxocluster". In: XIV International Sol-Gel Conference: Book of abstracts , Montpellier:ENSCM Communication, 2007. p. 260-260. . Atti del convegno:

- "XIV Sol-Gel Conference", Montpellier, 2nd-7th September 2007, URL : <http://www.enscm.fr/sol-gel2007.html>
- Di Maggio R., Dire' S., Callone E., Girardi F., "Self-assembling of Si and Zr based NBBs for hybrid O/I macromolecular materials starting by preformed zirconium oxo-clusters". In: XIV International Sol-Gel Conference: Book of abstracts , Montpellier:ENSCM Communication, 2007. p. 153-153. . Atti del convegno: "Sol-Gel 2007", Montpellier, 2nd-7th September 2007, URL : <http://www.enscm.fr/sol-gel2007.htm>
 - Di Maggio R., Dire' S., Girardi F., "Self-assembling of Si and Zr based NBBs for hybrid O/I macromolecular ". In: 2006 SAMIC : syntheses and methodologies in organic chemistry : From molecules to nanosystem, Padova:[Legatoria Artigiana-Trevisan], 2006. Atti del convegno: "SAMIC 2006", Bressanone, 3-7 December , 2006
 - Di Maggio R., Graziola F., Girardi F., Gross S., "Zirconium Oxocluster-Based Inorganic-Organic Hybrid Materials as protecting structural coating". In: 2006 SAMIC : syntheses and methodologies in organic chemistry : From molecules to nanosystems, Padova:[Legatoria Artigiana-Trevisan], 2006. Atti del convegno: "SAMIC 2006", Bressanone, 3-7 December , 2006
 - Di Maggio R., Fambri L., Girardi F., Moser M., "Polyhydroxyethylmethacrylate reinforced by preformed zirconium oxo-clusters". In: 2006 SAMIC : syntheses and methodologies in organic chemistry : From molecules to nanosystems, Padova:[Legatoria Artigiana-Trevisan], 2006. Atti del convegno: "SAMIC 2006", Bressanone, 3-7 December , 2006
 - Di Maggio R., Vaona W., Girardi F., Deflorian F., "Resistenza all'attacco chimico prodotto dal trasporto di liquami di fognatura". Contributo a "Convegno 'Sistemi Fognari ed Ambiente'", Roma (Italia), 4 Marzo 2005

Conference:

VI Workshop Sol-Gel Italiano, Lecce , 21-22 June 2008:

- Girardi F., Di Maggio R., Dire' S., Callone E., Kickelbick G., "Zr and Si based hybrid I/O macromolecular materials with zirconium oxoclusters". Oral communication

TICME 2007 Trento Innovation Conferences in Materials Engineering: Advances in Polymers, Composites and Biomaterials, Trento, 2007:

- Girardi F., Di Maggio R., Fambri L., "Poly-Hydroxyethyl-Methacrylate (PHEMA) reinforced by preformed zirconium oxo-cluster", Poster
- F. Graziola, F. Girardi, M. Bauer, H. Bertagnolli, C. Sada, R. Di Maggio, S. Gross, "UV - photopolymerised poly(methylmethacrylate)-based organic-inorganic hybrid coatings and bulk samples: effect of clusters on thermal stability and mechanical properties" - Poster

XIV International Sol-Gel Conference, Montpellier, 2-7 September, 2007:

- Di Maggio R., Fambri L., Girardi F., "Polymerization of 2-hydroxyethyl-methacrylate (HEMA) with zirconium oxoclusters", Poster
- Graziola F., Girardi F., Fambri L., Di Maggio R., "UV-photopolymerisation of PMMA-based inorganic-organic hybrid coatings and bulk samples reinforced with methacrylate-modified zirconium oxocluster", Poster
- Girardi F., Di Maggio R., Fambri L., Ischia M., "A study on titanium and zirconium alkoxides modified by 2-hydroxyethyl methacrylate (HEMA)" – Poster

SAMIC 2006, Bressanone, 3-7 December , 2006:

- Di Maggio R., Dire' S., Girardi F., "Self-assembling of Si and Zr based NBBs for hybrid O/I macromolecular ", Poster

- Di Maggio R., Fambri L., Girardi F., Moser M., "Polyhydroxyethylmethacrylate reinforced by preformed zirconium oxo-clusters", Poster
- Di Maggio R., Fambri L., Girardi F., Moser M., "Polyhydroxyethylmethacrylate reinforced by preformed zirconium oxo-clusters", Poster